



INSTITUTO SUPERIOR TÉCNICO
Universidade Técnica de Lisboa

Attitude Determination Using Multiple L1 GPS Receivers

João Miguel Mendes Cóias

Dissertação para obtenção do Grau de Mestre em
Engenharia Aeroespacial

Júri

Presidente: Prof. Doutor João Manuel Lage de Miranda Lemos
Orientador: Prof. Doutor Paulo Jorge Coelho Ramalho Oliveira
Co-orientador: Prof. Doutor José Eduardo Charters Ribeiro da Cunha Sanguino
Vogal: Prof. Doutor Fernando Duarte Nunes

Mai 2012

AGRADECIMENTOS

O concluir de uma tese de mestrado é o culminar de um processo, repleto de obstáculos, que nunca seria possível de alcançar por conta própria. Assim, é inevitável endereçar os meus agradecimentos a todos os que, com o seu importante contributo, tornaram possível chegar até aqui.

Ao Professor Paulo Oliveira e ao Professor José Sanguino, que sempre se mostraram disponíveis para partilhar o seu conhecimento e cuja orientação foi essencial para seguir sempre o caminho certo e ultrapassar os mais difíceis obstáculos.

À namorada, aos pais, à irmã e à restante família, que demonstraram sempre apoio incondicional e ajudaram a ter uma visão mais optimista nos momentos mais difíceis.

Aos colegas de laboratório pelo companheirismo e entreaajuda durante esta dura jornada.

A todos os restantes amigos que, perto ou longe, sempre demonstraram total apoio.

A todos, um sincero obrigado.

Esta tese de mestrado foi elaborada com o apoio parcial do Instituto de Telecomunicações (IT) e da Fundação para a Ciência e Tecnologia (FCT), no âmbito do projecto PTDC/EEA-TEL/122086/2010.

RESUMO

O uso de múltiplos receptores de GPS (Global Positioning System) permite a determinação de posicionamento relativo, isto é, a determinação do vector posição entre a antena de referência e as restantes. Para atingir níveis elevados de exatidão e precisão é necessário o uso de medições de fase. Contudo, estas medições contêm uma ambiguidade inteira. A determinação da ambiguidade de fase é um problema normalmente resolvido recorrendo a receptores de dupla frequência L1/L2. Devido ao elevado custo destes receptores, existe uma necessidade de desenvolver técnicas para resolver este problema usando receptores mais baratos de frequência única L1. Com o intuito de determinar correctamente a ambiguidade de fase com receptores de frequência única, nesta dissertação é proposto o uso do método de *LAMBDA* e o uso do *Ambiguity Filter*, permitindo a determinação do vector de posicionamento relativo com precisões milimétricas. As melhorias do *Ambiguity Filter*, propostas nesta dissertação, demonstraram um aumento da confiança na correcta determinação da ambiguidade de fase e, conseqüentemente, na determinação do vector de posicionamento relativo, e permitiram a adaptação às variações na constelação de satélites sem que fosse perdida a solução milimétrica do vector de posicionamento relativo.

Através da combinação de diversos vectores de posicionamento relativo, com normas conhecidas, obtidos utilizando quatro receptores L1, colocados em posições previamente conhecidas, é possível determinar os ângulos de atitude de um corpo rígido com elevados níveis de exatidão e precisão. Assim, são propostos dois modelos, um utilizando o método dos mínimos quadrados e a matriz de rotação, e o segundo utilizando um Filtro de Kalman Estendido para estimar o quaternião de rotação. As duas técnicas demonstraram bons resultados, permitindo a determinação dos ângulos de atitude com precisões inferiores a 1°, em cenários susceptíveis à presença de multi-percurso.

Todos os resultados apresentados foram obtidos com recurso a dados reais.

Palavras-chave: ambiguidade de fase inteira, Ambiguity Filter, determinação de atitude, duplas diferenças, GPS, método LAMBDA.

ABSTRACT

The use of multiple Global Positioning System (GPS) receivers allows the determination of relative position, that is, the baseline vector between a reference antenna and the remaining ones. To achieve high levels of accuracy and precision it is mandatory the use of the carrier-phase measurements. However, these measurements are biased by an unknown integer ambiguity. The integer ambiguity determination problem is usually addressed in a context of dual-frequency L1/L2 receivers. Due to the high cost of these receivers, strong motivations exist to explore techniques with cheaper single-frequency L1 receivers. In order to correctly solve the integer ambiguity problem with L1 GPS receivers, this thesis proposes the use of the LAMBDA method and the Ambiguity Filter, allowing the determination of the baseline vector with millimeter level precision. Improvements proposed within the Ambiguity Filter showed an increased confidence in the determination of the correct integer ambiguity, and hence the baseline vector, and the adaptation to the dynamic variation of the satellites' constellation, without the loss of the baseline solution with millimeter precision.

By combining multiple baselines, with known lengths, obtained by four L1 GPS receivers, placed in known positions, it is possible to determine a rigid body's attitude angles with high accuracy and precision levels. Thus, two attitude determination techniques are presented, one using a Least Squares estimation algorithm and the rotation matrix, and the second one using the rotation quaternion that is determined resorting to an Extended Kalman Filter. Both techniques showed good results allowing the determination of the attitude angles with precisions smaller than 1° , in scenarios affected by multipath.

All the presented results were obtained with real data.

Keywords: Ambiguity Filter, attitude determination, double differences, GPS, integer ambiguity, LAMBDA method.

ACRONYMS

ECEF	Earth-Centered Earth-Fixed
EKF	Extended Kalman Filter
ENU	East North Up
GNSS	Global Navigation Satellite Systems
GPS	Global Positioning System
INS	Inertial Navigation Systems
KF	Kalman Filter
LoS	Line of Sight
LS	Least Squares
NED	North East Down
RTK	Real Time Kinematics
SBAS	Satellite-Based Augmentation System
TD	Triple Difference
UERE	User Equivalent Range Error
WLS	Weighted Least Squares

SYMBOLS

$\nabla\Delta$	Double Difference
Δ	Single Difference
θ	Pitch Angle
μ	Mean
σ	Standard Deviation
ψ	Heading Angle
ϕ	Roll Angle

INDEX

AGRADECIMENTOS	ii
RESUMO	iii
ABSTRACT	iv
ACRONYMS	v
SYMBOLS	v
LIST OF FIGURES	viii
LIST OF TABLES	xi
1 INTRODUCTION	1
1.1 Motivation	1
1.2 State of the Art	1
1.3 Objectives and Structure	3
2 BASIC CONCEPTS	5
2.1 Introduction	5
2.2 Global Positioning System: Fundamentals and Operation	5
2.3 Measurement Errors	7
2.3.1 Satellite Clock Error	7
2.3.2 Ephemeris Error	7
2.3.3 Relativistic Effects	7
2.3.4 Ionospheric Effects	8
2.3.5 Tropospheric Delay	8
2.3.6 Receiver Noise	8
2.3.7 Multipath	9
2.3.8 Pseudorange Error Budget	9
2.4 Single Point Positioning	9
2.5 Coordinate Systems and Euler Angles	10
2.6 Accuracy and Precision	12
3 BASELINE DETERMINATION AND INTEGER AMBIGUITY RESOLUTION	13
3.1 Introduction	13
3.2 System Definition	13
3.2.1 Observables	13
3.2.2 Observation Model	15
3.2.3 Observables Covariance	17
3.3 Integer Ambiguity Resolution	18
3.3.1 Float Solution	19
3.3.2 Code Smoothing	19
3.3.3 LAMBDA Method	22
3.3.4 Ambiguity Filter	23
3.3.5 Constellation Changes: Recovery Techniques	25
4 ATTITUDE DETERMINATION	31
4.1 Introduction	31

4.2	Attitude Determination Using a Rotation Matrix	31
4.3	Quaternion-Based Extended Kalman Filter for Attitude Determination.....	33
4.3.1	Quaternion and Euler Angles.....	33
4.3.2	Extended Kalman Filter	34
4.3.3	Reachability and Observability.....	37
5	SOLUTION IMPLEMENTATION	41
5.1	Introduction.....	41
5.2	GPS Receivers and Antennas	41
5.2.1	Magellan AC12 GPS Receivers.....	41
5.2.2	U-Blox 6 GPS Receivers.....	42
5.2.3	Antennas	42
5.3	Algorithm Overview	43
5.4	Trials Description	45
5.4.1	Static Trials.....	45
5.4.2	Dynamic Trial.....	47
6	RESULTS	49
6.1	Introduction.....	49
6.2	Static Trials Results	49
6.2.1	Single Baseline Results	49
6.2.2	Multiple Baselines Results.....	55
6.3	Dynamic Trial Results	66
7	CONCLUSIONS	73
	REFERENCES	75

LIST OF FIGURES

Figure 1.1 – Illustration of the baselines’ definition.....	1
Figure 2.1 – Trilateration’s principle [18]	10
Figure 2.2 – Body fixed frame (xyz).....	10
Figure 2.3 – ECEF frame and ENU frame, [24].....	11
Figure 2.4 – Euler angles: a) Body fixed frame rotation about the East axis (pitch angle); b) Body fixed frame rotation about the North axis (roll angle); c) Body fixed frame rotation about the Down axis (heading angle) ..	12
Figure 2.5 – Illustration of both accuracy and precision concepts	12
Figure 3.1 – Comparison between the triple differences of both carrier phase and code double differences.....	15
Figure 3.2 – Zoom of the carrier-phase triple differences	15
Figure 3.3 – GPS interferometer for one satellite [1]	16
Figure 3.4 – Illustration of the KF loop	20
Figure 3.5 – Carrier phase double differences evolution with a cycle slip, in static environment.....	26
Figure 3.6 – Carrier phase triple difference evolution with a cycle slip, in static environment	27
Figure 3.7 – Carrier phase double differences evolution without cycle slips, in static environment.....	27
Figure 3.8 – Carrier phase triple differences evolution without cycle slips, in static environment	28
Figure 3.9 – Histogram of triple differences without cycle slips, in static environment.....	28
Figure 5.1 – a) AC12 sensor evaluation and development kit; b) AC12 OEM board [36]	41
Figure 5.2 – U-Blox 6 GPS receiver [37]	42
Figure 5.3 – Novatel model 531 GPS antenna with Chocke Ring Model A032 [38].....	42
Figure 5.4 – NAIS magnetic antenna [36]	43
Figure 5.5 – Flowchart of the developed algorithm.....	44
Figure 5.6 – Top view of the antennas’ position, for the single baseline static trial (Google Earth, [40])	46
Figure 5.7 – GPS receivers’ disposition and baseline vectors.....	46
Figure 5.8 – Top view of the platform’s orientation for the multiple baselines static trial (Google Earth, [40])..	47
Figure 5.9 – Top view of the platform’s path and orientation, for initial and final position, for the dynamic trial (Google Earth, [40])	48
Figure 6.1 – Baseline length evolution, using the Ambiguity Filter’s metrics 1 and 2 to solve the integer ambiguity problem for the single baseline static trial.....	50
Figure 6.2 – Baseline ENU coordinates evolution, using the Ambiguity Filter metrics 1 and 2 to solve the integer ambiguity problem for the single baseline static trial.....	50
Figure 6.3 – Zoom of the baseline ENU coordinates evolution, using the metric 2 of the Ambiguity Filter to solve the integer ambiguity problem for the single baseline static trial.....	51
Figure 6.4 – Number of satellites visible during the data acquisition in the single baseline static trial	51
Figure 6.5 – Baseline length evolution using different techniques to solve the integer ambiguity problem	52
Figure 6.6 – Baseline ENU coordinates evolution using different techniques to solve the integer ambiguity problem	53

Figure 6.7 – Heading angle evolution using different techniques to solve the integer ambiguity problem.....	54
Figure 6.8 – Pitch angle evolution using different techniques to solve the integer ambiguity problem.....	54
Figure 6.9 – Zoom of the heading and pitch angles, using the solution from the Ambiguity Filter	55
Figure 6.10 – Baseline ENU coordinates evolution, between the GPS receivers 1 and 2, with the Ambiguity Filter solution using metrics 1 and 2.....	56
Figure 6.11 – Baseline ENU coordinates evolution, between the GPS receivers 1 and 3, with the Ambiguity Filter solution using metrics 1 and 2.....	56
Figure 6.12 – Baseline ENU coordinates evolution, between the GPS receivers 1 and 4, with the Ambiguity Filter solution using metrics 1 and 2.....	57
Figure 6.13 – Zoom of the baseline ENU coordinates evolution, between the GPS receivers 1 and 2, with the Ambiguity Filter solution using metrics 2	58
Figure 6.14 – Zoom of the baseline ENU coordinates evolution, between the GPS receivers 1 and 3, with the Ambiguity Filter solution using metrics 2	58
Figure 6.15 – Zoom of the baseline ENU coordinates evolution, between the GPS receivers 1 and 4, with the Ambiguity Filter solution using metrics 2	59
Figure 6.16 – Number of visible satellites for the three baseline vectors	59
Figure 6.17 – Baseline ENU coordinates evolution, between the GPS receivers 1 and 2, using different techniques to solve the integer ambiguity problem	60
Figure 6.18 – Baseline ENU coordinates evolution, between the GPS receivers 1 and 3, using different techniques to solve the integer ambiguity problem	61
Figure 6.19 – Baseline ENU coordinates evolution, between the GPS receivers 1 and 4, using different techniques to solve the integer ambiguity problem	61
Figure 6.20 – Comparison between the attitude angles obtained with the rotation matrix technique and with the quaternion based EKF	63
Figure 6.21 – Zoom of the comparison between the attitude angles obtained with the rotation matrix technique and with the quaternion based EKF	63
Figure 6.22 – Angular velocities estimated with the quaternion base EKF during the static trial	64
Figure 6.23 – Innovation process between the measured baseline 1-2 and the one obtained with the estimated quaternion	65
Figure 6.24 – Innovation process between the measured baseline 1-3 and the one obtained with the estimated quaternion	65
Figure 6.25 – Innovation process between the measured baseline 1-4 and the one obtained with the estimated quaternion	66
Figure 6.26 – Comparison between the attitude angles obtained with the rotation matrix technique and with the quaternion based EKF, for the dynamic trial.....	67
Figure 6.27 – Zoom of pitch and roll angles obtained with the rotation matrix technique and with the quaternion based EKF, for the dynamic trial	67
Figure 6.28 – Up coordinate evolution of the three baselines after stabilization.....	68

Figure 6.29 – Zoom of heading and roll angles, during a positive rotation about the x axis (positive roll angle), obtained with the rotation matrix technique and with the quaternion based EKF, for the dynamic trial..... 68

Figure 6.30 – Evolution of the angular velocities estimated by the EKF during the dynamic trial 69

Figure 6.31 – Evolution of the innovation process between the measured baseline1-2 and the one obtained by the estimated quaternion, during the dynamic trial..... 70

Figure 6.32 – Evolution of the innovation process between the measured baseline1-3 and the one obtained by the estimated quaternion, during the dynamic trial..... 70

Figure 6.33 – Evolution of the innovation process between the measured baseline1-4 and the one obtained by the estimated quaternion, during the dynamic trial..... 71

LIST OF TABLES

Table 2.1 – Pseudorange typical error budget, [1].....	9
Table 6.1 – Performance of the baseline length using different techniques to solve the integer ambiguity problem	52
Table 6.2 – Performance of the baseline ENU coordinates in the single baseline static trial using different techniques to solve the integer ambiguity problem	53
Table 6.3 – Heading and pitch angles’ performance using different techniques to solve the integer ambiguity problem	55
Table 6.4 – Performance of the baseline ENU coordinates in the multiple baseline static trial using different techniques to solve the integer ambiguity problem	62
Table 6.5 – Performance of the attitude angles estimation, using the rotation matrix technique and the quaternion based EKF.....	64
Table 6.6 – Performance of the innovation process for each baseline, during the static trial	66
Table 6.7 – Performance of the innovation process for each baseline, during the dynamic trial.....	71

1 INTRODUCTION

1.1 Motivation

The Global Positioning System (GPS) is a powerful navigation tool that falls within the Global Navigation Satellite System (GNSS). The GPS may be used in numerous applications, such as the single point positioning (i.e. the position determination of a single GPS receiver). The GPS also allows high accuracy and precision in the determination of the vector between different antennas, which is called the baseline vector, [1], as illustrated in Figure 1.1.

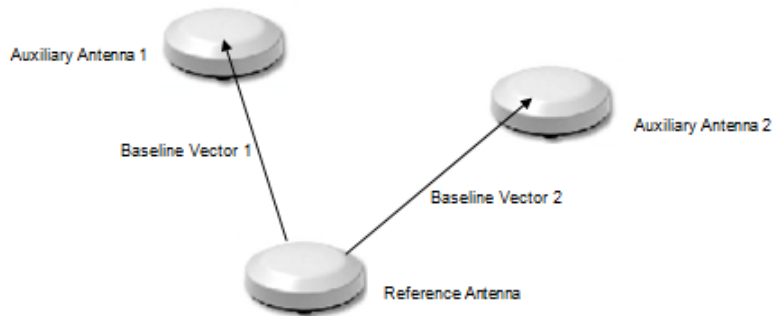


Figure 1.1 – Illustration of the baselines' definition

By placing multiple GPS antennas (at least three) along a vehicle or a rigid body in known positions and combining the corresponding baselines, it is possible to fully estimate the vehicles' orientation angles in space, known as the attitude angles or the Euler angles (i.e. heading, pitch and roll angles), with high accuracy and precision levels. The attitude determination is an important issue for the navigation and control of vehicles and rigid bodies.

1.2 State of the Art

In the recent decades, following the path started by the USA with the GPS, completely operational since 1995, a great effort has been employed by numerous governmental authorities, like Russia, the European Union, China, Japan and India, which have embraced their own GNSS programs. The Russian GLONASS, with 24 operational satellites since 2011, aims a worldwide coverage. The European Galileo positioning system is intended for a worldwide coverage, like the GPS and the GLONASS, and is projected to be fully operational on 2019 and to have a constellation with 30 satellites. The first Galileo's satellite was launched in 2011, [2]. The Chinese BeiDou (Compass) and the Indian IRNSS are regional GNSS systems that are being developed. In the future, the integration between different GNSS systems could be a powerful tool in different precise positioning techniques, from the stand-alone user to differential scenarios (i.e. with multiple GNSS antennas).

State of the art GPS receivers are able to tracking and read the GPS signals, which are provided by the GPS satellites' constellation. The GPS signals are transmitted at a carrier frequency L1 or at a carrier frequency L2. Some GPS receivers are capable of tracking both carrier frequencies and are called dual-frequency L1/L2 receivers, [1], [3]. Despite the higher precision levels that may be achieved by tracking the carrier signal with frequency L2, these receivers have higher costs than the single-frequency L1 devices. Resorting to Real Time Kinematic (RTK) techniques, [3], it is possible to estimate the baseline vector by using the carrier cycles information provided by the GPS receiver – carrier-phase measurements. However, this information is biased by an unknown integer number of cycles, which is called the integer ambiguity, [1], [3].

In order to determine the unknown integer ambiguity, and hence determine the baseline vector, many techniques have been developed. Accordingly to [4], the more common techniques are: the Least-Squares Ambiguity Search Technique (LSAST); the Fast Ambiguity Resolution Approach (FARA); the modified Cholesky decomposition method; the Least-Squares AMBIGUITY Decorrelation Adjustment (LAMBDA); the null space method; the Fast Ambiguity Search Filter (FASF); and the Optimal Method for Estimating GPS Ambiguities (OMEGA). From all the existing search techniques in the ambiguity domain, the LAMBDA method proposed in [5], is considered the most efficient one, accordingly to [6] and [4]. Recently, constrained versions of the LAMBDA method (C-LAMBDA), that take into account the baseline length have been proposed, [7], leading to faster and better solutions for the integer ambiguity, and hence to the baseline vector between two GPS antennas. The constraint imposed by the baseline length is also used in the Ambiguity Filter, which selects the best solution provided by the standard LAMBDA method, as described in [8], [9], [10] and [11] .

For attitude determination Inertial Navigation Systems (INS) may be used, combined or not with different sensors, such as vision sensors and range finders, [12], [13], [14]. Regarding the GPS based attitude determination, different types of techniques have been proposed through time. There are solutions using the INS/GPS coupling with a single-antenna configuration, like [15], where the position and velocity broadcasted by the GPS receiver is coupled with the measurements of acceleration and angular velocity from an accelerometer and a gyroscope. Other solutions use the coupling INS/GPS but with a multiple-antenna configuration, [16], where the baseline vector between GPS antennas is obtained, neglecting the determination of the integer ambiguity, and coupled with the measurements given by a gyroscope and an accelerometer. Finally, some solutions make use of multiple GPS receivers without the aid of INS sensors, as described in [17], where the technique proposed makes use of a constrained version of the LAMBDA method for the integer ambiguity resolution, and hence determine the Euler angles.

The work developed in this thesis falls within the attitude determination techniques using multiple single-frequency L1 GPS receivers, without INS sensors' aiding, using the LAMBDA method and the Ambiguity Filter for the integer ambiguity determination.

1.3 Objectives and Structure

The main objective of this thesis is the implementation of a tool, in MatLab environment, that is capable of determining the attitude of a vehicle by combining multiple single frequency L1 GPS receivers. This is done following the research line that led to the development of the Ambiguity Filter for the correct determination of the integer ambiguity, [8]. With that in mind, this thesis follows a structure that allows the understanding of fundamental concepts and implementation of important tools aiming the final goal of a GPS based attitude determination algorithm.

The Chapter 2 is the starting point of the developed work, where the basic principles underlying this thesis are presented, from the fundamentals of GPS operation to the concepts behind the attitude angles (i.e. the Euler angles).

In Chapter 3 the developed systems, using RTK techniques are presented, along with different types of solutions for the integer ambiguity resolution. New additions and improvements in the implementation of the Ambiguity Filter are proposed for the correct determination of the integer ambiguity.

In Chapter 4 the two proposed techniques regarding the attitude determination, using the baselines' solutions as observations, are presented in detail.

More practical issues in the implementation of the proposed algorithms are presented in Chapter5, with focus on the used GPS receivers and the description of the executed trials. This chapter also includes a general characterization of the implemented tool.

In Chapter 6 the practical results are presented and discussed. The main focus of this chapter is the performance evaluation of the Ambiguity Filter, regarding the improvements made in the algorithm, the comparison between different techniques that allows the integer ambiguity determination and the performance analyzes of the used techniques for attitude determination. The presented test results were obtained resorting to real data acquisition and respective post-processing, for static and dynamic environments.

Finally, the results depicted in Chapter 6 are used as support for the conclusions presented in Chapter 7. Along with the conclusions of this thesis, topics for future work regarding the improvement to the used techniques and possible applications are proposed.

After the conclusions, are presented the references that were used as support for the developed work.

2 BASIC CONCEPTS

2.1 Introduction

In this chapter the reader is presented with the basic concepts regarding GPS based attitude determination. It introduces fundamental topics that are essential for a better understanding of this thesis' work. With that in mind, the fundamentals of GPS technology are briefly presented, from the operational basis to its measurements and characteristics. Finally, the definition of the Euler angles is presented, along with the characterization of the coordinate systems used during this work.

2.2 Global Positioning System: Fundamentals and Operation

The GPS operation is well documented in a great number of bibliographies related to Geodesy and Navigation Systems, such as [1], [3] and [18]. It provides raw code and carrier-phase measurements, which may be used for single point positioning and precise point positioning algorithms. The system is constituted by three segments: space segment, control segment, and user segment.

The space segment comprises the constellation of satellites in orbit that transmits the ranging signals and the constellation ephemerides to the passive user receiver. The constellation ephemerides consist in a series of parameters that describe the orbital movement of the respective satellite and are used to compute the satellite position. Presently, there are 31 healthy satellites in operation, [19], flying in medium Earth orbits at an altitude approximately 20,200 Km, in six different orbital planes with a nominal inclination of 55°, relative to the equator, [1], [3].

The control segment is responsible for tracking the GPS satellites, monitoring their status, and sending commands (to keep them in the ideal orbital position) and data (such as clock, ephemeris and almanac updates) to each satellite. For this, the control segment comprises a master control station located in the United States territory, responsible for uploading navigation messages to update each satellite parameters, and monitoring the system integrity, sixteen monitoring stations around the world responsible for tracking the satellites and sending status reports to the master control station.

The user segment comprises the hardware devices, portable or fixed, that are able to processing the signals transmitted by GPS satellites, which are called GPS receivers, in the L-band, that comprises frequencies between 1 GHz and 2 GHz.

The GPS carrier signals are centered in two frequencies: L1 ($f_{L1} = 1575.42 \text{ MHz}$), intended for civil and military use; and L2 ($f_{L2} = 1227.60 \text{ MHz}$), planned for military use and with better accuracy when compared with L1. However, due to the GPS modernization program, new civil signals, such as the L2C, the L5 and the L1C, are being developed, accordingly with [20]. Each signal is constituted by three components: the carrier, the ranging code, and the navigation data, [3]. The carrier is the

sinusoidal signal with frequency L1 or L2. The ranging code is a set of binary PRN codes, where PRN stands for pseudo-random noise, which allows accurate range measurements and the transmission of multiple signals in the same carrier having different spreading sequences (code division multiple access – CDMA). The C/A code (standing for course/acquisition code) and P(Y) code (standing for precise and encrypted code) are transmitted in L1 frequency, while only P(Y) code is transmitted in L2 frequency. Each C/A code is a unique sequence of 1023 *chips*, with a chipping rate of 1.023 *Mchips/s* and a chipping width of 300 *m*. The P code is a unique sequence of approximately 10^{14} *chips*, with a chipping rate of 10.23 *Mchips/s* and a chipping width of 30 *m*. With a smaller wavelength, represented by the chipping width, the P code allow a higher accuracy than the C/A code, [3]. Finally, the navigation data is a binary message containing the satellite information, such as the ephemeris, status and clock correction, essential information to compute each satellite's position.

After the characterization of the GPS operational system, a briefly description of the concepts behind the code and carrier-phase measurements is presented

Code measurements (or pseudoranges) are obtained measuring the time of arrival (TOA) of the GPS signals, that is, the time that required for the signal to travel from the satellite to the receiver. That is, the TOA is defined as the difference between the signal reception time, T_R , as determined by the receiver clock, and the transmission time at the satellite, T_T , which is generated by the receiver's code loops based on replicas of the code transmitted by the satellite. After the estimation of the satellites' transmission time, it is possible to compute the respective pseudorange between the satellite and the receiver, knowing that GPS signals travel at the speed of light, c (where $c \approx 3 \times 10^8$ *m/s*), given by,

$$PR = c(T_R - T_T) \quad (2.1)$$

Note that these two time measurements are in different timescales, which are asynchronous.

The carrier phase measurement is the accumulated phase variation from an initial phase offset, and it is measured in cycles (i.e. modulo 2π), that is, for an error-free model at a generic instant t the carrier phase measurement is given by

$$\phi(t) = \phi(t_0) + \int_{t_0}^t f(s) ds, \quad (2.2)$$

where $f(s)$ is the time-varying frequency and $\phi(t_0)$ is the initial phase that contains an unknown number of cycles, which are referred to as the integer ambiguity. It is obtained resorting to a phase lock loop that monitors the phase changes from the initial phase difference measurement. The carrier phase measurement has a centimeter level precision, better than the code measurement that has a meter level precision.

As aforementioned, this work focuses on techniques using L1 single-frequency GPS receivers. Thus from this point, all GPS related topics are discussed regarding single-frequency L1 GPS receivers.

2.3 Measurement Errors

In order to solve the attitude determination problem with high levels of precision, precise positioning techniques regarding the GPS measurements may be used. The knowledge of the main disturbances that affect those measurements is mandatory.

2.3.1 Satellite Clock Error

The GPS time estimated by the satellite is obtained with atomic clocks, which are stable and highly accurate. However, atomic clocks drift over time leading to errors in the measured TOA of the transmitted signal. A drift of 1 ms in the satellite clock leads to an error of 300 km in the code measurement, [1]. The satellite clock drift may be corrected resorting to a second-order polynomial. The Control Segment is responsible for the determination and transmission, in the navigation message, of the correction polynomial parameters for the satellite clock drift.

2.3.2 Ephemeris Error

The ephemerides of each satellite are generated by the Control Segment, and transmitted in the navigation message, using a curve-fit, which leads to residual errors in the satellites positioning. These error in the satellites position could be translated in code errors on the order of 0.8 m (1σ), [1]. To minimize the effect of errors in the ephemerides' parameters, the Control Segment updates the contents of the navigation message at two-hour intervals.

2.3.3 Relativistic Effects

There are several errors in the GPS measurements associated to the satellite's orbit and to the Earth's rotation. The first effect is based on Einstein's general and special theories of relativity. Since the two clocks are at different gravitational potentials and moving at different velocities, both clocks will have different rates. To correct this effect, accordingly to [1], before launch the satellite clock frequency is set to $10.22999999543\text{ MHz}$, so that the frequency observed at sea level is 10.23 MHz .

The second effect arises from the fact that the satellite's orbit is not circular, having a small eccentricity. This leads to different velocities and gravitational potentials along the satellite's trajectory, which is translated in differential velocity of the satellite clock through time. This effect is corrected by a parameter that is in the navigation message, along with the ephemerides.

The Earth's rotation during the GPS signal transmission, from the satellite to the receiver, leads to errors in the computation of the satellites' position at the user level, since the observed signal does not match the actual positions but the positions at the time of transmission. This effect is known as the Sagnac effect and it is corrected in the positioning iterative process, until the correct satellite positions at the time of transmission are obtained.

2.3.4 Ionospheric Effects

The ionosphere is a layer of the atmosphere, approximately between heights 70 Km and 1,000 Km, composed by ions and free electrons originated by sun's ultraviolet rays. Since it is a dispersive medium affects the electromagnetic waves' propagation by delaying the group velocity and advancing the signal's carrier-phase. That is, the ionospheric error in code measurements is symmetric to the ionospheric error present in carrier-phase measurements.

The values of the ionospheric delay are function of the satellite's elevation angle, since for small elevation angles (less than 10°) the electromagnetic waves path inside the ionosphere is bigger than the path for high elevation angles. An average value, for all elevation angles, for the ionospheric delay is approximately 7 m (1σ), [1].

For single-frequency GPS receivers, the ionospheric delay correction is obtained resorting to the Klobuchar model, as characterized in [21], by using the Klobuchar coefficients that are included in the navigation message.

2.3.5 Tropospheric Delay

The troposphere is the first layer of the atmosphere and is not a dispersive medium for the GPS signals. However, due to the refraction phenomenon both phase and group velocities are equally delayed. Thus, the delay imposed by the troposphere, supported by the Snell's law [22], is function of the refractive index, which depends on the conditions of the medium (such as temperature, pressure and humidity), and function of the signal's angle of refraction, which is equal to the satellite's elevation angle. The troposphere is composed of dry gases and water vapor, and hence the troposphere delay comprises both dry and wet components. This delay is typically translated in an error of 0.2 m (1σ) in code measurements, [1]. This delay is corrected using mapping functions relating the local meteorological parameters and the satellite's elevation angle. One example of such technique is the Hopfield model, described in [1], [3] and [23].

2.3.6 Receiver Noise

The measurements are affected by noise present in the signal acquisition process, induced by the thermal noise caused by the used hardware and by the interference between the GPS signals and other signals in the same band. Typically, the values of the error in the code measurements are on the order of the decimeter (1σ) and in the carrier phase measurements on the order of the millimeter (1σ), [1].

2.3.7 Multipath

In real environments multiple versions of the same signal reach the GPS receiver. Besides the direct signal (i.e. the one received from the line-of-sight path), reflected versions (on natural or man-made surfaces) of the same signal reach the antenna, versions that have longer paths than the direct one and smaller amplitudes, which introduces errors in both code and carrier phase measurements. This phenomenon is highly related with the scenario surrounding the receiving device. Urban scenarios are rich in multipath sources, since there are multiple surfaces that allow the reflection of the GPS signal before reaching the antenna. Also the satellites' elevation angle may influence the multipath error, since signals transmitted by satellites with smaller elevation angles are more likely to be reflected. The multipath effect can be reduced by applying specific techniques in the antenna design and in the signal processing of the GPS signal, as described in [3].

2.3.8 Pseudorange Error Budget

After the description of each error source, it is possible to determine the User Equivalent Range Error (UERE), which is a estimation of the pseudorange error and is given by the root-sum-squared between all error components. Thus, the 1σ typical value for each error source and the UERE are present in Table 2.1.

Table 2.1 – Pseudorange typical error budget, [1]

Error Source	1σ Error (m)
Satellite Clock	1.1
Ephemeris	0.8
Ionospheric Delay	7.0
Tropospheric Delay	0.2
Receiver Noise	0.1
Multipath	0.2
UERE	7.1

2.4 Single Point Positioning

Code measurements allow the determination of the receiver's position by using the trilateration's principle, which basic idea is illustrated in Figure 2.1. However, along with the three coordinates of the user position, it is also necessary to estimate the receiver clock offset, leading to a system where all unknowns are only determined with at least four code measurements, that is, four satellites.

Thus, a Weighted Least Squares (WLS) algorithm, using the code measurements, the satellites' positions and the geometric range, allows the estimation of the user position. Note that in order to improve the estimation's accuracy, the code measurements may be corrected using some of the techniques previously presented. The geometric range, ρ , between the satellite and the receiver is

given by

$$\rho = \sqrt{(x_{sat} - x_u)^2 + (y_{sat} - y_u)^2 + (z_{sat} - z_u)^2}, \quad (2.3)$$

where the terms x_{sat} , y_{sat} and z_{sat} represent the coordinates of the satellite position, and the terms x_u , y_u and z_u represent the coordinates of the user position. The coordinates of the satellite position are obtained by using the respective satellite's ephemeris for a specific time instant, taking into account the correction of the relativistic effect due to the Earth's rotation.

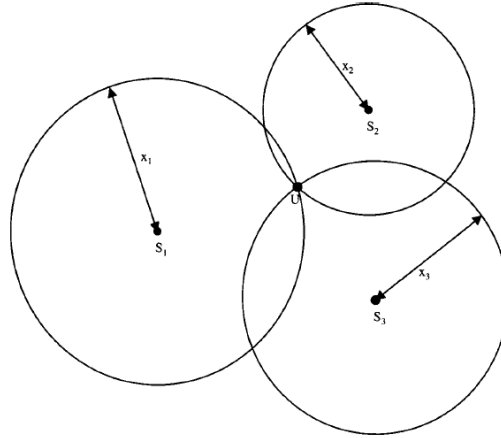


Figure 2.1 – Trilateration's principle [18]

The single point positioning is not the main focus of this thesis, but it is an essential step in the definition of the reference position to the local coordinate system, as presented in next section.

2.5 Coordinate Systems and Euler Angles

In attitude determination problems using multiple GPS receivers, the first step is to place the receivers in specific positions along the test platform, defined in the body fixed frame. In the body fixed frame, depicted in Figure 2.2, the $+x$ axis is pointing in the movement direction, the $+z$ axis is pointing down and the $+y$ axis is pointing in the right side of the platform, forming a right handed coordinate system. The term fixed frame entails that the reference frame follows the platform movement, in terms of translation and rotation. Thus, the positions of the receivers will be constant in the body fixed frame.

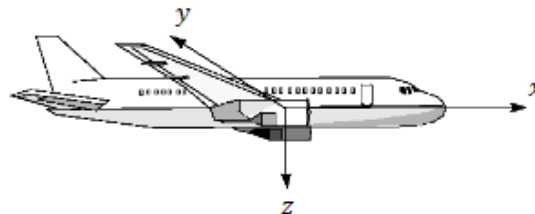


Figure 2.2 – Body fixed frame (xyz)

The attitude angles characterize the transformation of the receivers' positions in the body fixed frame to the reference space frame. In the previous chapter, the reference space frame used was the ENU (East-North-Up) coordinate system, which is represented in Figure 2.3 along with the ECEF (Earth-Centered Earth-Fixed) coordinate system. In the ECEF system the $+x$ axis is pointing in the direction of the null longitude (0°) position, the $+y$ axis is pointing in the direction of the longitude $90^\circ E$ and the $+z$ axis is perpendicular to the equatorial plane, pointing in the direction of the North Pole. The ECEF coordinate system rotates with the Earth's motion and is used in the determination of the user position.

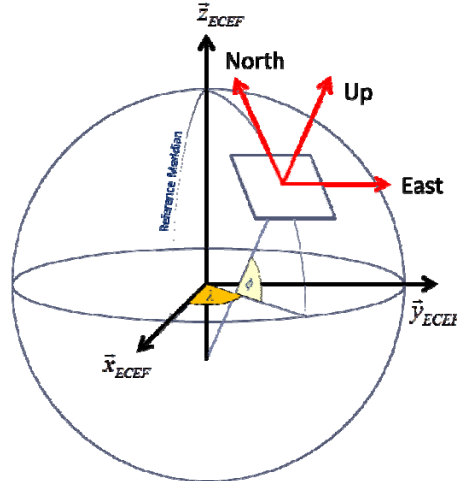


Figure 2.3 – ECEF frame and ENU frame, [24]

The ENU coordinate system is a local system and it is appropriate to describe the relative position between two stations. As the name states, the $+e$ axis is pointing in the East direction (i.e. along a fixed latitude line), the $+n$ axis is pointing in the North direction (i.e. along a fixed longitude line) and the $+u$ axis is pointing in the geodetic Up direction. However, in attitude determination problems the reference space frame used is the NED (North-East-Down) coordinate system. As it looks, it is an alternative form to compute the ENU coordinates. Thus, the transformation between the two coordinate systems is straightforward, that is

$$b_{NED} = \begin{bmatrix} 0 & 1 & 0 \\ 1 & 0 & 0 \\ 0 & 0 & -1 \end{bmatrix} b_{ENU}. \quad (2.4)$$

The attitude angles (or the Euler angles) relate the orientation of the body frame to the reference space frame. These two frames are related by the pitch, roll and heading angles, respectively, θ , ϕ and ψ . As depicted in Figure 2.4, the pitch angle relates the about the y axis, the roll angle relates the rotation about the x axis and the heading angle relates the rotation about the z axis.

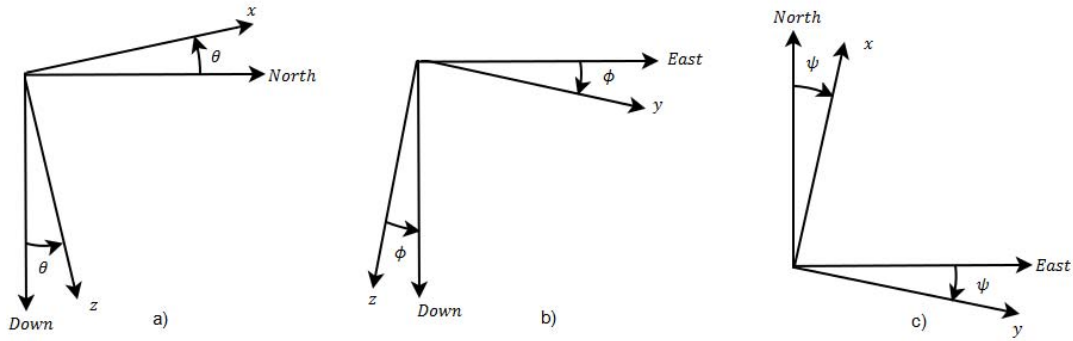


Figure 2.4 – Euler angles: a) Body fixed frame rotation about the East axis (pitch angle); b) Body fixed frame rotation about the North axis (roll angle); c) Body fixed frame rotation about the Down axis (heading angle).

2.6 Accuracy and Precision

Two important concepts when using estimation techniques for the determination of disturbed variables are the accuracy and precision concepts. A variable is accurately estimated if its value is equally distributed around the correct value. Contrarily, a variable is estimated with precision if its value has small oscillations over time, that is, if its value has a small standard deviation. These two concepts are illustrated in Figure 2.5.

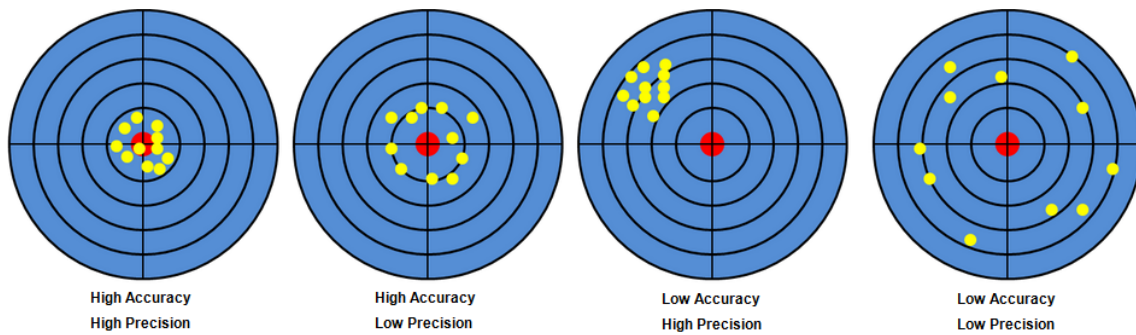


Figure 2.5 – Illustration of both accuracy and precision concepts

3 BASELINE DETERMINATION AND INTEGER AMBIGUITY RESOLUTION

3.1 Introduction

The determination of the baseline vector is done by using interferometric techniques. This technique consists on the differentiation of two receivers' measurements. Thus, in the GPS case the measurements at hand lead to both carrier phase and code (pseudoranges) double differences, which are used as observations in the developed system. However, to use carrier phase measurements the integer ambiguities must be determined. In this chapter the developed system and the techniques used for the baseline determination are presented.

3.2 System Definition

3.2.1 Observables

Generation of both carrier-phase and code double differences is essential for the determination of the baseline vector between two GPS antennas. The double differences allow the cancellation of the receiver and satellite clock biases and great part of ionospheric propagation delay. Considering that the distance between both antennas is small, when compared with the receiver-satellite distance, one may assume that the elevation angle is the same for both receivers. Hence, the tropospheric propagation delay will largely cancel as well.

The carrier phase measured, in meters, for satellite p and receiver k has the form

$$\phi_k^p = \rho_k^p + \lambda N_k^p + c(t_p + t_k + T_k^p - I_k^p) + \epsilon_k^p, \quad (3.1)$$

where,

- ρ_k^p is the geometric distance between the satellite and the receiver (in meters);
- λ is the carrier wavelength (in meters);
- N_k^p is the unknown integer ambiguity (in cycles);
- c is the speed of light in vacuum (meters per second);
- t_p and t_k are the satellite and the receiver clock offset (in seconds), respectively;
- T_k^p and I_k^p are the tropospheric and ionospheric delay (in seconds), respectively;
- ϵ_k^p is unmodeled noise due to different factors (hardware, multipath).

The carrier phase integer ambiguity, N_k^p , is kept constant within the receiver as long as the satellite is continuously tracked.

Adding another receiver measurement (let the new receiver be m) and assuming that both phase measurements Φ_k^p and Φ_m^p correspond to the same instant, it is possible to generate a single difference by subtracting both measurements. That is, the single difference for phase measurements ($\Delta\Phi_{km}^p$) would have the form

$$\Delta\Phi_{km}^p = \Phi_k^p - \Phi_m^p = \Delta\rho_{km}^p + \lambda\Delta N_{km}^p + c\Delta t_{km} + \Delta\epsilon_{km}^p. \quad (3.2)$$

Equation (3.2) proves the cancellation of the satellite clock bias and the tropospheric and ionospheric delays, since they are common term between the two receivers. However, the receiver clock bias is not cancelled by operation (3.2). This can be done by double differencing.

Adding a new satellite (q) it is possible to generate a double difference. This is done by subtracting two single differences, the first one relative to receivers k , m and satellite p and the second one relative to the same set of receivers but for satellite q . That is,

$$\nabla\Delta\Phi_{km}^{pq} = \Delta\Phi_{km}^p - \Delta\Phi_{km}^q = \nabla\Delta\rho_{km}^{pq} + \lambda\nabla\Delta N_{km}^{pq} + \nabla\Delta\epsilon_{km}^{pq}. \quad (3.3)$$

As previously said, the formation of double differences the receiver clock bias now cancelled. In order to use the carrier phase double differences it is necessary the integer ambiguity determination.

The same process can be applied to code measurements that are defined as

$$PR_k^p = \rho_k^p + c(t_p + t_k + T_k^p + I_k^p) + \epsilon_k^p, \quad (3.4)$$

and the code double difference generation is straightforward, based on the process presented above. Thus, code double differences are given by

$$\nabla\Delta PR_{km}^{pq} = \nabla\Delta\rho_{km}^{pq} + \nabla\Delta\epsilon_{km}^{pq}. \quad (3.5)$$

Despite unambiguous, code double differences are noisier when compared with carrier phase double differences. Accordingly with [3] and [1], the standard deviation of the error in code double differences is meter level, while in the carrier phase double differences is centimeter level, as illustrated in Figure 3.1 where the triple differences, that consist in the differentiation through time and whose definition is presented in the following sections, are used for comparison the precision levels between carrier phase and code double differences. In Figure 3.2 is presented a zoom of the carrier-phase triple differences depicted in Figure 3.1. Thus, for a precise baseline determination, one must make use of carrier phase double differences and, consequently, calculate the integer ambiguities.

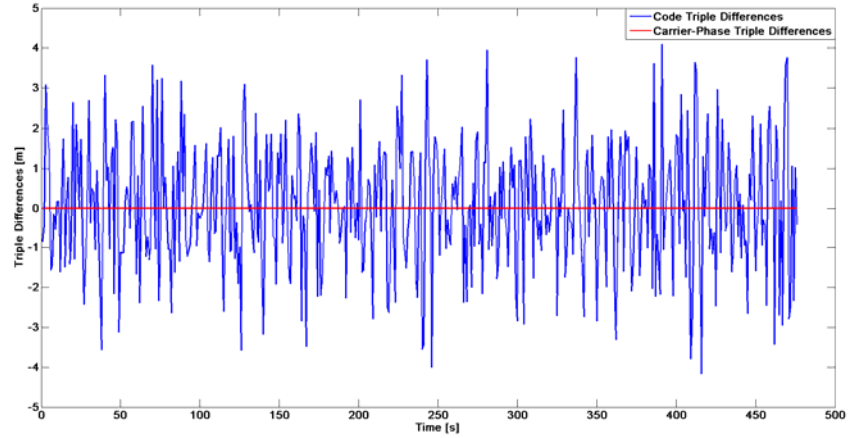


Figure 3.1 – Comparison between the triple differences of both carrier phase and code double differences

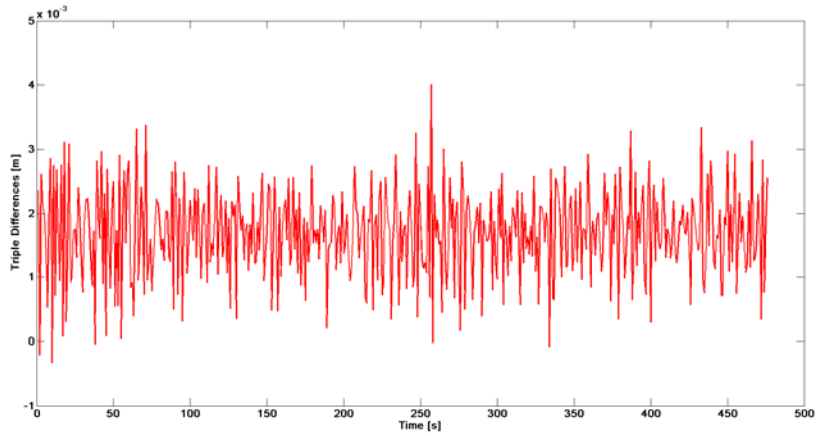


Figure 3.2 – Zoom of the carrier-phase triple differences

3.2.2 Observation Model

With the definition of the double differences at hand, the next step is the description of the relation between them and the baseline, which is the vector between a reference antenna and an auxiliary antenna, as aforementioned. The single differences can be calculated by the inner product between the baseline vector, b , and the Line of Sight (LoS), or direction cosine, unit vector to the used satellite, e . Recovering the situation with satellite p and receivers k and m

$$\Delta\rho_{km}^p = b \cdot e^p. \quad (3.6)$$

That is, the single difference corresponds to the projection of the baseline vector onto the LoS to the respective satellite, as depicted in Figure 3.3. It is assumed that the paths of propagation between the satellite and the two receivers are parallel, due to the distance between them (satellites are in orbit at a mean distance of 20,200 km [1], while the distance between antennas is meter level).

By differentiating equation (3.6) for satellites p and q , the double difference obtained would have the form

$$\nabla \Delta \rho_{km}^{pq} = b \cdot (e^p - e^q) = b \cdot e^{pq}. \quad (3.7)$$

The determination of the direction cosines e^p and e^q , which are assumed to be equal for both receivers due to the big difference between the baseline length and the satellite-receiver distance, is done by computing the user position and the respective satellite position.

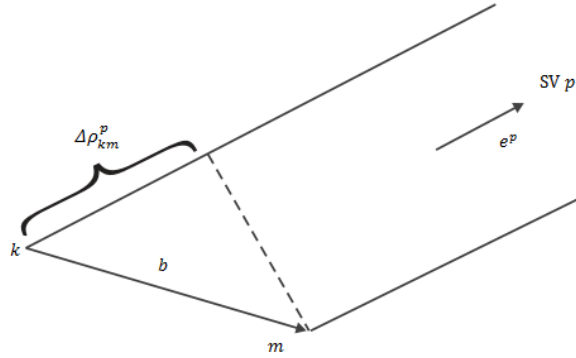


Figure 3.3 – GPS interferometer for one satellite [1]

Combining (3.3) and (3.5) with (3.7), and expanding to a case with n satellites, one would obtain the system

$$\begin{bmatrix} \nabla \Delta P_{km}^{12} \\ \nabla \Delta P_{km}^{13} \\ \vdots \\ \nabla \Delta P_{km}^{1n} \\ \nabla \Delta \Phi_{km}^{12} \\ \nabla \Delta \Phi_{km}^{13} \\ \vdots \\ \nabla \Delta \Phi_{km}^{1n} \end{bmatrix} = \begin{bmatrix} e_{km_x}^{12} & e_{km_y}^{12} & e_{km_z}^{12} \\ e_{km_x}^{13} & e_{km_y}^{13} & e_{km_z}^{13} \\ \vdots & \vdots & \vdots \\ e_{km_x}^{1n} & e_{km_y}^{1n} & e_{km_z}^{1n} \\ e_{km_x}^{12} & e_{km_y}^{12} & e_{km_z}^{12} \\ e_{km_x}^{13} & e_{km_y}^{13} & e_{km_z}^{13} \\ \vdots & \vdots & \vdots \\ e_{km_x}^{1n} & e_{km_y}^{1n} & e_{km_z}^{1n} \end{bmatrix} \begin{bmatrix} b_x \\ b_y \\ b_z \end{bmatrix} + \begin{bmatrix} 0 & 0 & \dots & 0 \\ 0 & 0 & \dots & 0 \\ \vdots & \vdots & \ddots & \vdots \\ 0 & 0 & \dots & 0 \\ \lambda & 0 & \dots & 0 \\ 0 & \lambda & \dots & 0 \\ \vdots & \vdots & \ddots & \vdots \\ -0 & 0 & 0 & \lambda \end{bmatrix} \begin{bmatrix} \nabla \Delta N_{km}^{12} \\ \nabla \Delta N_{km}^{13} \\ \vdots \\ \nabla \Delta N_{km}^{1n} \end{bmatrix} + \begin{bmatrix} \nabla \Delta \epsilon_{km}^{12} \\ \nabla \Delta \epsilon_{km}^{13} \\ \vdots \\ \nabla \Delta \epsilon_{km}^{1n} \\ \nabla \Delta \epsilon_{km}^{12} \\ \nabla \Delta \epsilon_{km}^{13} \\ \vdots \\ \nabla \Delta \epsilon_{km}^{1n} \end{bmatrix}. \quad (3.8)$$

Note that the superscript 1 present in all differential terms is relative to the reference satellite, which is the one with highest elevation. This definition of reference satellite is in order to maximize the constellation geometry and stability.

The system (3.8) can be reduced to the form

$$y_{2(n-1) \times 1} = B_{2(n-1) \times 3} b_{3 \times 1} + A_{2(n-1) \times (n-1)} a_{(n-1) \times 1} + e_{2(n-1) \times 1}, \quad (3.9)$$

in which the subscript in each matrix represents its dimension and,

- y is the measured double differences' vector;
- B is the system matrix for the baseline coordinates, containing the differenced direction cosines;
- b is the baseline coordinates' vector;
- A is the system matrix for the ambiguity set, containing the carrier wavelength;
- a is the aforementioned ambiguity set;
- e is the measurement noise vector.

Defining the augmented system matrix $H = [A \ B]$, with dimension $2(n-1) \times ((n-1) + 3)$, one would have an augmented state vector $x = [a^T \ b^T]^T$, with dimension $((n-1) + 3) \times 1$. Analyzing the augmented system is possible to conclude that there are enough equations to estimate all the states (i.e. baseline vector coordinates and the double differences integer ambiguities), if the full rank of the augmented system matrix H is equal to the number of states, that is, equal to $((n-1) + 3)$. This equality is only verified when the constellation has, at least, four satellites, that is for $n \geq 4$.

To use the system defined above, one must define the covariance matrix of the measurement error, e , which is the next step of this thesis.

3.2.3 Observables Covariance

Both carrier phase and code measurements' noise is assumed to be Gaussian distributed, with expected value zero and variance σ_ϕ^2 and σ_ρ^2 , respectively and assumed to be equal for all satellites. Considering that measurements from different satellites are independent, this entails that those measurements are uncorrelated. Hence, for a generic set of measurements, given by the column vector z and with the disturbance column vector ϵ , distributed like code and carrier phase (with expected value zero and variance σ_z^2), the respective covariance matrix is defined by,

$$cov(z) = E\{(\epsilon - E(\epsilon))(\epsilon - E(\epsilon))^T\} = E\{\epsilon\epsilon^T\} = \sigma_z^2 I_{n \times n}, \quad (3.10)$$

for a constellation with n satellites and where $I_{n \times n}$ represents the identity matrix.

By the definition of single difference, as shown in equation (3.2) for receivers k and m (which for each satellite leads to measurement error $\Delta\epsilon_{km} = \epsilon_k - \epsilon_m$), the derivation of the corresponding covariance matrix is straightforward

$$\begin{aligned} cov(\Delta z_{km}) &= E\{(\Delta\epsilon_{km} - E(\Delta\epsilon_{km}))(\Delta\epsilon_{km} - E(\Delta\epsilon_{km}))^T\} = E\{(\epsilon_k - \epsilon_m)(\epsilon_k - \epsilon_m)^T\} \\ &= E\{\epsilon_k\epsilon_k^T + \epsilon_m\epsilon_m^T\} = 2\sigma_z^2 I_{n \times n}. \end{aligned} \quad (3.11)$$

Equation (3.11) results in a diagonal matrix and this shows that the single differences are uncorrelated.

As showed in the two previous sections, double differences are formed by the difference between the single difference of the reference satellite and the single difference of the other satellites. Thus, the double differences' vector, for n satellites, is given by

$$\nabla\Delta z_{km} = M\Delta z_{km} \quad (3.12)$$

where $M_{(n-1)\times n} = \begin{bmatrix} 1 & -1 & 0 & \dots & 0 \\ 1 & 0 & -1 & \dots & 0 \\ \vdots & \vdots & \vdots & \ddots & \vdots \\ 1 & 0 & 0 & \dots & -1 \end{bmatrix}$. Finally, it is possible to determinate the double differences' covariance matrix

$$\begin{aligned} cov(\nabla\Delta z_{km}) &= E\{(\nabla\Delta\epsilon_{km} - E(\nabla\Delta\epsilon_{km}))(\nabla\Delta\epsilon_{km} - E(\nabla\Delta\epsilon_{km}))^T\} \\ &= E\{M\Delta\epsilon_{km}\Delta\epsilon_{km}^T M^T\} = 2\sigma_z^2 M M^T \\ &= 2\sigma_z^2 \begin{bmatrix} 2 & 1 & \dots & 1 \\ 1 & 2 & \dots & 1 \\ \vdots & \vdots & \ddots & \vdots \\ 1 & 1 & 1 & 2 \end{bmatrix}. \end{aligned} \quad (3.13)$$

Thus, one may conclude that the double differences are correlated, which is evident since all double differences are generated for the same reference satellite.

To conclude, both carrier phase and code double differences have the following covariance matrices, correspondingly,

$$cov(\nabla\Delta\Phi_{km}) = 2\sigma_\phi^2 M M^T, \quad (3.14)$$

$$cov(\nabla\Delta PR_{km}) = 2\sigma_{PR}^2 M M^T. \quad (3.15)$$

3.3 Integer Ambiguity Resolution

The system defined in (3.9) can be solved by a weighted least squares algorithm. From [6] it is known that the usual problem in WLS is to minimize the error norm of the type $\|u\|_W^2 = u^T W u$, that is

$$\min_{a,b} \|y - Aa - Bb\|_W^2, \quad (3.16)$$

where W is the weight matrix.

The minimization gives floating point solutions that are highly contaminated by code's noise and we know that the correct ambiguities are integers, which is called the fixed solution. Such estimates are called float solutions. This noisy solution can be improved by smoothing code double differences. The correct integer ambiguities can be determined by search techniques that make use of the float solution. All these tools will be better explained in next subsections.

3.3.1 Float Solution

As aforementioned, the system (3.9) can be solved by a weighted least squares estimator. For a generic system $Hx = b$, the estimator is given by, [6],

$$\hat{x} = (H^TWH)^{-1}H^TWb. \quad (3.17)$$

Remembering the notion of augmented system introduced before, where $H = [A \ B]$ and $x = [a^T \ b^T]^T$, the estimator (3.17) can be applied to the problem at hand. The weight matrix is given by the inverse of the measurements covariance matrices (3.14) and (3.15), that is

$$W = \begin{bmatrix} cov(\nabla\Delta PR_{km}) & 0 \\ 0 & cov(\nabla\Delta\Phi_{km}) \end{bmatrix}^{-1}. \quad (3.18)$$

Thus, our estimator should have the form

$$\begin{bmatrix} \hat{a} \\ \hat{b} \end{bmatrix} = ([A \ B]^TW[A \ B])^{-1}[A \ B]^TWy. \quad (3.19)$$

It is important to obtain the float solution estimation's covariance matrix, since it will have an important role on fixed solution determination. Defining the estimation error as $\tilde{x} = x - \hat{x}$ and using some mathematical manipulation, one should obtain

$$\tilde{x} = -([A \ B]^TW[A \ B])^{-1}[A \ B]^TWe, \quad (3.20)$$

where e represents the double differences' noise with covariance matrix W , as defined above. The covariance matrix for the estimation error can be calculated from (3.20) with the form

$$\begin{aligned} Q_{\tilde{x}} = Q_{\hat{x}} &= E\{(\tilde{x} - E(\tilde{x}))(\tilde{x} - E(\tilde{x}))^T\} = ([A \ B]^TW[A \ B])^{-1} \\ &= \begin{bmatrix} A^TWA & A^TWB \\ B^TWA & B^TWB \end{bmatrix}^{-1} = \begin{bmatrix} Q_{\hat{a}} & Q_{\hat{a}\hat{b}} \\ Q_{\hat{b}\hat{a}} & Q_{\hat{b}} \end{bmatrix}. \end{aligned} \quad (3.21)$$

3.3.2 Code Smoothing

In this section, a code smoothing technique to improve the accuracy of the float solution is presented. But for a better comprehension of this technique, the Kalman Filter will be briefly described.

Kalman Filter

The Kalman Filter (KF), introduced by [25], is a recursive mathematical model to estimate the state of a system minimizing the mean of the squared error. In a first step, the filter "predicts" the system's state in that instant, and then in a second step using a feedback control, based on the noisy measurements, the filter "updates" the system's state. Thus, two different steps constitute the KF: the prediction step, and the update step, as depicted in Figure 3.4.

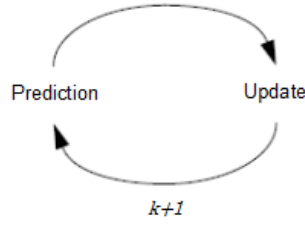


Figure 3.4 – Illustration of the KF loop

The model of a generic linear discrete system, at instant k , is represented by

$$x_k = Ax_{k-1} + Bu_{k-1} + w_{k-1}, \quad (3.22)$$

which has measurements in the form

$$z_k = Hx_k + v_k. \quad (3.23)$$

Both w and v are random variables, respectively the process and measurement noise, with zero mean normal probability distributions, that is

$$p(w) \sim N(0, Q), \quad (3.24)$$

$$p(v) \sim N(0, R), \quad (3.25)$$

where Q is the process noise covariance and R is the measurement noise covariance.

The equations of the prediction step are given by

$$\hat{x}_k^- = A\hat{x}_{k-1} + Bu_{k-1}, \quad (3.26)$$

$$P_k^- = AP_{k-1}A^T + Q. \quad (3.27)$$

In equation (3.26), the state at the previous instant, \hat{x}_{k-1} , is projected to the new instant, based on the system's dynamic. The same is done with the error covariance matrix, P_{k-1} , in equation (3.27). The state estimation and the error covariance matrix at this step, \hat{x}_k^- and P_k^- , are called the *a priori* estimate.

For the update step equations are defined as

$$K_k = P_k^- H^T (HP_k^- H^T + R)^{-1}, \quad (3.28)$$

$$\hat{x}_k = \hat{x}_k^- + K_k(z_k - H\hat{x}_k^-), \quad (3.29)$$

$$P_k = (I - K_k H)P_k^-, \quad (3.30)$$

where K_k is the Kalman gain and it is obtained using (3.28). The residual, or innovation process, which is calculated by the difference between the measurements and the *a priori* estimates, that is, $z_k - H\hat{x}_k^-$, is weighted by the Kalman gain and is used to correct the *a priori* estimate, as represented

in equation (3.29). In equation (3.30) the new error covariance matrix is obtained. Note that the term I is the identity matrix. After these two steps, the process is repeated for a new instant, $k + 1$, using the previous estimated state, \hat{x}_k , and the estimation covariance matrix, P_k , as inputs for the new prediction step.

For linear systems, the KF ensures stability, reachability and observability, and converges to the optimal solution, [26] and [27]. However, for non-linear systems the direct application of the algorithm presented above is not possible. The estimation for non-linear systems will be addressed during this thesis.

Complementary Kalman Filter

Based on the KF, described in the previous section, the reader is now presented with the technique used for code smoothing. This technique, used by [28], makes use of the combination between the noisy code double differences and the less noisy carrier phase double differences with a Complementary Kalman Filter. The technique uses the average of the noisier measurement to center the quieter one, limiting the size of the integer ambiguity. Thus, the filter's output, at instant, k , is a smoothed (less noisier) code double difference, $\nabla\Delta S$.

For that, the filter has the form

$$\nabla\Delta S_k^- = \nabla\Delta S_{k-1}^+ + (\nabla\Delta\phi_k - \nabla\Delta\phi_{k-1}), \quad (3.31)$$

$$P_k^- = P_{k-1}^+ + cov(\nabla\Delta\phi), \quad (3.32)$$

$$K_k = P_k^- (P_k^- + cov(\nabla\Delta PR))^{-1}, \quad (3.33)$$

$$\nabla\Delta S_k^+ = \nabla\Delta S_k^- + K_k (\nabla\Delta PR_k - \nabla\Delta S_k^-), \quad (3.34)$$

$$P_k^+ = (I - K_k)P_k^-. \quad (3.35)$$

The first two lines (equations (3.31) and (3.32)) compose the prediction step. In the first one, the smoothed code double differences are propagated from the previous instant with the change rate of the carrier phase double differences. By differencing two carrier phase double differences, the integer ambiguity is canceled, hence the propagated $\nabla\Delta S_k^-$ is unambiguous. In the second line, the error covariance matrix is obtained by adding the new covariance matrix of the carrier phase measurements to the previous error covariance.

For the update step, the Kalman gain is calculated as described in equation (3.33). In equation (3.34), the predicted smoothed code double differences are propagated with the weighted residual between the measured code double differences and the smoothed code double differences. Finally, in equation (3.35) the estimation error covariance is propagated to the new instant, maintaining the balance between the unambiguous but noisier code measurements and the ambiguous but smoother carrier phase measurements.

3.3.3 LAMBDA Method

As aforementioned, the LAMBDA method was chosen as the search technique to use in this thesis and it will be presented in detail. It has three steps: float solution, integer ambiguity estimation, and fixed solution, [29].

The float solution step consists in the initialization of the LAMBDA method. The inaccurate solution obtained by the weighted least squares estimator, \hat{a} in equation (3.19), is used in the search process as the central point. The error estimation covariance, $Q_{\hat{a}}$, defines the search space to finding the correct integer ambiguity vector, \check{a} , that minimizes the cost function,

$$\check{a} = \text{arg} \left(\min_{a \in \mathbb{Z}} \|\hat{a} - a\|_{Q_{\hat{a}}^{-1}}^2 \right), \quad (3.36)$$

that is the integer ambiguity estimation step.

Note that, the float solution obtained using the code smoothing technique, instead of the unsmoothed float solution, could be used as an input in the LAMBDA method. However, it was decided to use the unsmoothed float solution as an input rather than the smoothed float solution, which is only used as comparison in the results section

The correlated nature of double differences leads to a non diagonal covariance matrix, as depicted in the derivation of (3.13), which entails that the covariance matrix of the float solution is also not diagonal, leading to an elliptical search space. This means that the search space can be more elongated in one direction than in another, which results in integer ambiguity sets that have lower values of the cost function but appear much farther away than those which appear nearby but are outside of the search space. To fix this issue, the LAMBDA method uses a transformation matrix to decorrelate the error and, therefore, diagonalizing (as much as possible, where the non diagonal elements are close to zero) the covariance matrix of the float solution. This process will create a search space that is nearly spherical, leading to an easier and faster search process.

This diagonalization process is accomplished by a Z transformation defined as

$$Q_Z = Z^T Q_{\hat{a}} Z, \quad (3.37)$$

where both Z and Z^{-1} must have integer entries, so that the original and the transformed ambiguities remain integer.

Next, the covariance matrix of the float solution can be decomposed as

$$Q_{\hat{a}} = L^T D L, \quad (3.38)$$

where L is a lower matrix and D is a diagonal matrix. Assuming that Z is close to L^{-1} one must have

$$Q_z = \tilde{L}^T \tilde{D} \tilde{L}, \quad (3.39)$$

where the non diagonal elements of this new covariance matrix, represented by \tilde{L} , are close to zero, leading to a nearly diagonal covariance matrix.

After the Z transformation and the decorrelation process, the new cost function is defined as

$$\check{z} = \arg \left(\min_z \|\hat{z} - z\|_{Q_z^{-1}}^2 \right), \quad (3.40)$$

where $z = Z^T a$ and $\hat{z} = Z^T \hat{a}$.

The volume of the search space is controlled by the value χ^2 , that is constant during the search process and takes into account the new nearly diagonal covariance matrix and the number of candidates desired by the user. That is, the LAMBDA method outputs those ambiguities that verify the inequality

$$(\hat{z} - z)^T Q_z^{-1} (\hat{z} - z) \leq \chi^2. \quad (3.41)$$

The number of candidates selected by the user must consider the distance between the float solution and the true integer solution, and the computation time available. That is, a number of candidates too small could lead to a solution that do not include the true integer solution and a number of candidates too big won't permit the adaptation to real-time applications. A study on the influence of the number of candidates is presented in [8].

At the end of the LAMBDA method, the required number of candidates is transformed back to the initial form, resorting to

$$\check{\alpha} = Z^{-T} \check{z}, \quad (3.42)$$

where the solution remains integer, due to the aforementioned nature of Z and Z^{-1} . Note that the candidates outputted from the LAMBDA method are sorted in ascending order of the distance to the float solution.

3.3.4 Ambiguity Filter

Following the methodology developed in [8], the Ambiguity Filter developed in this thesis chooses the best integer ambiguity set from LAMBDA method's output. For each candidate set $\check{\alpha}$, as resulting from LAMBDA method, the corresponding baseline, $\check{b}(\check{\alpha})$, is computed with the objective of attributing merit to each candidate. For that, the developed method has three steps: validation, selection and stabilization. Before the description of these three steps, the tests used in this thesis for merit attribution are presented.

Merit Attribution

In merit attribution were used three types of metrics. The first two, also present in [8], were the residual ratio and the baseline length constraint. The third one, proposed in this thesis, makes use of the Up coordinate while the ambiguity set is not stabilized.

The residual ratio: for each ambiguity set and the respective baseline solution, the phase residual vector V is calculated as the difference between the estimated phase double differences and the measured ones. That is, the phase residual vector is given by

$$V = B\check{b} + A\check{\alpha} - \nabla\Delta\Phi, \quad (3.43)$$

and its Euclidean norm is obtained by

$$\|V\|^2 = V^T(\text{cov}(\nabla\Delta\Phi))^{-1}V. \quad (3.44)$$

The baseline length constraint: with the knowledge of the truth baseline distance, l , the error of the estimated baseline is obtained as

$$\delta_b = \left| \|\check{b}(\check{\alpha})\| - l \right|. \quad (3.45)$$

The Up coordinate constraint: this test is similar to the previous one, but only considers the Up coordinate resulting from the candidate set that is being tested. It is assumed that during the initialization (i.e. while there is no stabilized solution) the platform is stopped, which leads to a constant baseline vector. By measuring the altitude difference between the reference antenna and the auxiliary antenna, it is possible to obtain the real Up coordinate, u_{real} . Thus, the Up coordinate error is given by

$$\delta_u = |\check{u}(\check{\alpha}) - u_{real}|. \quad (3.46)$$

For each of the three tests defined above, the errors of the candidates are grouped in a vector with ascending order of the respective error, which is the descending order of merit. So, the merit, M , of a candidate set will be attributed according with the position, i , of the error in the sorted vector, that is

$$M_i = \frac{1}{i}. \quad (3.47)$$

Validation Step

The validation step makes use of the baseline length error, described in (3.45), and defining a threshold. This threshold was set to be 10 *cm*, due to the nature of the errors present in the baseline vector. That is,

$$\delta_b = \left| \|\check{b}(\check{\alpha})\| - l \right| \leq 0.1. \quad (3.48)$$

The candidates that have a baseline length error bigger than the threshold are excluded.

Selection Step

This step is where the merit is attributed. This is done by combining two of the tests defined previously in two different metrics:

1. Residual ratio and baseline length constraint;
2. Baseline length constraint and Up coordinate constraint.

The candidate set with higher merit, using the metric 1 or the metric 2, will be selected as the fixed solution for the respective epoch.

Stabilization Step

The candidate set selected as the fixed solution by the Ambiguity Filter in each epoch is stored in a data base. As debated in [8], the ambiguity set that first achieves 50 occurrences as the fixed solution (i.e. a candidate is selected as the fixed solution in 50 different epochs) is the correct fixed solution. Thereafter the correct baseline vector will be determined by the best fixed solution.

In dynamic environments variations in the satellite constellation occur quite often (i.e. change of the reference satellite, loss of lock, cycle slips), that entails to the lost of the correct ambiguity set. The algorithm proposed in this thesis uses the same constellation in the maximum number of epochs. Even if a new satellite becomes visible, the algorithm uses those satellites for which the correct integer ambiguity set is known. When the number of satellites falls to less than four, the algorithm uses the last baseline's estimate (i.e. calculated using the correct ambiguity set) and recovers the correct ambiguity set for the new constellation. Then the recovered ambiguity set is used to calculate the present baseline vector. This adaptation to a new constellation represents an improvement in the use of the Ambiguity Filter and the techniques used will be presented next. If neither of the recovery techniques is capable of maintaining the integer ambiguity solution, the Ambiguity Filter must be reinitialized and start the process from the beginning.

3.3.5 Constellation Changes: Recovery Techniques

As said before, constellation changes lead to the loss of both correct ambiguity set, obtained after stabilization, and the ambiguities stored through the different epochs. However, some techniques can be used to recover from this scenario, without resetting the system.

Reference Satellite Transformation

As aforementioned, the reference satellite is the one with highest elevation. However, during the

acquisition time the reference satellite may change, due to the variation of elevation or to the loss of lock of the actual reference satellite.

Remembering the definition of the carrier phase double differences, in equation (3.3), for a reference satellite p , a rover satellite q and receivers k and m , one must have

$$\nabla\Delta\phi_{km}^{pq} = \Delta\phi_{km}^p - \Delta\phi_{km}^q = \nabla\Delta\rho_{km}^{pq} + \lambda\nabla\Delta N_{km}^{pq} + \nabla\Delta\epsilon_{km}^{pq}. \quad (3.49)$$

Assuming that a new reference satellite is used (e.g. satellite g), through manipulation of the equation (3.49), [8], the integer ambiguity element for the reference satellite g and the rover satellite q is given by

$$\nabla\Delta N_{km}^{gq} = \nabla\Delta N_{km}^{pq} - \nabla\Delta N_{km}^{pg} + \frac{\nabla\Delta\phi_{km}^{gq} - \nabla\Delta\phi_{km}^{pq} + \nabla\Delta\phi_{km}^{pg}}{\lambda}. \quad (3.50)$$

Using this technique, if the reference satellite changes the new correct ambiguity set (or for the ambiguity sets stored as previous solutions) can be obtained. However, it is mandatory that the new reference satellite had been visible in previous epochs, or the term $\nabla\Delta N_{km}^{pg}$ is unknown and this technique cannot be applied.

Cycle Slips

A cycle slip occurs when there is a loss of signal continuity, between the satellite and the receiver, resulting in a gain of carrier cycles when the signal is reacquired by the receiver. From the observables used, the cycle slips can be detected in carrier phase measurements and, consequently, in carrier phase double differences, as depicted in Figure 3.5 for data acquisition in static environment.

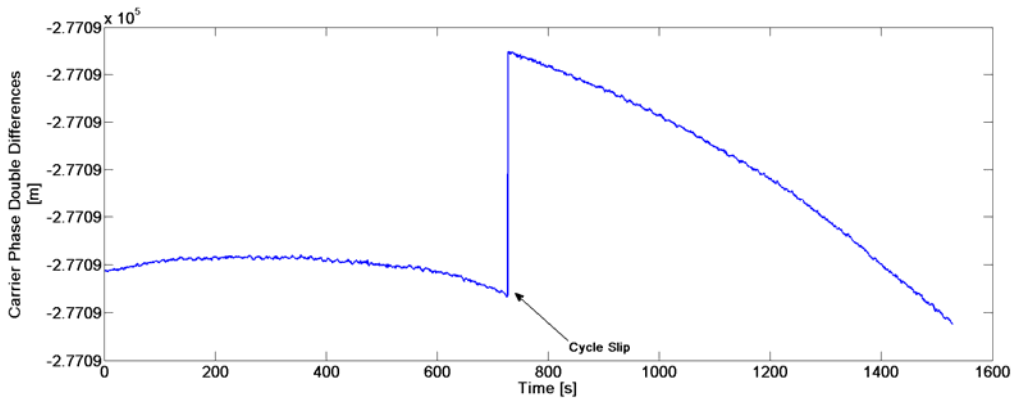


Figure 3.5 – Carrier phase double differences evolution with a cycle slip, in static environment

At this point, it is clear that double differences affected by cycle slips should have new ambiguities.

Thus, it is mandatory that the algorithm track the evolution of the carrier phase double differences in order to detect these events. This may be done by using triple differences (TD), which is the difference between two epochs' measurements, and defining a threshold. That is,

$$TD = \nabla\Delta\phi_t - \nabla\Delta\phi_{t-1} \leq \alpha, \quad (3.51)$$

where α is the user defined threshold, in meters. As discussed in [8], the threshold must be chosen by taking into account the platform's dynamic. For surveying scenarios, triple differences' variation is low and the threshold may be set up to $\alpha = 0.01m$. In Figure 3.6 the triple differences evolution for the case in Figure 3.5, where the cycle slip is easily identified by the peak, respecting the previously defined threshold.

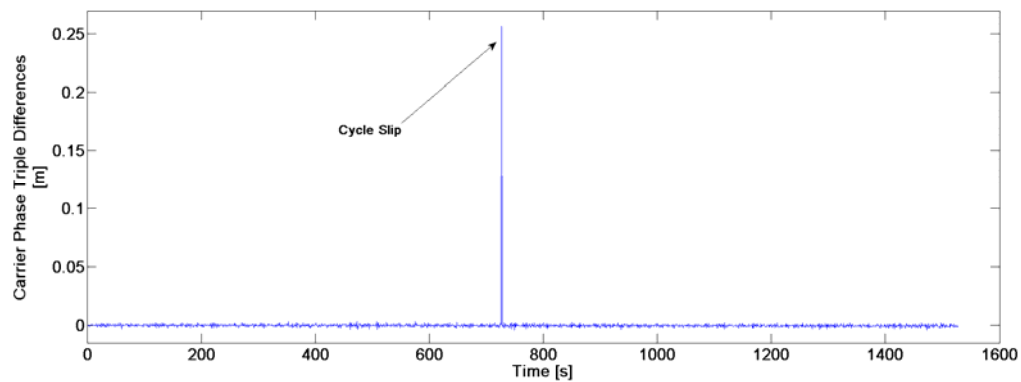


Figure 3.6 – Carrier phase triple difference evolution with a cycle slip, in static environment

In Figure 3.7, the evolution in static environment of the carrier phase double difference without a cycle slip is illustrated, followed by the respective triple differences, in Figure 3.8. By analyzing the histogram for the carrier phase triple differences, in Figure 3.9, one may see that the triple differences are characterized only by the normal distributed residuals of the carrier phase double differences and that the threshold defined as $\alpha = 0.01 m$ allow a confidence interval of $\approx 10\sigma$ ($\mu = 0$ and $\sigma = 0.001$).

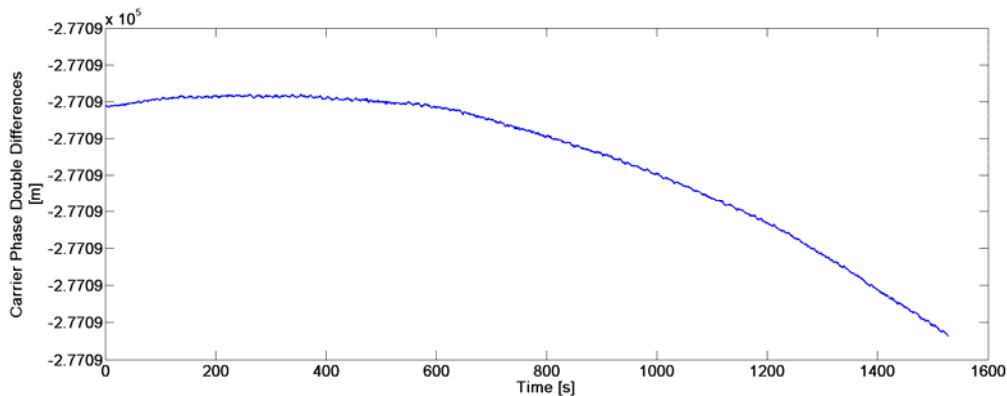


Figure 3.7 – Carrier phase double differences evolution without cycle slips, in static environment

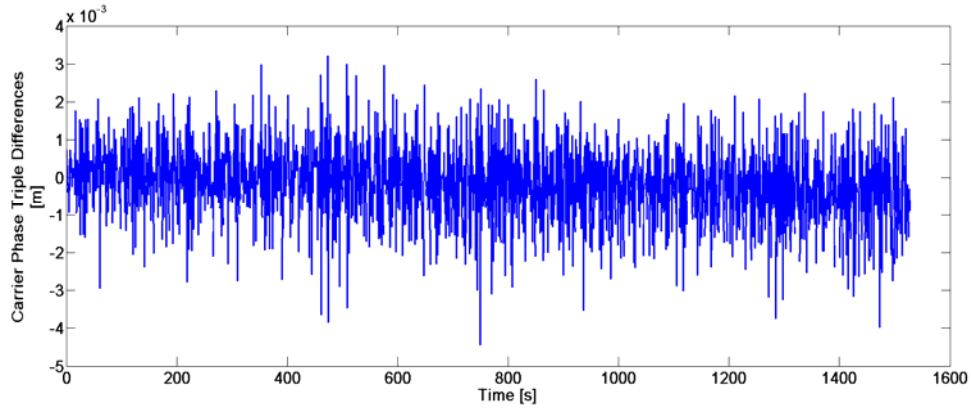


Figure 3.8 – Carrier phase triple differences evolution without cycle slips, in static environment

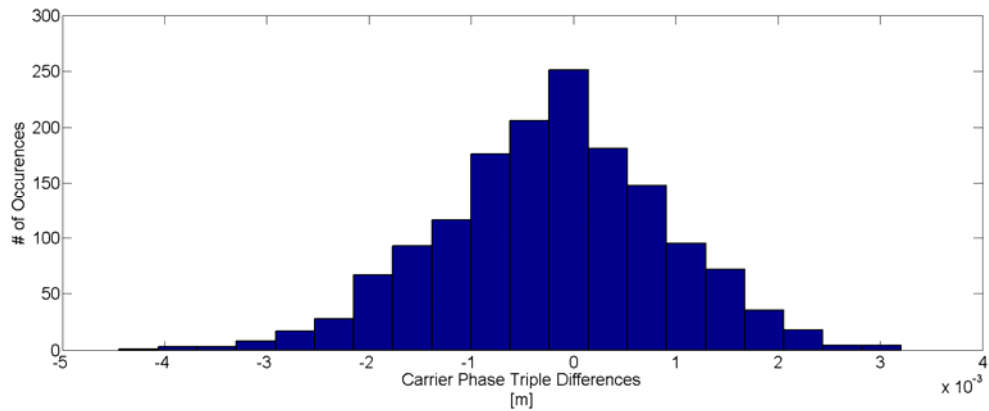


Figure 3.9 – Histogram of triple differences without cycle slips, in static environment

As described in [8], the worst scenario is the type of movement with high angular velocities, which imposes a sinusoidal evolution to the double differences, that is,

$$\nabla\Delta\phi_k = l \sin(\omega t), \quad (3.52)$$

where l is the baseline length and ω is the maximum angular velocity of the vehicle. Thus from the conclusions described in [8], the maximum value for the TD in this type of scenario is function of the baseline length and the vehicle's angular velocity, that is,

$$\max(TD) = 2l \sin\left(\pi - \frac{\omega T}{2}\right). \quad (3.53)$$

Since the dynamic trials were performed with slow movements, a small value for the vehicle's angular velocity ($\approx 0.5 \text{ rad/s}$) was considered. However, improvements in the estimation of the vehicle's angular velocity could be addressed, in order to validate this technique for different dynamics.

When a cycle slip is detected in an explicit double difference, the stored integer ambiguities and the correct integer ambiguity, if known, must be corrected. In this thesis, the recovery of an ambiguity set

from a cycle slip is done by adding the rounded triple difference to the previous integer ambiguity. That is,

$$\nabla \Delta N_{km}^{pq} = \nabla \Delta N_{km}^{pq} + \text{round}(TD). \quad (3.54)$$

Variation in the Number of Satellites

During the data acquisition in real environments the number of satellites used to compute the baseline vector changes quite often, due to the loss of signal or even loss of data in the interface. Instead of resetting the Ambiguity Filter, the algorithm deletes the ambiguity component relative to the lost satellite and keeps tracking the remaining satellites with the previously obtained ambiguities.

As aforementioned, the algorithm uses the same satellites as much as possible, so that the stability is maximized, that is, even if a new satellite becomes visible the algorithm uses the satellites for which the correct ambiguities are known.

When the number of used satellites falls to less than four, the algorithm uses the last estimation of the baseline vector to estimate the ambiguity set for all visible satellites, that is, from (3.19) one may obtain

$$\nabla \Delta N = (A^T W A)^{-1} (A^T W y - A^T W B b_{t-1}), \quad (3.55)$$

where b_{t-1} is the last baseline's estimation. It is assumed that between two epochs the baseline vector has small changes and can be used to estimate the new ambiguity set.

4 ATTITUDE DETERMINATION

4.1 Introduction

The configuration of multiple baselines allows the attitude determination. By using the Ambiguity Filter, described in the previous chapter, for baseline determination, two techniques for attitude determination are proposed.

With the definition of the Euler angles presented in the Chapter 2 in mind, two techniques for the attitude determination are presented. First, a simple technique using rotation matrices is presented. Finally, a more complex solution using a rotation quaternion and a generalization of the Kalman Filter (KF) is proposed.

4.2 Attitude Determination Using a Rotation Matrix

As discussed in [1] and in [28], among other possible solutions assume that the attitude is defined by the rotation transformation which relates a coordinate frame fixed in space NED to a coordinate frame fixed in the body (xyz). Due to its nature, the coordinates of the baselines will be constant in the body frame and are known.

The rotation of the body fixed frame can be represented as a series of rotations from the body fixed frame to the reference space frame. First a rotation about the z axis (angle ψ), followed by a rotation about the new y axis (angle ϕ) and , finally, a rotation about the newest x axis (angle θ). That is,

$$Rot(\psi, \theta, \phi) = Rot_z(\psi)Rot_y(\theta)Rot_x(\phi), \quad (4.1)$$

where each rotation matrix is a 3×3 square matrix and with $|Rot_z(\psi)| = |Rot_y(\theta)| = |Rot_x(\phi)| = +1$. The resulting rotation matrix, also a 3×3 square matrix and with $|Rot(\psi, \theta, \phi)| = +1$, is represented by

$$Rot(\psi, \theta, \phi) = \dots \quad (4.2)$$

$$\begin{bmatrix} \cos(\psi) \cos(\theta) & \begin{pmatrix} -\sin(\psi) \cos(\phi) + \\ \cos(\psi) \sin(\theta) \sin(\phi) \end{pmatrix} & \begin{pmatrix} \sin(\psi) \sin(\phi) + \\ \cos(\psi) \sin(\theta) \cos(\phi) \end{pmatrix} \\ \sin(\psi) \cos(\theta) & \begin{pmatrix} \cos(\psi) \cos(\phi) + \\ \sin(\psi) \sin(\theta) \sin(\phi) \end{pmatrix} & \begin{pmatrix} -\cos(\psi) \sin(\phi) + \\ \sin(\psi) \sin(\theta) \cos(\phi) \end{pmatrix} \\ -\sin(\theta) & \cos(\theta) \sin(\phi) & \cos(\theta) \cos(\phi) \end{bmatrix}$$

The transformation from the body fixed frame to the space frame is given by

$$B_{NED} = Rot(\psi, \theta, \phi)B_{xyz}, \quad (4.3)$$

where $B_{NED} = \begin{bmatrix} | & \dots & | \\ b_{NED}^{12} & \dots & b_{NED}^{1i} \\ | & \dots & | \end{bmatrix}$ and $B_{xyz} = \begin{bmatrix} | & \dots & | \\ b_{xyz}^{12} & \dots & b_{xyz}^{1i} \\ | & \dots & | \end{bmatrix}$ are matrices of baselines (as columns) in the respective coordinate frame.

Thus, using the baselines vectors, in the space frame, calculated in each epoch, the rotation matrix at each epoch may be calculated by solving as a simple Least Squares (LS) problem, that is

$$Rot(\psi, \theta, \phi) = B_{NED}B_{xyz}^T(B_{xyz}B_{xyz}^T)^{-1}. \quad (4.4)$$

After the determination of the rotation matrix, one may obtain the attitude angles using simple trigonometric relations, as represented next

$$\theta = \sin^{-1}(-Rot_{31}), \quad (4.5)$$

$$\phi = \sin^{-1}(Rot_{32}/\cos(\theta)), \quad (4.6)$$

$$\psi = \cos^{-1}(Rot_{11}/\cos(\theta)), \quad (4.7)$$

where the subscript in the rotation matrix represents its index. The expressions for the pitch and roll angles (equations (4.5) and (4.6), respectively) assume a rotation between $[-\pi/2; \pi/2]$, and the expression for the heading angle (equation (4.7)) assume a rotation between $[0; \pi]$, thus one cannot have all possible orientations. To correct this issue, depending on the signal of the baselines' coordinates the attitude angles must be corrected to the real quadrant.

This approach has singularities for pitch angles of $\pm \pi/2$. However, it is easy to obtain the attitude angles for situations where such attitude is not experienced. For a more robust and stable implementation, a rotation quaternion may be used.

4.3 Quaternion-Based Extended Kalman Filter for Attitude Determination

4.3.1 Quaternion and Euler Angles

As described in [30], instead of rotation matrices, a quaternion may be used as rotation operator. A quaternion is a hyper-complex number of rank 4, and it is defined as

$$q = q_0 + iq_1 + jq_2 + kq_3, \quad (4.8)$$

where q_0 is called the scalar part and $iq_1 + jq_2 + kq_3$ are called the vector part.

The computation of a baseline vector in the coordinate frame NED from the Body fixed frame, in terms of a rotation quaternion, is given by

$$b_{NED} = q^* b_{xyz} q, \quad (4.9)$$

where $q^* = q_0 - iq_1 - jq_2 - kq_3$ represents the complex conjugate of the quaternion q . An important property is that the quaternion q is a unit vector, that is

$$\|q\|^2 = q_0^2 + q_1^2 + q_2^2 + q_3^2 = 1, \quad (4.10)$$

which consists in a crucial constraint when using a quaternion for attitude determination, as presented in the development of the Extended Kalman Filter (EKF) proposed in next section.

Thus, the rotation matrix Rot , in terms of quaternions is represented by

$$A_q = \begin{bmatrix} -1 + 2(q_0^2 + q_1^2) & 2(q_1q_2 - q_0q_3) & 2(q_1q_3 + q_0q_2) \\ 2(q_1q_2 + q_0q_3) & -1 + 2(q_0^2 + q_2^2) & 2(q_2q_3 - q_0q_1) \\ 2(q_1q_3 - q_0q_2) & 2(q_2q_3 + q_0q_1) & -1 + 2(q_0^2 + q_3^2) \end{bmatrix}.$$

By substituting the matrix $Rot(\psi, \theta, \phi)$ with the quaternion matrix, A_q , equation should have the new form

$$B_{NED} = A_q B_{xyz}. \quad (4.11)$$

The Euler angles can be obtained from the quaternion matrix as

$$\theta = \sin^{-1}(-A_q^{31}), \quad (4.12)$$

$$\phi = \tan^{-1} \left(\frac{A_q^{32}}{A_q^{33}} \right), \quad (4.13)$$

$$\psi = \tan^{-1} \left(\frac{A_q^{21}}{A_q^{11}} \right), \quad (4.14)$$

where the superscript in the matrix represents its index.

4.3.2 Extended Kalman Filter

Instead of the LS presented in Section 4.2, which provide an epoch-by-epoch solution, the KF allow better results since it is a recursive estimation algorithm. However, with the observables at hand it is not possible to apply the linear KF due to the measurement model, as depicted during this section.

To obtain the Euler angles based on the rotation quaternion it is necessary to estimate the parameters q_0 , q_1 , q_2 and q_3 . The system dynamics of the quaternion is represented by

$$\dot{q} = \frac{1}{2} \Omega q, \quad (4.15)$$

where q is the vector with the quaternion components, that is, $q = [q_0 \ q_1 \ q_2 \ q_3]^T$, and Ω is the skew-symmetric matrix, defined as

$$\Omega = \begin{bmatrix} 0 & \omega_z & -\omega_y & \omega_x \\ -\omega_z & 0 & \omega_x & \omega_y \\ \omega_y & -\omega_x & 0 & \omega_z \\ -\omega_x & -\omega_y & -\omega_z & 0 \end{bmatrix}, \quad (4.16)$$

where $\omega = [\omega_x \ \omega_y \ \omega_z]^T$ are the angular velocities in the body frame axis. The observations of angular velocities may be provided by a rate gyro. However, in this thesis only GPS observables and its derivations are used as observations. Thus, the angular velocities must be estimated along with the quaternion components. It is assumed a constant angular velocity model, which is a good approximation for a short measurement interval and for a vehicle with low dynamics, [31], with the disturbances being interpreted as inputs to the system.

So, this leads to a linear time-varying discrete system defined as

$$x_{k+1} = F(x_k)_k + G_k w_k, \quad (4.17)$$

with each component being

$$x_{k+1} = \begin{bmatrix} q_{k+1} \\ \omega_{k+1} \end{bmatrix}, \quad (4.18)$$

$$F_k = \begin{bmatrix} q_k + \frac{1}{2} \Delta t \Omega_k q_k \\ \omega_k \end{bmatrix}, \quad (4.19)$$

$$G_k = \begin{bmatrix} -\frac{1}{2} \Xi & 0 \\ 0 & I \end{bmatrix}, \quad (4.20)$$

$$\Xi = \begin{bmatrix} q_4 & -q_3 & q_2 \\ q_3 & q_4 & -q_1 \\ -q_2 & q_1 & q_4 \\ -q_1 & -q_2 & -q_3 \end{bmatrix}, \quad (4.21)$$

where Δt is the sampling time ($\Delta t = 1$ s for the GPS case), w_k is the process noise, Gaussian distributed with zero mean and covariance Q , and $\Xi \omega = \Omega q$, accordingly with [32].

By using the baselines' coordinates, from the previously presented Ambiguity Filter, as measurements, the relation between measurements and the system's state vector is given by equation (4.11). In addition, the measurement model takes into account the constraint imposed by the quaternion nature, which is a unit vector as represented in equation (4.10). This is done by using this constraint as a perfect measurement, as described in [27]. So, the measurement model is non linear time-varying and has the form

$$z_k = h(x_k)_k + v_k, \quad (4.22)$$

where v_k is the measurement noise, Gaussian distributed with zero mean and covariance R , and

$$z_k = \begin{bmatrix} b_{NED}^{12} \\ b_{NED}^{13} \\ b_{NED}^{14} \\ 1 \end{bmatrix}, \quad (4.23)$$

(4.24)

$$h(x_k)_k = \begin{bmatrix} A_q b_{NED}^{12} \\ A_q b_{NED}^{13} \\ A_q b_{NED}^{14} \\ q^T q \end{bmatrix}.$$

Since the system model is linear time-varying and the observation model is non linear time-varying, to estimate the quaternion components and the angular velocities it is necessary to implement an EKF. The EKF consists in the system's linearization around the nominal solution that results from the KF estimation.

Thus with the system at hand, it is mandatory the linearization of the measurement model. This is done by Taylor Series expansions, where neglecting the high order terms (assumed to have small numeric value), [33], leads to the Jacobian matrix defined as

(4.25)

$$H_k = \begin{bmatrix} \frac{\partial h(x_k)_k}{\partial q} & \frac{\partial h(x_k)_k}{\partial \omega} \end{bmatrix}.$$

The process noise characterizes the small disturbance in the system's dynamics and is given by, [33] and [34],

$$Q_k = E[w_k w_k^T] = \int_{t_k}^{t_{k+1}} F(t_{k+1}, \tau) G(\tau) Q G^T(\tau) F^T(t_{k+1}, \tau) d\tau, \quad (4.26)$$

where Q , accordingly with [32], is a diagonal matrix and containing the covariance of the disturbances present in the angular velocities, that is,

$$Q = \begin{bmatrix} Q_\omega & 0 \\ 0 & Q_{\omega_{bias}} \end{bmatrix}_{6 \times 6}, \quad (4.27)$$

where Q_ω is the covariance of the angular velocity noise and $Q_{\omega_{bias}}$ is the covariance of the angular velocity bias noise. These two parameters must be tuned in order to obtain the best solution, but since it is not used any rate gyro, it is assumed that the value of $Q_{\omega_{bias}}$ is close to zero.

To solve the equation (4.26), in order to obtain the process covariance matrix, it is assumed that the time interval between two measurements (1s for the GPS) is small enough to use the approximation

(4.28)

$$Q_k \approx G_k Q G_k^T \Delta t.$$

Since the measurements used are the coordinates of the baseline vectors (assumed to be independent), the measurement covariance matrix is diagonal with each component regarding the corresponding coordinate, that is for a single baseline observation one must have

$$R_{NED} = \begin{bmatrix} \sigma_N^2 & 0 & 0 \\ 0 & \sigma_E^2 & 0 \\ 0 & 0 & \sigma_D^2 \end{bmatrix}. \quad (4.29)$$

Thus, for three baselines and the quaternion-norm perfect measurement, the observation covariance matrix of the EKF is defined as

$$R_k = E[v_k v_k^T] = \begin{bmatrix} R_{NED}^{12} & 0 & 0 & 0 \\ 0 & R_{NED}^{13} & 0 & 0 \\ 0 & 0 & R_{NED}^{14} & 0 \\ 0 & 0 & 0 & 0 \end{bmatrix}. \quad (4.30)$$

Finally, the EKF should have the form

$$\hat{x}_k^- = F(x_k)_k, \quad (4.31)$$

$$P_k^- = F_k P_{k-1} F_k^T + Q_k. \quad (4.32)$$

$$K_k = P_k^- H_k^T (H_k P_k^- H_k^T + R_k)^{-1}, \quad (4.33)$$

$$\hat{x}_k = \hat{x}_k^- + K_k (z_k - h(\hat{x}_k^-)_k), \quad (4.34)$$

$$P_k = (I - K_k H_k) P_k^-. \quad (4.35)$$

where, as previously described, the first two lines are the prediction step, where the state vector and the respective covariance matrix, estimated in the previous instant, are propagated to the new time step. The remaining lines correspond to the update step, where the Kalman gain is determined and is used to weight the state prediction, based on the innovation process given by the difference between the measured baseline vectors and the ones obtained from the estimated quaternion, $z_k - h(\hat{x}_k^-)_k$. This innovation process is used in the results section as a tool to evaluate the performance of the EKF.

Instead of the linear KF, the EKF solution is optimal only around the linearization nominal point and the conditions for stability are not necessarily sufficient. The stability in non-linear systems is possible only inside bounded regions, [27] and [33]. The reachability and observability will be addressed in next section.

4.3.3 Reachability and Observability

The concept of reachability for a discrete-time system, which is analogous to controllability for a continuous-time system, defines how well the system is reachable (or controllable). Thus, accordingly

with [27], a discrete-time system is reachable if for any initial state x_0 and some final time k_f there exists a control that transfers the state to any desired value at time k .

Accordingly with [35], this may be verified by the rank of the reachability matrix, which for the system defined in the previous section and for the time interval $[k_0, k_f]$ is defined by

$$R(k_0, k_f) = [G(k_f - 1) \quad F(k_f, k_f - 1)G(k_f - 2) \quad \dots \quad F(k_f, k_0 + 1)G(k_0)]. \quad (4.36)$$

That is, the linear time-varying system by (4.17), with n state variables, is reachable on the time interval $[k_0, k_f]$, if and only if the reachability matrix verifies

$$\text{rank}(R(k_0, k_f)) = n. \quad (4.37)$$

The next important concept is the observability, that relates how well it is possible to determinate the initial conditions through the observations. Thus, accordingly with [27], a discrete-time system is observable if for any initial state x_0 and some final time k_f , the initial state can be uniquely determined by the corresponding zero-input response z_k .

Accordingly with [35], this may be verified by the rank of the observability matrix, which for the system at hand and for the time interval $[k_0, k_f]$ is defined by

$$O(k_0, k_f) = \begin{bmatrix} Q(k_0) \\ Q(k_0 + 1)F(k_0 + 1, k_0) \\ \vdots \\ Q(k_f - 1)F(k_f - 1, k_0) \end{bmatrix}. \quad (4.38)$$

That is, the linear time-varying system by (4.17), with n state variables, is observable on the time interval $[k_0, k_f]$, if and only if the observability matrix verifies

$$\text{rank}(O(k_0, k_f)) = n. \quad (4.39)$$

In the system (4.17) the state variables are the quaternion elements and the angular velocities components, thus it is a system with $n = 7$ state variables. By computing the desired matrices for formation of both reachability and observability matrices, in a significant time interval, it was possible to verify that the conditions for reachability and observability were respected, that is,

$$\text{rank}(R(k_0, k_f)) = 7, \quad (4.40)$$

$$\text{rank}(O(k_0, k_f)) = 7. \tag{4.41}$$

Finally, based on the results of (4.40) and (4.41), it is possible to conclude that the EKF implemented can provide a solution for the problem at hand and is unique.

5 SOLUTION IMPLEMENTATION

5.1 Introduction

After the description of the tools used to solve the problem of the attitude determination using multiple baselines, and how to determine those baselines, this section addresses the practical issues of this thesis. Two types of GPS receivers were used: Magellan AC12 and U-Blox 6. Thus, it is important to introduce a general description for both receivers and the antennas used. Following the receivers' introduction, a description of the developed algorithm, using the previously discussed tools, is presented. Finally, the reader is presented with the description of the trials, static and dynamic, used to validate the developed algorithm.

5.2 GPS Receivers and Antennas

5.2.1 Magellan AC12 GPS Receivers

In order to have a three baselines system, four Magellan AC12 GPS receivers were used, two evaluation and development kits and two OEM boards as illustrated in Figure 5.1, [36], respectively.

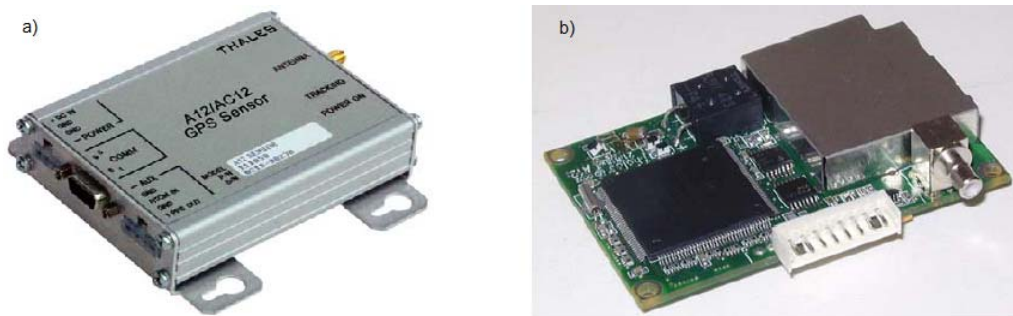


Figure 5.1 – a) AC12 sensor evaluation and development kit; b) AC12 OEM board [36]

The receiver processes signals, on the L1 frequency band, from the GPS satellite constellation, for which uses ten channels, and SBAS, in two channels, leading to a total of twelve signal tracking channels. The receiver provides real-time position, velocity, and time measurement, amongst other significant information, in NMEA format. The receiver also provides the satellites ephemeris, which are essential for the development of single positioning algorithms, through a binary message. However, this receiver does not provide the ionospheric correction parameters, which allow an improvement on the single positioning. Regarding the double differences computation, the AC12 receiver provides a binary message containing both carrier phase and code raw measurements. The communication with the receiver is made with RS-232 interface.

5.2.2 U-Blox 6 GPS Receivers

The single positioning of the reference antenna is part of the developed algorithm. In order to improve the positioning accuracy, one may use the ionospheric parameters to correct the code measurements. Since the Magellan AC12 receivers do not provide such parameters, one U-Blox 6 GPS receiver, illustrated in Figure 5.2, was used for this purpose, [37]. As for the AC12, the U-Blox provides real-time positioning, velocity, and time measurements, amongst other significant information, through NMEA messages, and binary messages containing raw measurements, satellite ephemeris and ionospheric corrections, and along with other important information.



Figure 5.2 – U-Blox 6 GPS receiver [37]

The reader may ask why not use only U-Blox receivers. However, the performance of the Ambiguity Filter, using these receivers, was lower than the performance when using AC12 receivers. For this reason, it was decided to adopt the described set of GPS receivers.

The communications with the receiver is made using the RS-232 interface and through USB connection.

5.2.3 Antennas

For the Magellan AC12 GPS receivers presented above, three types of antennas were used. For static (or survey) tests with two GPS receivers, two Novatel model 531 GPS antennas with Chocke Ring model A032 [38], depicted in Figure 5.3. This type of antenna operates at the L1 frequency. Antenna optimization in the shape of the radiation pattern along with the Chocke Ring allows the minimization of multipath and interference errors.



Figure 5.3 – Novatel model 531 GPS antenna with Chocke Ring Model A032 [38]

For multiple baselines (more than two receivers) in static and dynamic trials, the AC12 receivers used a NAIS Magnetic antenna, [36], illustrated in Figure 5.4. Smaller than the previous antenna, allow more versatility in the set up. However, is subject to higher levels of interference and multipath errors.



Figure 5.4 – NAIS magnetic antenna [36]

Finally, the U-Blox 6 receiver uses an ANN-MS-0-005 magnetic antenna, [39], which is similar to the NAIS magnetic antenna depicted in Figure 5.4.

5.3 Algorithm Overview

Using the techniques presented so far in this thesis, the algorithm illustrated by the flowchart of Figure 5.3 was developed in MatLab. Note that the data acquisition of the GPS measurements was done previously and then inputted to the algorithm in post-processing mode. So, the first process with the name “Data Acquisition” regards the acquisition of the raw data previously stored. However, this program could be adapted in order to use data in real time, being the “Data Acquisition” process responsible for reading the measurements provided by the GPS receiver. With the data at hand, it is mandatory that measurements from different receivers are synchronized, which is done by the “Data Synchronization” process. This is done by comparing the measured time of week of each receiver, which represents the number of seconds passed since the beginning of the corresponding week (beginning at Saturday/Sunday midnight).

To determine the baseline vector coordinates it is mandatory to know the origin of the local coordinate system (ENU or NED) in the ECEF coordinate system, which coincides with the position of the reference antenna. This is done in the “Reference Antenna Stand-Alone Positioning” process, resorting to code measurements, code corrections and satellite ephemeris, as described in [21]. The “Double Differences Formation” process is responsible for the selecting satellites, common to the receivers that compose the baseline vector, and computing the double differences. For the satellite selection process an elevation mask of 5° was used, which neglect noisier satellite measurements.

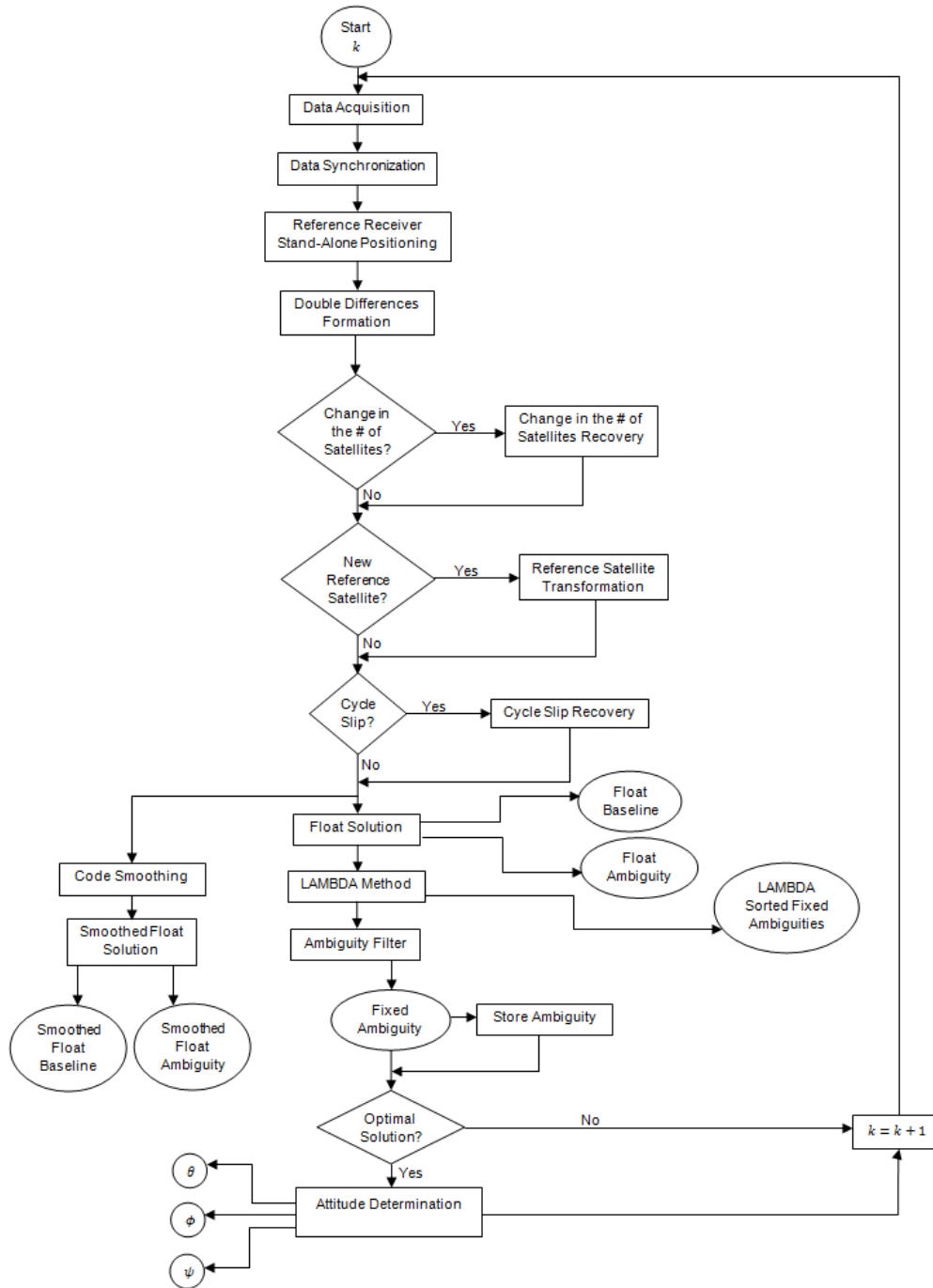


Figure 5.5 – Flowchart of the developed algorithm

After computing the double differences some tests must be accomplished. The first test is to verify if there is any change in the number of satellites. If this test outputs the logic value “true”, the respective algorithm corrects this issue by excluding the ambiguity (from the correct ambiguity set and from the stored ambiguities) corresponding to the lost satellite. After this correction, the flowchart converges with the node that would be reached if the test turned out “false”. The second test verifies if there is a new reference satellite. If the output is the logic true, the transformation of equation (3.50) must be

applied. The last test that is applied to the double differences is the cycle slip verification. If a cycle slip is detected, returning the logic true in the detection test, the respective correction is applied.

With the double differences accomplishing the previous tests, the algorithm determines the float solution of both baseline vector and ambiguity set, in “Float Solution” process, by solving the WLS defined in equation (3.19). An alternative float solution is obtained by smoothing the code double differences using the respective algorithm, and then determining the corresponding float solution.

By using the non-smoothed float solution as an input, the LAMBDA method outputs the intended number of candidates sorted by the distance from the float solution, as described in Section 3.3.3. From these candidates, the Ambiguity Filter selects the one with highest merit/confidence as the correct fixed ambiguity set, which is outlined in Section 3.3.4. The ambiguity set selected by the Ambiguity Filter is then stored in a data base, where is verified if the correct solutions was already achieved, which consists on the stabilization process of the Ambiguity Filter. If there is not an optimal solution, the Algorithm proceeds to the next iteration from this point. However, if the optimal solution was already achieved, the attitude angles are obtained resorting to one of the two methods presented in Sections 4.3 and 4.4. After obtaining the attitude angles, the algorithm proceeds to the next iteration.

Note that in multiple baseline scenarios, each vector is calculated separately and only in the attitude determination step all the baselines are computed to obtain the Euler angles.

5.4 Trials Description

To validate the developed algorithm, static and dynamic trials were made. For the static trials, the first type is a test using a single baseline (i.e. two GPS receivers), and the second type is a test using three baselines (i.e. four GPS receivers). For the dynamic trials, the platform using multiple baselines was in motion along a route.

5.4.1 Static Trials

Single Baseline

The objective of this first type of static test is the performance evaluation of the Ambiguity Filter. For high accuracy in the baseline determination, minimizing the multipath effect, the Novatel 531 antennas with Chocke Ring were used. These antennas are placed in the rooftop of the North Tower, at Instituto Superior Técnico, as depicted in Figure 5.6, which allow a scenario with very low levels of multipath.



Figure 5.6 – Top view of the antennas’ position, for the single baseline static trial (Google Earth, [40])

For this configuration, the distance between the two GPS antennas is 10.665 m and the south antenna is the reference one, as illustrated in the above figure. This leads to a baseline vector pointing to north and to an expected heading angle between $[-4^\circ; -3.5^\circ]$. Both antennas’ support structures are placed at the same height, and hence it is expected that the baseline’s Up coordinate is close to zero.

With this trial, a comparison between the baseline vector obtained with various solutions (i.e. unsmoothed float baseline, smoothed float baseline, baseline with the best ambiguity set from LAMBDA method and baseline with the best ambiguity set from Ambiguity Filter) is possible.

Multiple Baselines

Since multiple baselines are used, this trial is intended to validate the attitude determination techniques and it is made in an urban scenario. For that, the GPS antennas were placed accordingly with Figure 5.7, leading to the baseline vectors depicted in the same figure. In the results section, different baselines are distinguished by the respective GPS receivers’ number, that is, “baseline 1-2” corresponds to the vector between GPS receivers 1 and 2.

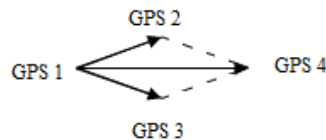


Figure 5.7 – GPS receivers’ disposition and baseline vectors

Both baselines’ length, between receivers 1 and 2, and between receivers 1 and 3, is approximately 0.8 m . The baseline length between receivers 1 and 4 is approximately 1.34 m . Accordingly with the

studies presented in [11], these values for the baseline length allow high accuracy in the baseline determination.

For this trial, four NAIS magnetic antennas were used. Since the data acquisition was made in an urban scenario and the antennas used are more exposed to multipath, than the ones used in the single baseline trial, it is expected to increase the multipath effect, when compared with the single baseline test. The scenario in which the data acquisition took place and the platform's orientation, with an expected heading angle between $[-120^\circ; -110^\circ]$, are depicted in Figure 5.8. Since the platform was stopped in a flat surface, it is expected that the Up coordinate of each baseline is close to zero.



Figure 5.8 – Top view of the platform's orientation for the multiple baselines static trial (Google Earth, [40])

5.4.2 Dynamic Trial

This trial intended to evaluate the performance of the attitude determination techniques in a dynamic environment, that is, for data acquired in a moving platform. The GPS receivers and the antennas' disposition used were the same as presented in the previous section, that is, for the static trial in the multiple baselines case. The platform was in motion along a flat surface and with considerable variation on the heading angle, as depicted in Figure 5.9. The maneuvers made by the platform along the trajectory were slow, so it is not expected very aggressive angular velocities estimated by the EKF. During the trajectory it was imposed to the platform a positive rotation about the x axis, that is, a positive roll angle. This test was made between epochs $t \in [235; 255] s$, when the platform's heading was $\approx -30^\circ$. Despite this test, the remaining variations in pitch and roll angles are due to surface irregularities and multipath noise.

The orientation of the initial and the final position, as depicted in Figure 5.9, is expected to be between $[-30^\circ; -20^\circ]$ and $[-115^\circ; -110^\circ]$, respectively.



Figure 5.9 – Top view of the platform’s path and orientation, for initial and final position, for the dynamic trial (Google Earth, [40])

6 RESULTS

6.1 Introduction

In this chapter the results from the trials previously described are presented. Along with the results, a critical discussion is made to evaluate the performance of the developed techniques.

The single baseline static trial is used to evaluate the Ambiguity Filter performance, by analyzing the corresponding baseline solution. This solution is compared with the one obtained from LAMBDA method's best candidate integer ambiguity set, with the float solution and with the smoothed version of the float solution. This performance evaluation is done by comparing the evolution and the precision levels given by the mean (μ) and standard deviation (σ) – with a confidence interval of 68.2 %. The same is done with pitch and heading angles, which can be determined with a single baseline configuration.

In the multiple baseline static trial it is done the same performance evaluation made in the single baseline case, for a more conclusive and robust evaluation of the developed techniques since the scenario introduces higher disturbance levels. Along with the comparison between the different techniques for baseline determination, the multiple baselines configuration allows the full determination of the attitude angles. Thus the performance of the developed algorithms for attitude determination is discussed. For the EKF, the respective innovation process, between the measured baseline coordinates and the ones estimated based in the quaternion elements, and the estimated angular velocities are analyzed.

Finally, the dynamic trial is analyzed in terms of the attitude angles' performance. This is done by comparing both attitude solutions, along with the performance of the EKF, that is given by the innovation process and the performance of the estimated angular velocities.

6.2 Static Trials Results

6.2.1 Single Baseline Results

Ambiguity Filter Performance

The first exercise is the performance comparison between the Ambiguity Filter's metrics. Using the metric 1, taking into account the carrier-phase residual ratio and the knowledge of the baseline length, or the metric 2, with the previous knowledge of the baseline Up coordinate in the place of the carrier-phase residual ratio, the evolution of the baseline solution may be different. As depicted in Figure 6.1, both metrics have different baseline lengths through time. While the baseline length of the solution using metric 2, characterized by the red line, instantaneously converges to the correct solution, the first metric's solution, sketched by the blue line, takes more epochs to stabilize. However, both

solutions converge to the correct solution, despite the longer time needed by the first metric's solution.

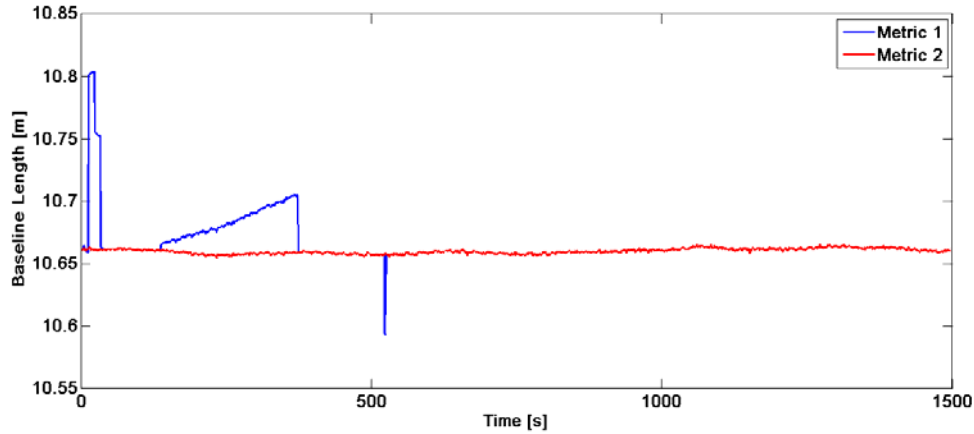


Figure 6.1 – Baseline length evolution, using the Ambiguity Filter’s metrics 1 and 2 to solve the integer ambiguity problem for the single baseline static trial

This is emphasized by the evolution of the baseline coordinates for both metrics, illustrated in Figure 6.2. As presented during the trials description, both GPS antennas are at the same height, and thus it is expected that the correct solution is the one with an Up coordinate close to zero. Since the baseline solution using the metric 2, again depicted by the red line, shows a better performance than the solution using metric 1 (blue line), since converges faster to the correct solution (with the Up coordinate being close to zero). In Figure 6.3 is presented a zoom of the baseline ENU coordinates using metric 2. By analyzing it, along with the evolution of the number of visible satellites in Figure 6.4, it is possible to verify that the baseline solution is not affected, despite the variation in the number of visible satellites. This is possible due to technique developed to manage the stored ambiguity candidates and the correct solution determined by the Ambiguity Filter.

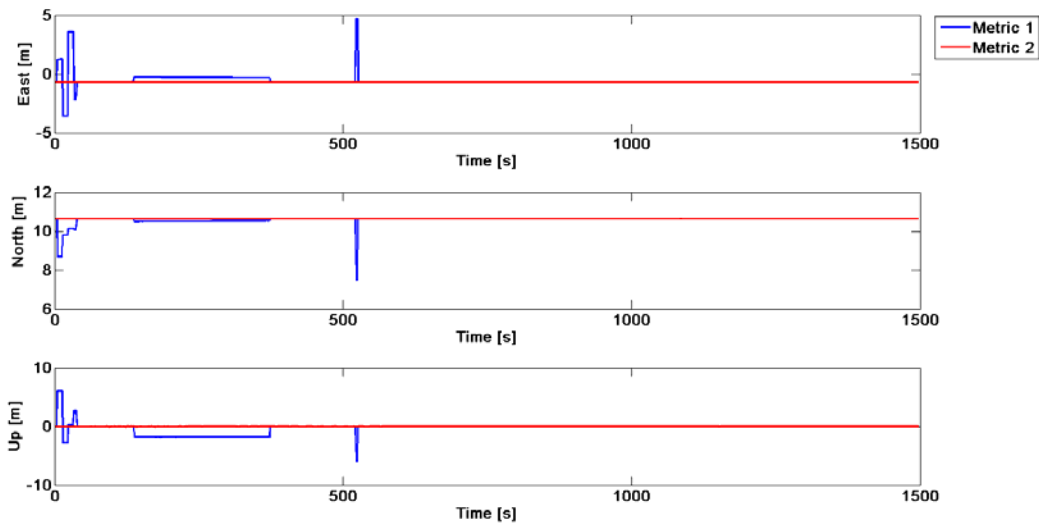


Figure 6.2 – Baseline ENU coordinates evolution, using the Ambiguity Filter metrics 1 and 2 to solve the integer ambiguity problem for the single baseline static trial

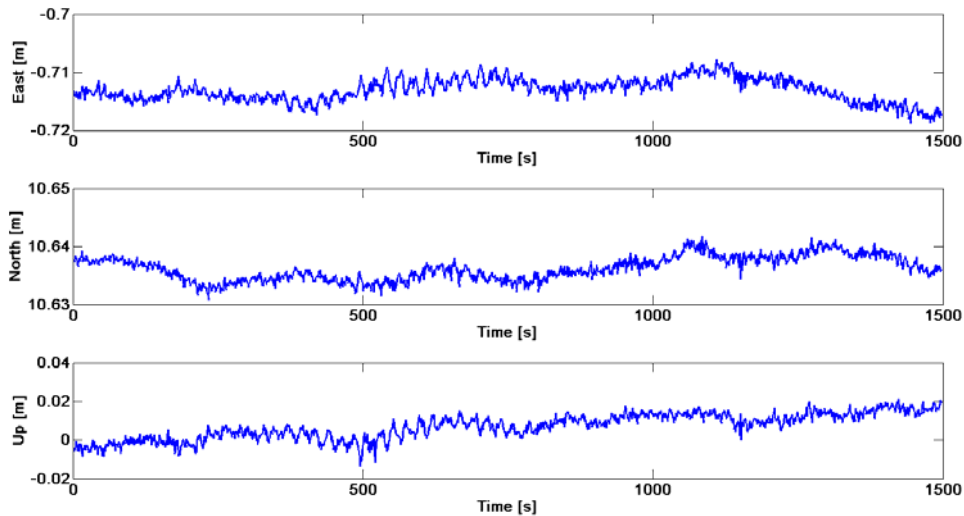


Figure 6.3 – Zoom of the baseline ENU coordinates evolution, using the metric 2 of the Ambiguity Filter to solve the integer ambiguity problem for the single baseline static trial

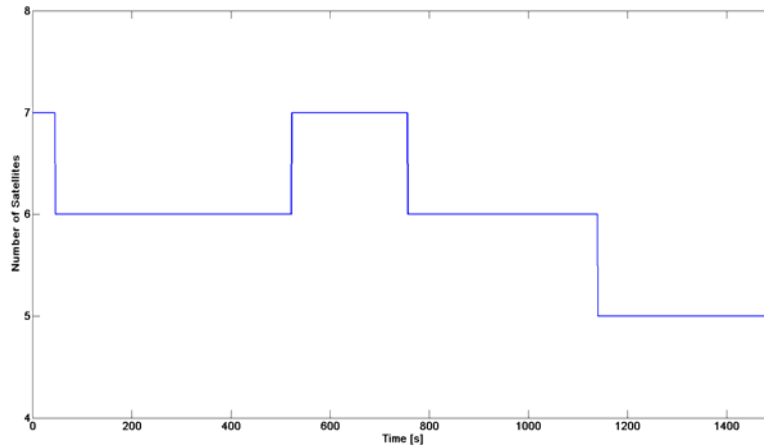


Figure 6.4 – Number of satellites visible during the data acquisition in the single baseline static trial

Comparison between Ambiguity Filter, LAMBDA Method, Float Solution and Smoothed Float Solution

At this point, it is important the comparison between the Ambiguity Filter's solution, using the better solution given by metric 2, with other techniques for the integer ambiguity resolution, as described in this thesis. From Figure 6.5, where the evolution of the baseline length is depicted, and from Figure 6.6, where the evolution of the baseline ENU coordinates is illustrated, it is possible to verify that the solution obtained from the LAMBDA method's best candidate in this, method's sense, and the float solution are very similar. In fact, the float solution has better precision, which is proved by the performance results present in Table 6.1, for the baseline length, and in Table 6.2, for the baseline ENU coordinates. This approximation between the two solutions is expected, since the best integer ambiguity candidate of the LAMBDA method is the integer that is close to the center of the search

space, which is defined by the float solution. As expected the smoothed float solution has a better precision than the first two techniques since it uses a smoothed version of the code measurements. However, the technique that has better precision is the solution using the Ambiguity Filter. Comparing the four techniques, in the scale of the Figure 6.5, the baseline length is noise free, which is not completely correct as depicted in Figure 6.3 with the appropriate scale. The same fact is illustrated by Figure 6.6 with the baseline's ENU coordinates.

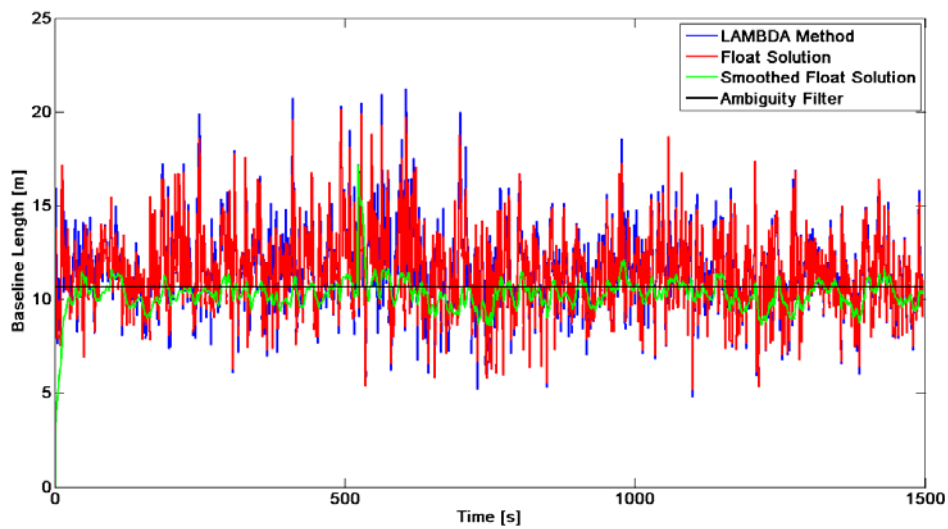


Figure 6.5 – Baseline length evolution using different techniques to solve the integer ambiguity problem

Table 6.1 – Performance of the baseline length using different techniques to solve the integer ambiguity problem

	Ambiguity Filter	LAMBDA method	Float Solution	Smoothed Float Solution
μ (m)	10.660	11.411	11.329	10.274
σ (m)	0.002	2.308	2.210	0.745

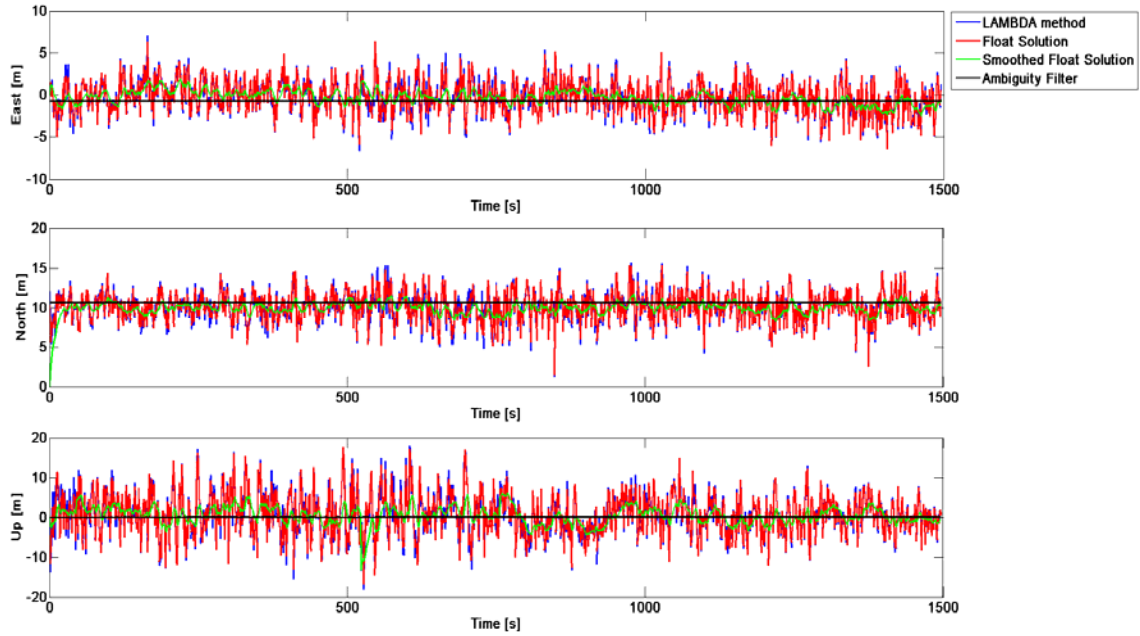


Figure 6.6 – Baseline ENU coordinates evolution using different techniques to solve the integer ambiguity problem

Table 6.2 – Performance of the baseline ENU coordinates in the single baseline static trial using different techniques to solve the integer ambiguity problem

	Ambiguity Filter	LAMBDA method	Float Solution	Smoothed Float Solution
μ_{East} (m)	-0,713	-0,371	-0,346	-0,327
σ_{East} (m)	0,002	1,953	1,889	0,804
μ_{North} (m)	10,636	9,981	9,977	9,935
σ_{North} (m)	0,002	1,878	1,809	0,816
μ_{Up} (m)	0,007	0,446	0,414	0,408
σ_{Up} (m)	0,007	5,311	5,149	2,247

By analyzing both tables above, for the baselines' length and ENU coordinates, it is possible to evaluate quantitatively each technique. The Ambiguity Filter solution has millimeter level precision, which is much better than any of the other techniques. With the smoothed float solution it is possible to achieve a centimeter level horizontal precision ($\approx 80\text{ cm}$), that is, with the East and North coordinates. A common characteristic to all the techniques is the degradation of the Up coordinate when compared with the horizontal precision, from a decrease of few millimeters with the Ambiguity Filter to several meters with the other techniques. These results ensure a great confidence in the use of the Ambiguity Filter to determine the integer ambiguity and hence use the baseline vectors in attitude determination.

Single-Baseline Attitude: Heading and Pitch Angles

A single baseline configuration allows the determination of pitch and heading, since these two angles relate the rotation of the baseline vector in both vertical and horizontal planes. The heading angle is

obtained with the baseline's North and East coordinates, that is, the components in the horizontal plane. The pitch angle is calculated using the baseline's projection in the horizontal plane and the Up coordinate. Heading and pitch angles' evolution is depicted in Figure 6.7 and in Figure 6.8, respectively.

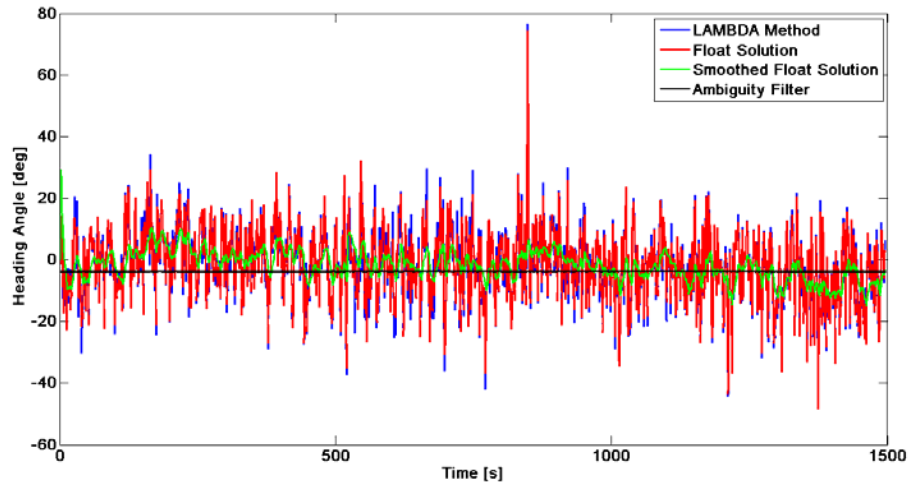


Figure 6.7 – Heading angle evolution using different techniques to solve the integer ambiguity problem

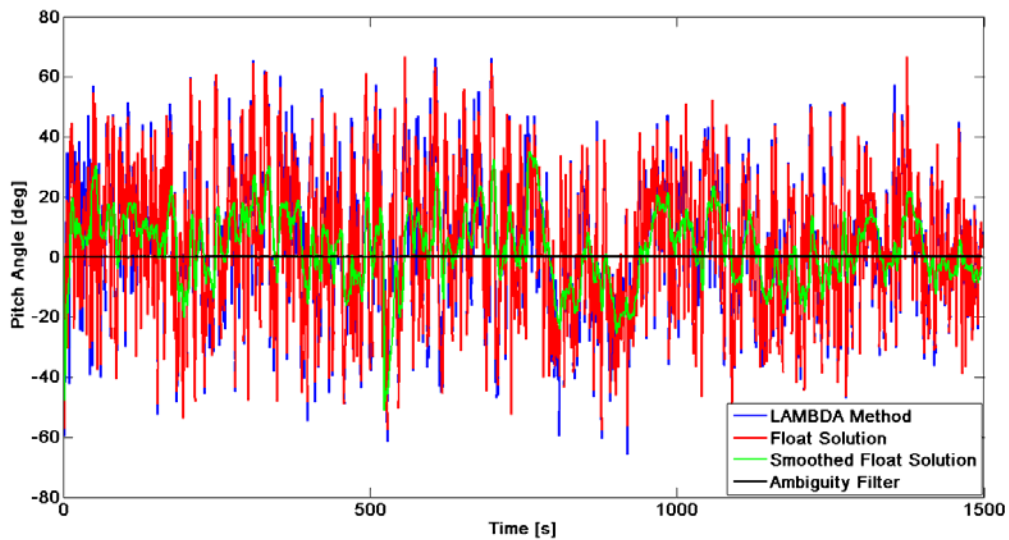


Figure 6.8 – Pitch angle evolution using different techniques to solve the integer ambiguity problem

As expected, the solution obtained by the Ambiguity Filter, which is zoomed in Figure 6.9, has higher precision than the other solutions. The dispersion of several centimeters, for the smoothed float solution, and a few meters for the LAMBDA method and the float solution is projected in heading and pitch angles with a precision of several degrees, which is not the best scenario when trying to determine a rigid body orientation. The worst case is the pitch angle that is obtained using the Up

coordinate, which is the component that is most affected by disturbances, as previously discussed. These results are resumed in Table 6.3.

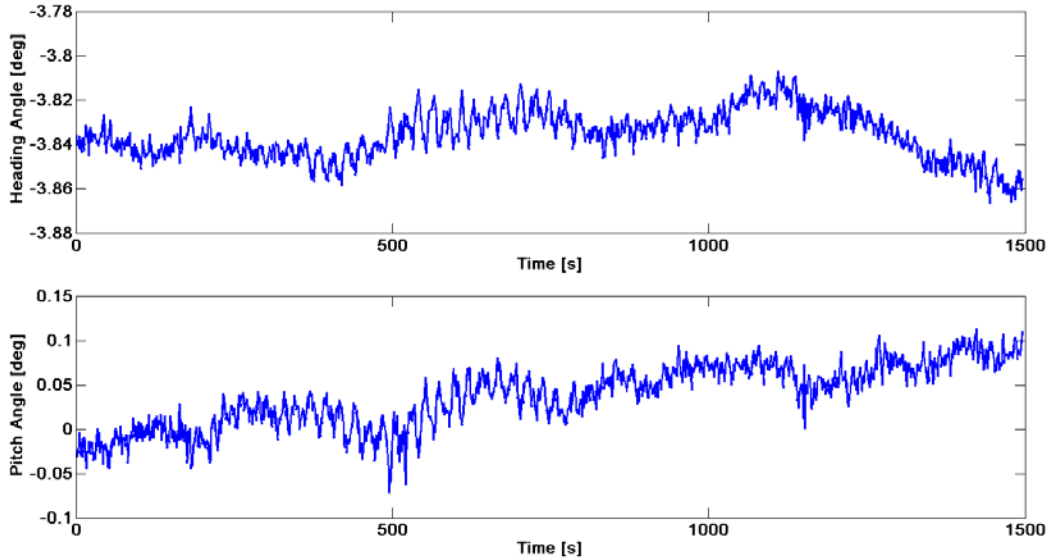


Figure 6.9 – Zoom of the heading and pitch angles, using the solution from the Ambiguity Filter

Table 6.3 – Heading and pitch angles’ performance using different techniques to solve the integer ambiguity problem

	Ambiguity Filter	LAMBDA method	Float Solution	Smoothed Float Solution
$\mu_{Heading} (^{\circ})$	-3.836	-2.466	-2.363	-1.867
$\sigma_{Heading} (^{\circ})$	0.011	11.679	11.319	4.801
$\mu_{Pitch} (^{\circ})$	0.037	2.382	2.322	2.368
$\sigma_{Pitch} (^{\circ})$	0.035	25.533	24.975	12.291

These results show that the best solution for attitude determination is the Ambiguity Filter, despite of only pitch and heading angles are considered in this single baseline case. The baseline vector obtained with the Ambiguity Filter allows the determination of angles with centesimal precision (in degrees).

6.2.2 Multiple Baselines Results

Ambiguity Filter Performance

The first exercise is, once again, the evaluation of the Ambiguity Filter’s performance, but in this case with multiple baselines. As described in the algorithm overview, each baseline is calculated separately. However, it is important to test again the ambiguity Filter performance since the scenario is more exposed to different types of disturbances, such as multipath, than the scenario of the single

baseline static trial.

In previous results it demonstrated that the Ambiguity Filter metric 2 gives more confidence (in accuracy) than the metric 1 in the determination of the correct integer ambiguity set. In the multiple baseline static trial, both Ambiguity Filter solutions using metric 1 and metric 2 converge to the correct integer ambiguity, which is proved by the Up coordinate that is expected to be close to zero, as depicted in Figure 6.10 and in Figure 6.11.

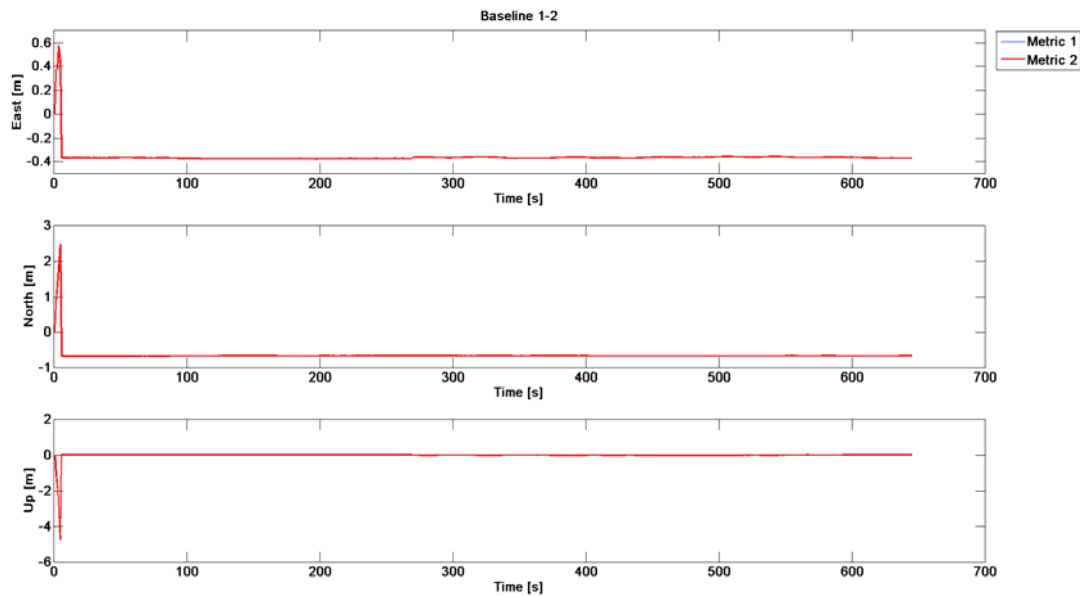


Figure 6.10 – Baseline ENU coordinates evolution, between the GPS receivers 1 and 2, with the Ambiguity Filter solution using metrics 1 and 2

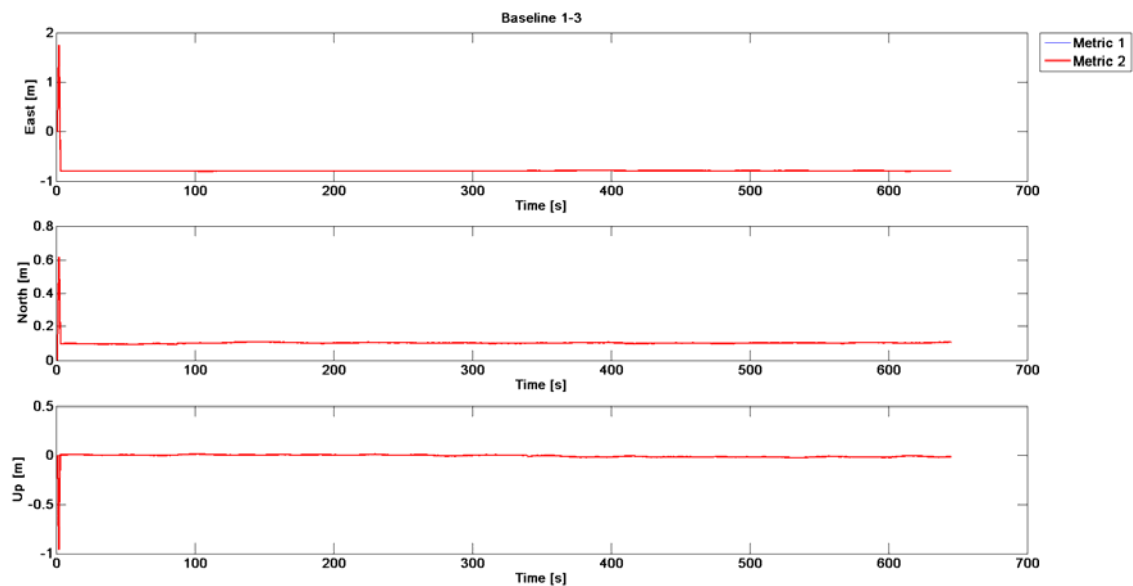


Figure 6.11 – Baseline ENU coordinates evolution, between the GPS receivers 1 and 3, with the Ambiguity Filter solution using metrics 1 and 2

However, for the baseline 1-4 only the solution obtained by metric 2 is correct. The solution obtained using the metric 1 stabilizes in an incorrect integer ambiguity set, since the baseline Up coordinate is $\approx -40\text{ cm}$, as depicted in Figure 6.12, which is not the correct baseline vector as presented in the trials description section. Thus these results prove that, in a scenario exposed to bigger disturbances, the metric 2 has better chances to determine the correct integer ambiguity, and hence is more accurate.

From the results presented in these two static trials, it was decided to use the Ambiguity Filter resorting only to metric 2, since in both scenarios are better with this technique. The following results presented in this thesis take into account this decision, and the results obtained resorting to metric 1 are neglected.

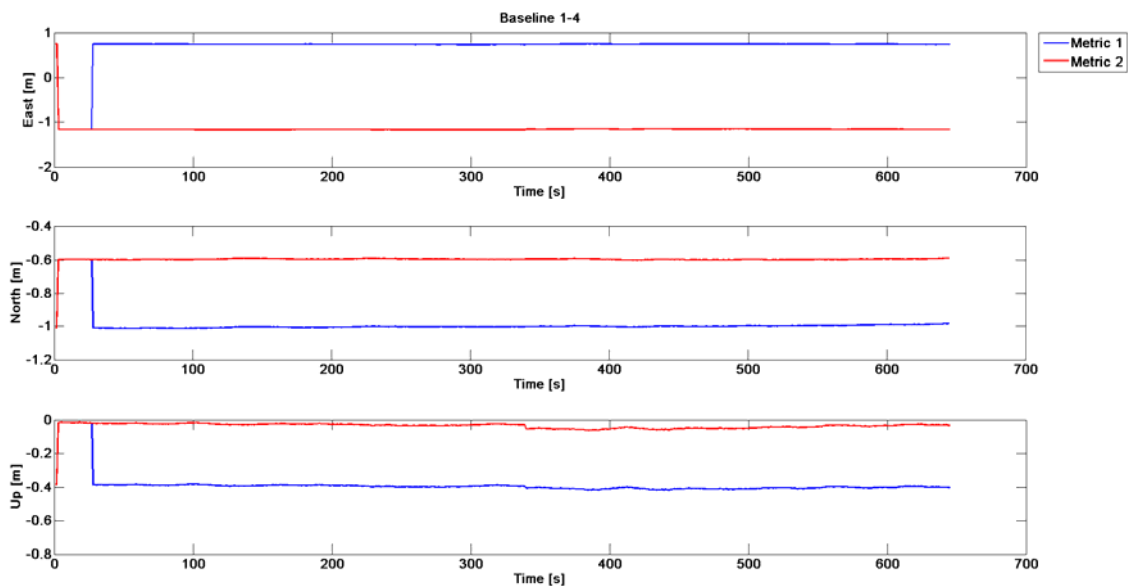


Figure 6.12 – Baseline ENU coordinates evolution, between the GPS receivers 1 and 4, with the Ambiguity Filter solution using metrics 1 and 2

In contrast with the results presented for the single baseline static trial, in this environment the baseline coordinates are more affected by the variation in the number of visible satellites. However, by comparing the ENU coordinates of each baseline vector in Figures 6.13, 6.14 and 6.15 with the evolution in the number of visible satellites in Figure 6.16, the oscillation is not bigger than a few centimeters, which guarantee that the precise and accurate solution is not lost. This oscillation may be seen in Figure 6.13 for the baseline 1-2 ENU coordinates, where the North component has a small increment due to the reduction of the number of visible satellites from 8 to seven before the instant 100 s, and where the East component is increased and Up component decreases few centimeters almost instantaneously between epochs [200;300] s, which is coincident with the reduction in the number of visible satellites from 6 to 5, as represented in Figure 6.16 for the respective baseline.

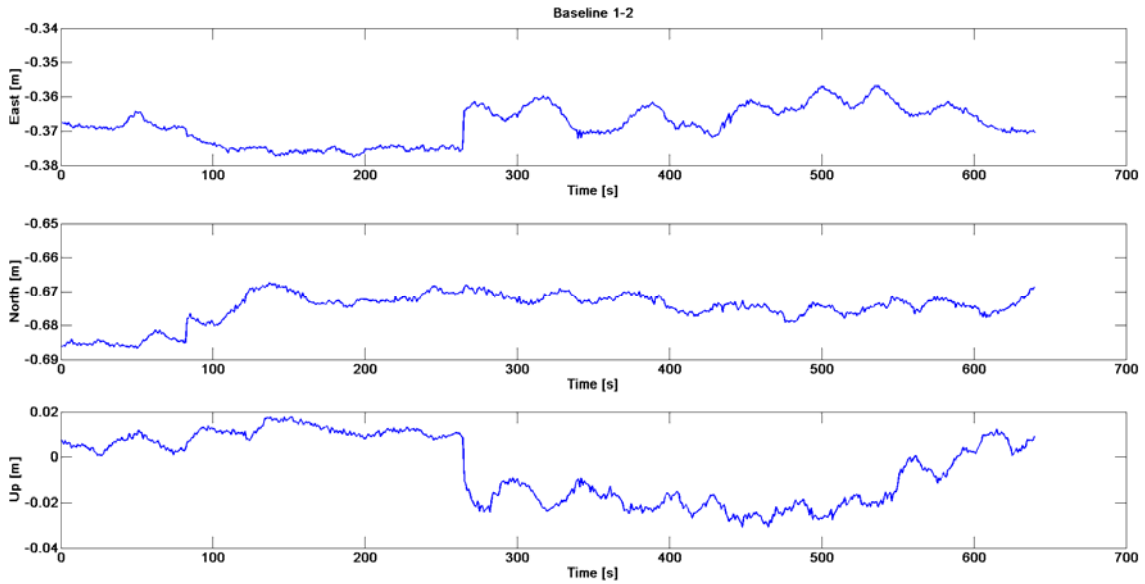


Figure 6.13 – Zoom of the baseline ENU coordinates evolution, between the GPS receivers 1 and 2, with the Ambiguity Filter solution using metrics 2

From the three baseline vectors, the baseline 1-3 is the one that is less affected by the variation in the number of visible satellites, since in Figure 6.14 is not possible to distinguish bigger oscillations despite small spikes that coincide with variations sketched in Figure 6.16, for the respective baseline.

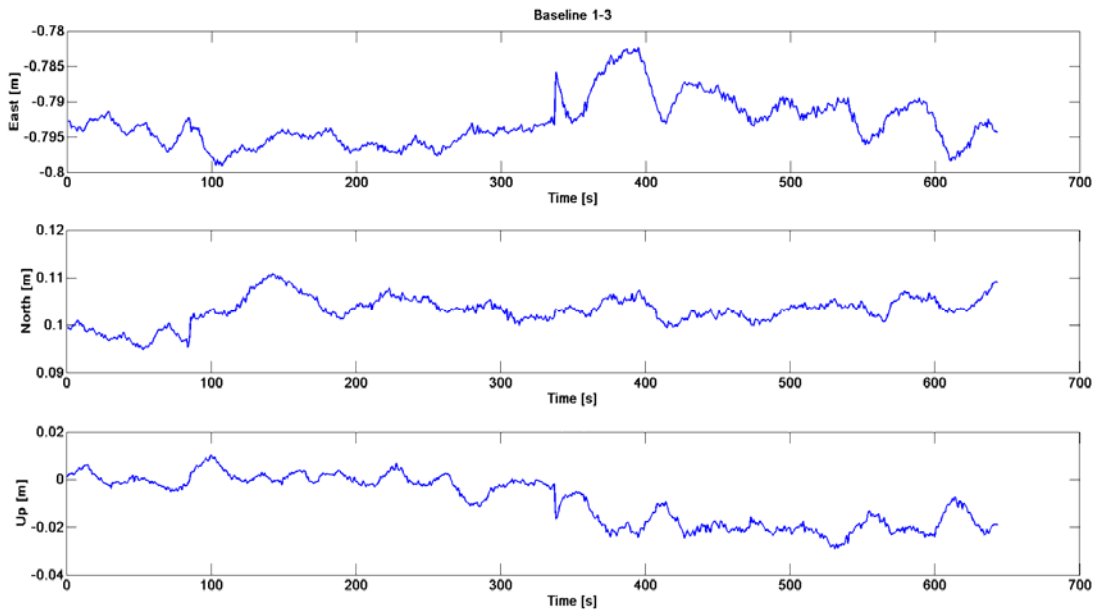


Figure 6.14 – Zoom of the baseline ENU coordinates evolution, between the GPS receivers 1 and 3, with the Ambiguity Filter solution using metrics 2

Finally, the baseline 1-4 is mostly affected by the variation in the number of visible satellites between the epochs [200; 300] s, from 7 to 6 satellites, as illustrated in Figure 6.16, for the respective baseline.

This centimeter-level oscillation is verified in an instantaneous increment of the East component and a decrease of the Up component.

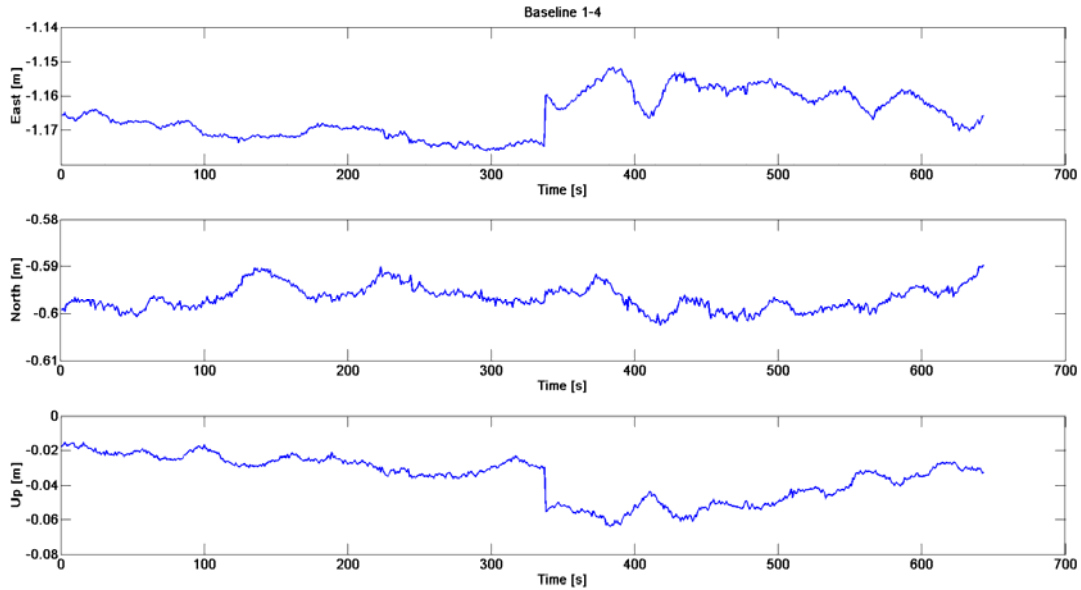


Figure 6.15 – Zoom of the baseline ENU coordinates evolution, between the GPS receivers 1 and 4, with the Ambiguity Filter solution using metrics 2

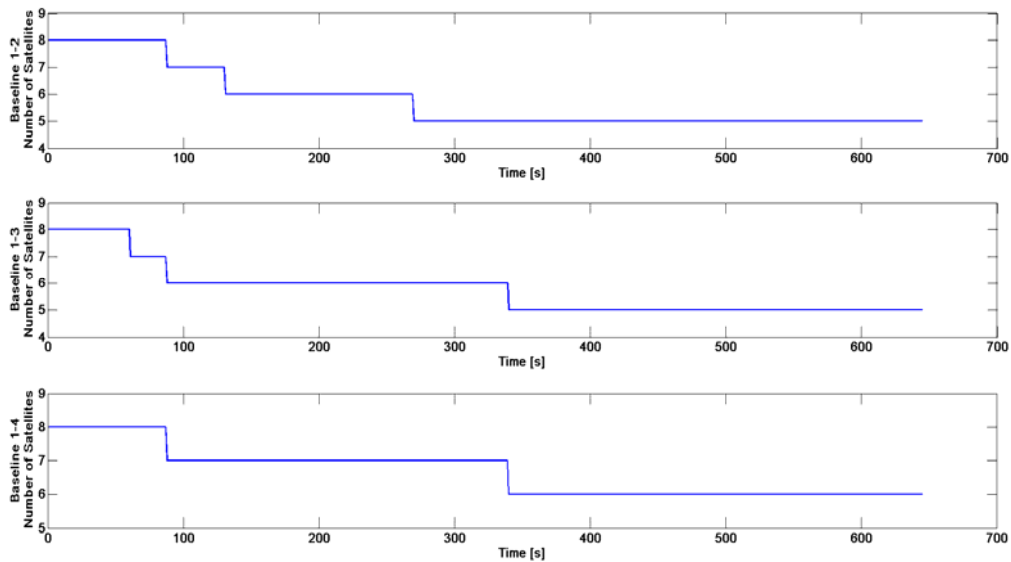


Figure 6.16 – Number of visible satellites for the three baseline vectors

These results prove that, even in noisier environments, the technique used to avoid the lost of the correct integer ambiguity set solution, by resetting the Ambiguity Filter, is a big addition to the algorithm improving the results presented in [8], keeping a precise and accurate solution for the baseline vectors.

Comparison between Ambiguity Filter, LAMBDA Method, Float Solution and Smoothed Float Solution

For the comparison between the Ambiguity Filter and the remaining techniques, the baseline vectors' ENU coordinates, obtained with different methods, are presented in Figures 6.17, 6.18 and 6.19, for the respective baseline.

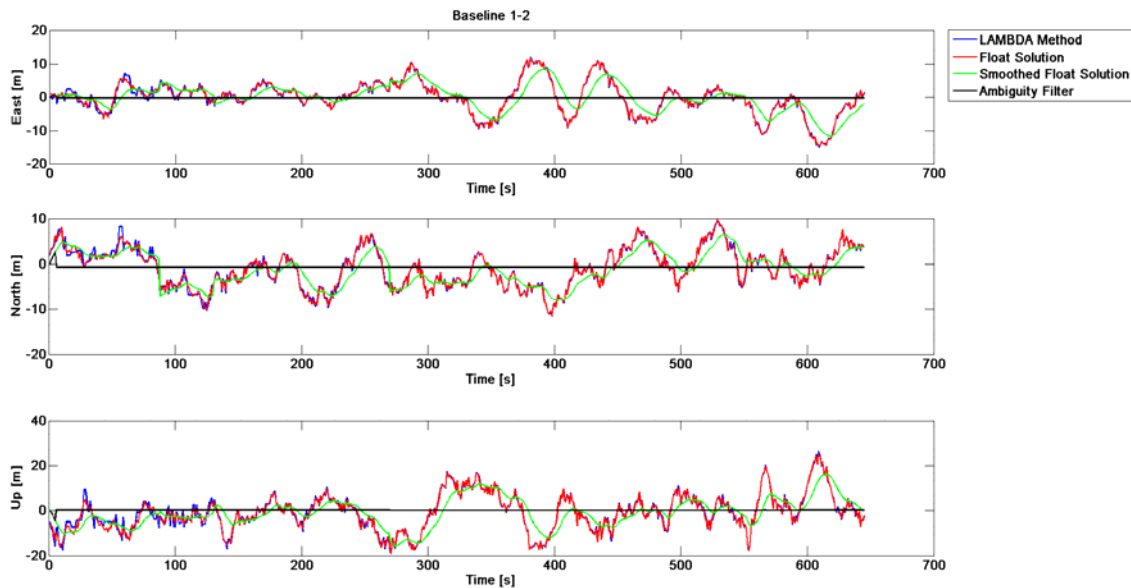


Figure 6.17 – Baseline ENU coordinates evolution, between the GPS receivers 1 and 2, using different techniques to solve the integer ambiguity problem

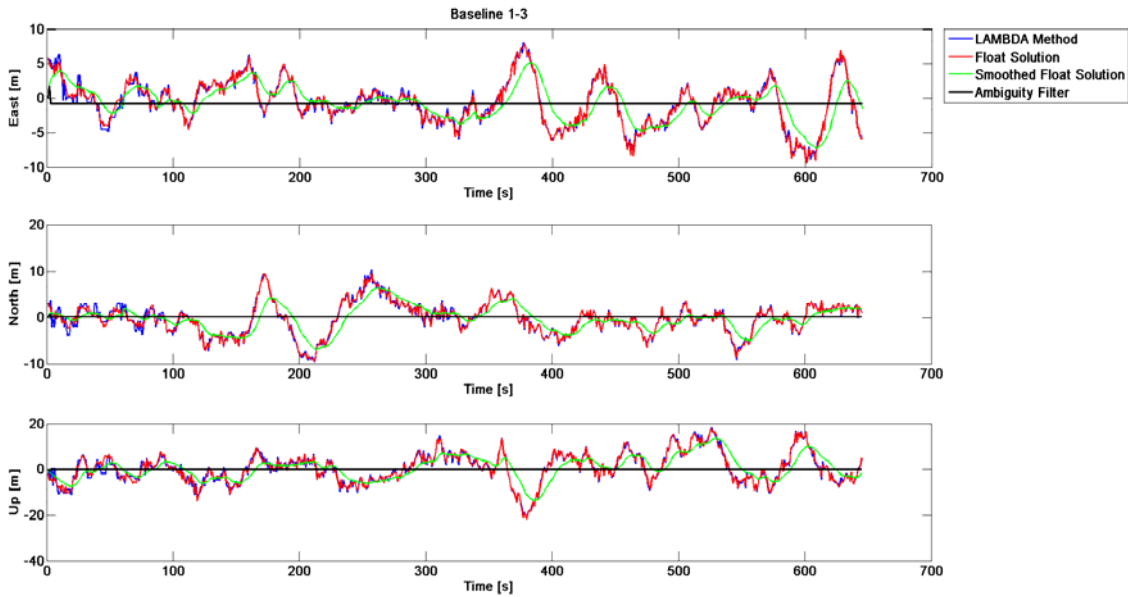


Figure 6.18 – Baseline ENU coordinates evolution, between the GPS receivers 1 and 3, using different techniques to solve the integer ambiguity problem

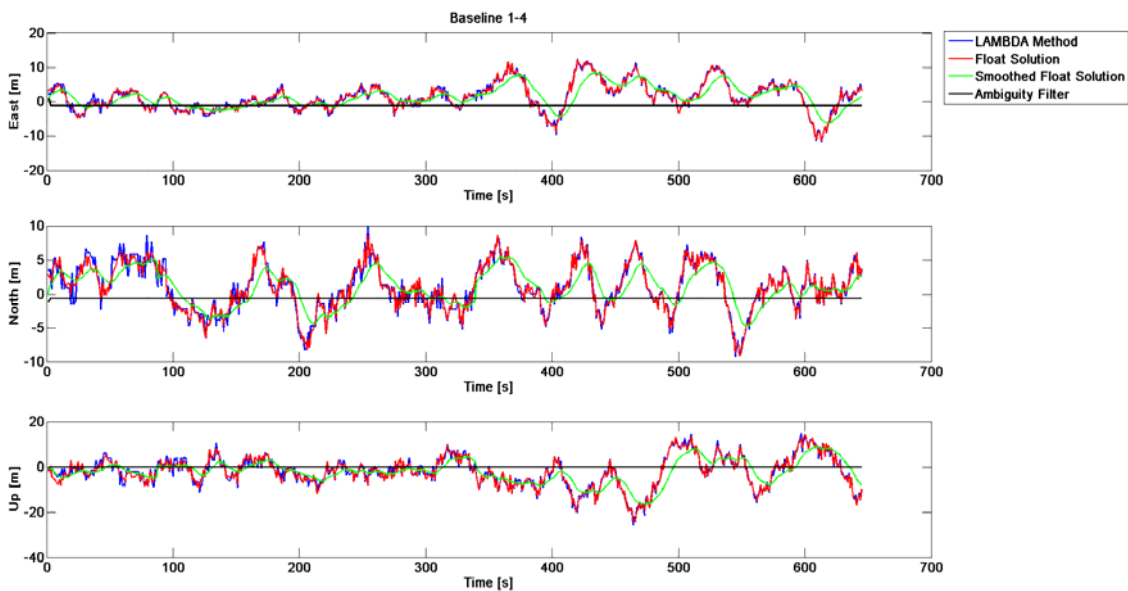


Figure 6.19 – Baseline ENU coordinates evolution, between the GPS receivers 1 and 4, using different techniques to solve the integer ambiguity problem

For the three baselines the results are analogous to the ones presented for the same comparison for the single baseline case. In fact, due to higher disturbances present in this scenario, there is degradation in the precision level, which may be verified by comparing Tables 6.2 and 6.4. By analyzing the Up coordinates' performance, in Table 6.4, for all techniques it is possible to demonstrate that in this case the precision of the solution obtained by using the Ambiguity Filter is close to 1.3 *cm*, which is worst when compared with an accuracy of 7 *mm* for the single baseline case. However this loss of precision is small when compared with the precision of the remaining solutions

that have levels in the order of several meters. This fact is illustrated in above Figures, where the Ambiguity Filter solution is almost undisturbed when compared with the remaining ones.

Table 6.4 – Performance of the baseline ENU coordinates in the multiple baseline static trial using different techniques to solve the integer ambiguity problem

		Ambiguity Filter	LAMBDA method	Float Solution	Smoothed Float Solution
Baseline 1-2	μ_{East} (m)	-0.368	-0.306	-0.262	-0.202
	σ_{East} (m)	0.005	4.855	4.820	3.861
	μ_{North} (m)	-0.675	-0.999	-1.017	-1.199
	σ_{North} (m)	0.005	4.232	4.176	3.489
	μ_{Up} (m)	-0.005	-0.964	-1.096	-1.131
	σ_{Up} (m)	0.015	8.034	7.991	6.217
Baseline 1-3	μ_{East} (m)	-0.793	-0.687	-0.677	-0.645
	σ_{East} (m)	0.003	3.201	3.183	2.373
	μ_{North} (m)	0.103	-0.328	-0.327	-0.326
	σ_{North} (m)	0.003	3.422	3.372	2.608
	μ_{Up} (m)	-0.009	0.487	0.544	0.550
	σ_{Up} (m)	0.010	6.727	6.662	5.003
Baseline 1-4	μ_{East} (m)	-1.166	1.353	1.328	1.355
	σ_{East} (m)	0.006	4.005	3.976	3.013
	μ_{North} (m)	-0.597	0.891	0.895	0.893
	σ_{North} (m)	0.003	3.508	3.413	2.455
	μ_{Up} (m)	-0.036	-2.189	-2.241	-2.152
	σ_{Up} (m)	0.013	6.638	6.579	4.936

From these results, along with the ones presented for the single baseline trial, it is proved that from the presented techniques only the Ambiguity Filter allow solutions with good precision to estimate the platform's attitude correctly

Attitude Determination

Using the baseline vectors obtained with the Ambiguity Filter as measurements, after the algorithm's stabilization, the attitude angles were obtained by employing both the rotation matrix technique and the quaternion based EKF. In Figure 6.20 both solutions are presented. The blue line illustrates the evolution of the Euler angles estimated by the rotation matrix LS. The red line depicts the evolution of the Euler angles obtained by the quaternion based EKF. Since this is a recursive algorithm, it takes a few seconds to stabilize in the correct values, which corresponds to the transitory in the EKF's solution.

In Figure 6.21 is presented a zoom of the attitude angles' evolution, where it is possible to see that both solutions are similar. However, the solution obtained through time by the EKF is smoother than the one obtained directly from the rotation matrix, which is emphasized by the numerical performance results depicted in Table 6.5. These results are expected, due to the recursive nature of the EKF.

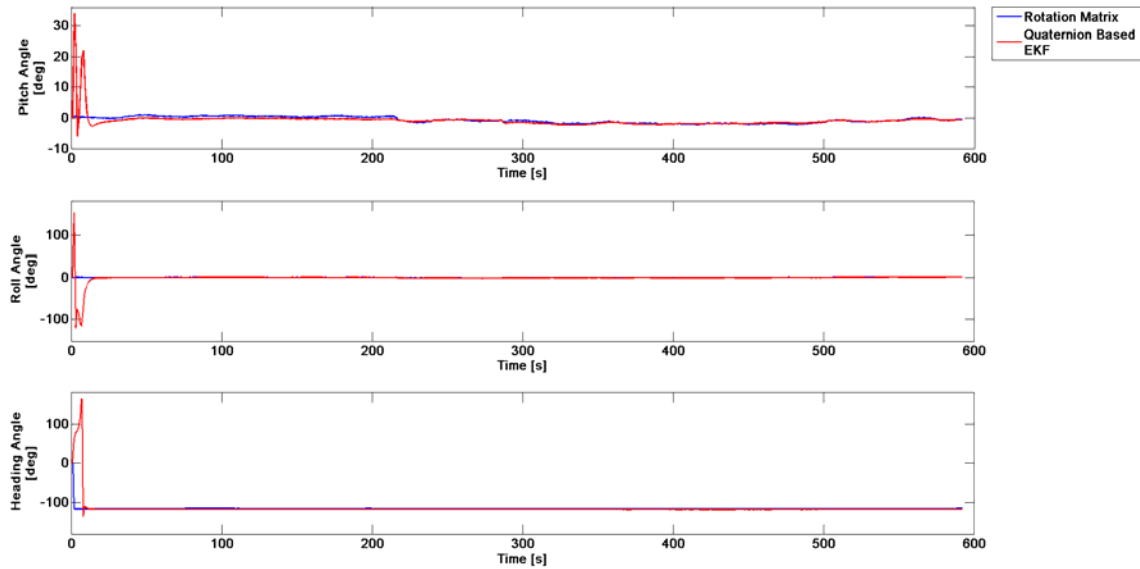


Figure 6.20 – Comparison between the attitude angles obtained with the rotation matrix technique and with the quaternion based EKF

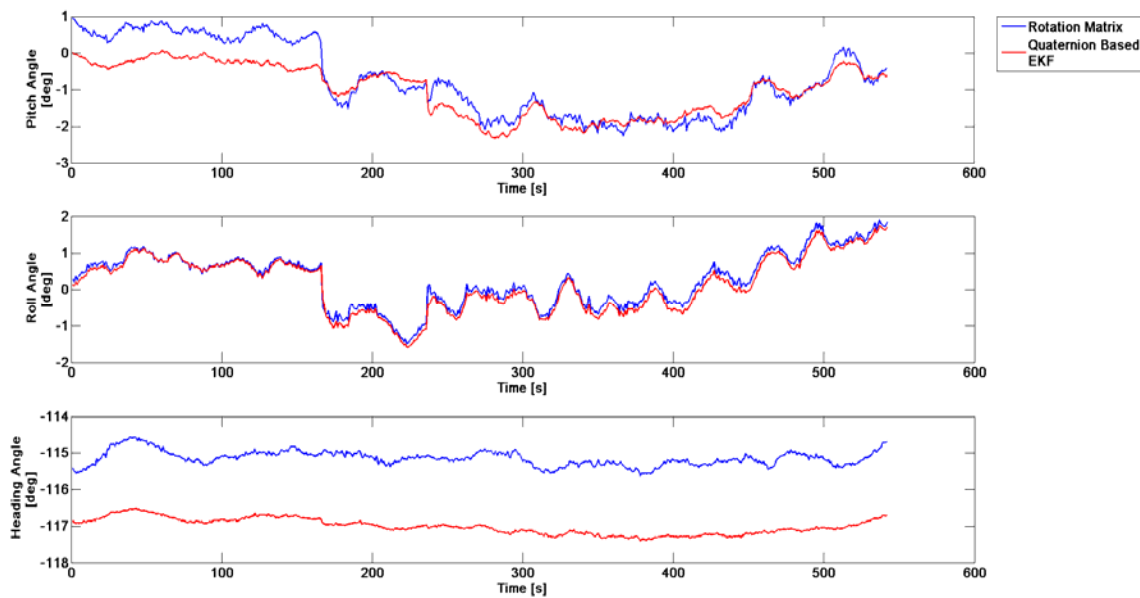


Figure 6.21 – Zoom of the comparison between the attitude angles obtained with the rotation matrix technique and with the quaternion based EKF

Table 6.5 – Performance of the attitude angles estimation, using the rotation matrix technique and the quaternion based EKF

		Rotation Matrix	Quaternion Based EKF
Pitch Angle	μ (°)	-0.666	-1.007
	σ (°)	1.001	0.708
Roll Angle	μ (°)	0.277	0.147
	σ (°)	0.709	0.751
Heading Angle	μ (°)	-115.193	-117.008
	σ (°)	0.261	0.212

As aforementioned, only the baseline vectors are used as measurements. Thus, the angular velocities are estimated in the EKF, and its evolution is depicted in Figure 6.22. As expected, the presented results for the angular velocities converge to zero, since the platform has no motion. This fact demonstrates that the dynamic system is correctly design, since the angular velocities are correctly estimated by using only the baseline vectors' measurements.

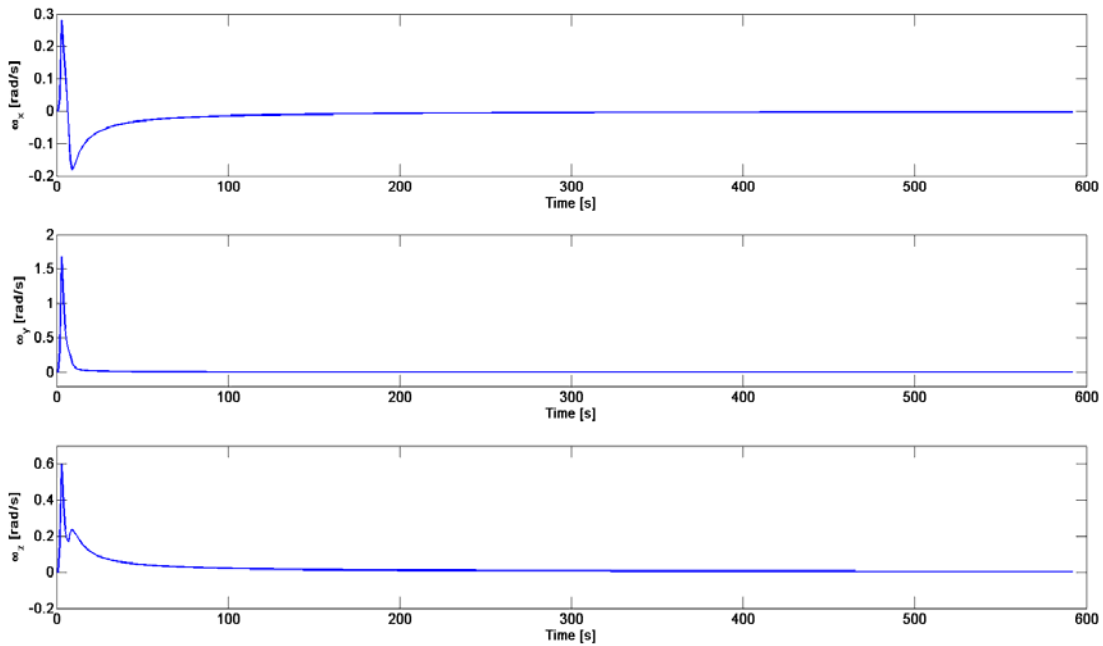


Figure 6.22 – Angular velocities estimated with the quaternion base EKF during the static trial

Since there is not information about the real value of the attitude angles, the innovation process may be used to evaluate the EKF performance. The evolution of the innovation for each baseline is depicted in Figures 6.23, 6.24 and 6.25, and the respective performance is resumed in Table 6.6. The results present that the mean value of the innovation process is close to zero and that its precision is close to the millimeter-level.

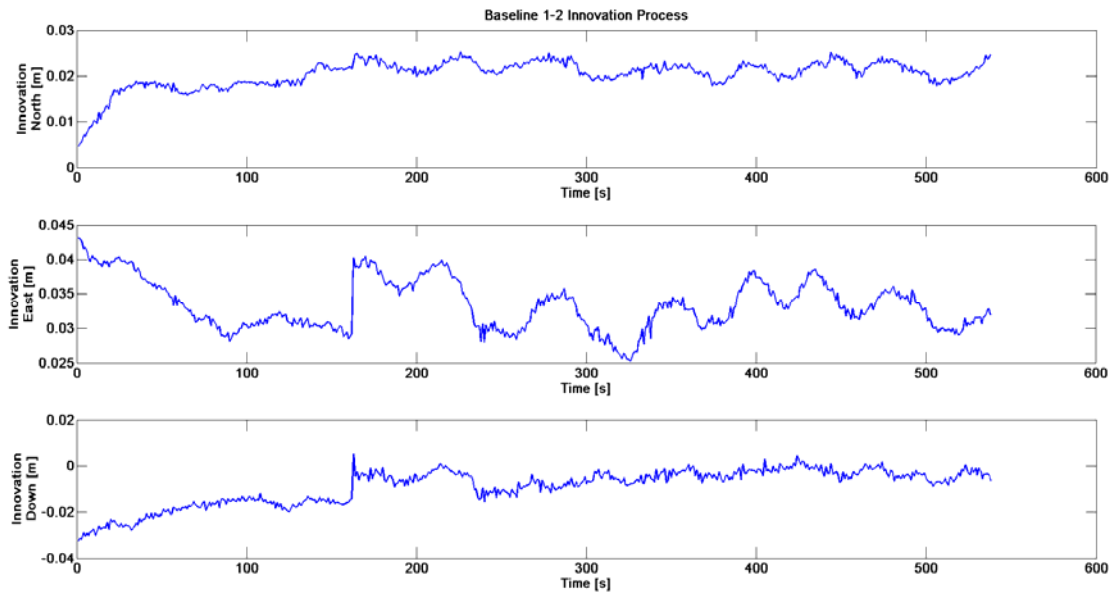


Figure 6.23 – Innovation process between the measured baseline 1-2 and the one obtained with the estimated quaternion

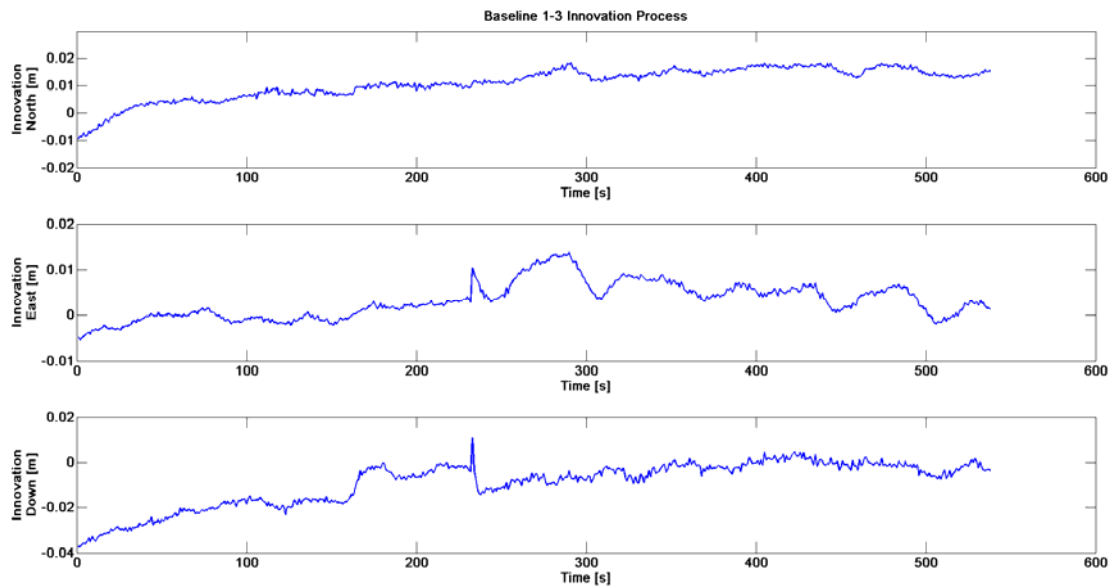


Figure 6.24 – Innovation process between the measured baseline 1-3 and the one obtained with the estimated quaternion

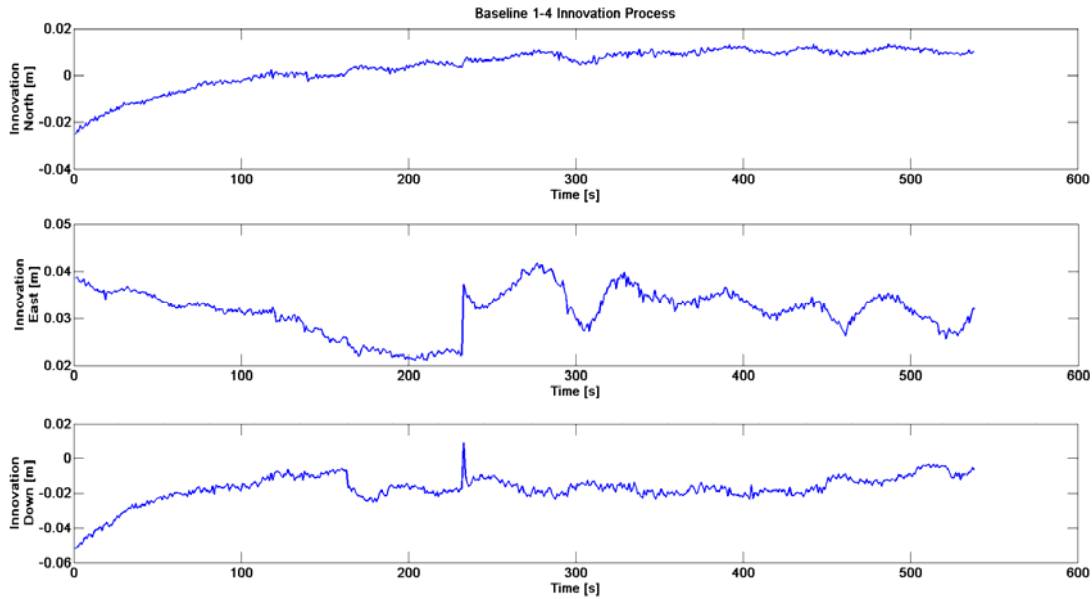


Figure 6.25 – Innovation process between the measured baseline 1-4 and the one obtained with the estimated quaternion

Table 6.6 – Performance of the innovation process for each baseline, during the static trial

	Baseline 1-2	Baseline 1-3	Baseline 1-4
$\mu_{Innov. North} (m)$	0.020	0.011	0.004
$\sigma_{Innov. North} (m)$	0.003	0.006	0.008
$\mu_{Innov. East} (m)$	0.033	0.003	0.032
$\sigma_{Innov. East} (m)$	0.004	0.004	0.005
$\mu_{Innov. Down} (m)$	-0.009	-0.009	-0.017
$\sigma_{Innov. Down} (m)$	0.008	0.010	0.008

6.3 Dynamic Trial Results

At this point it is clear that only the baseline solution obtained with the best integer ambiguities, provided by the Ambiguity Filter, allow high levels of confidence in attitude determination. As aforementioned, the same platform used for the multiple baseline static trial was in motion with the trajectory previously depicted by Figure 5.9. The corresponding Euler angles are depicted in Figure 6.26. The attitude algorithms' solution is only available after the correct integer ambiguity is known, that is, when the stabilization of the Ambiguity Filter is achieved. Around the epoch $t = 150 s$ the platform starts moving, which is characterized by the heading variation and the increase in the disturbances present in both pitch and roll angles. As for the static case, in the first epochs the EKF's solution is characterized by a transitory preceding the convergence of the state variables around the correct solution.

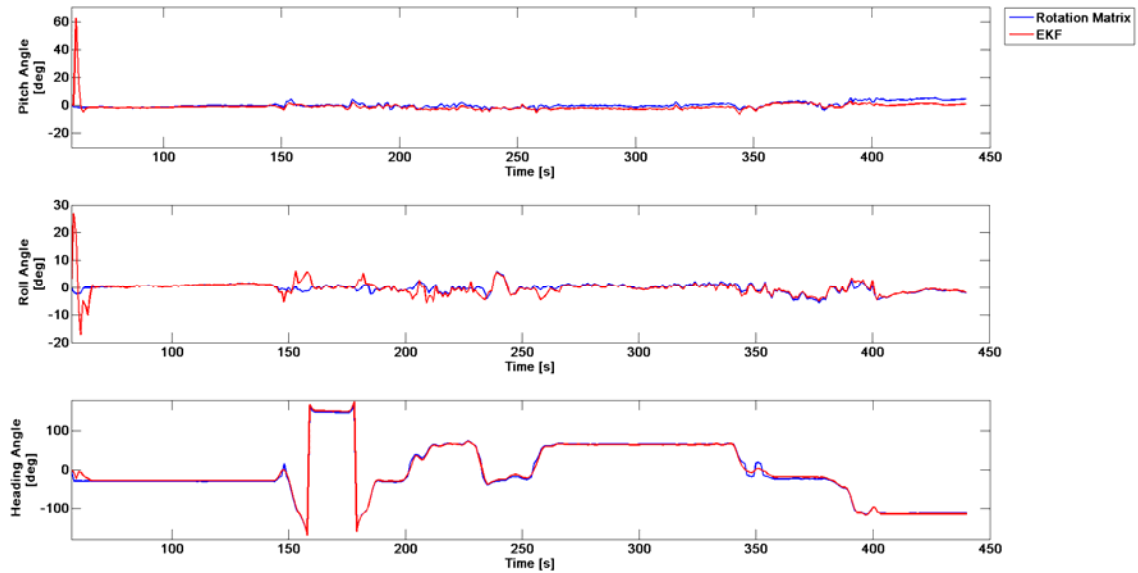


Figure 6.26 – Comparison between the attitude angles obtained with the rotation matrix technique and with the quaternion based EKF, for the dynamic trial

By analyzing Figure 6.26 along with the zoom of pitch and roll angles in Figure 6.27, one may verify that at the beginning, around epoch $t = 150\text{ s}$, of the trajectory the roll angle estimated by the EKF is highly disturbed when compared with the solution obtained by the rotation matrix. This fact is emphasized by the x term of the angular velocity after the platform start moving in Figure 6.30, which is not exact since the maneuvers made during the trial were with small accelerations. This may be explained by the decrease of precision in the Up coordinate after the platform started moving, which is represented in Figure 6.28. This could be improved by using an accelerometer output as measurement of the EKF and hence to better estimate the angular velocities.

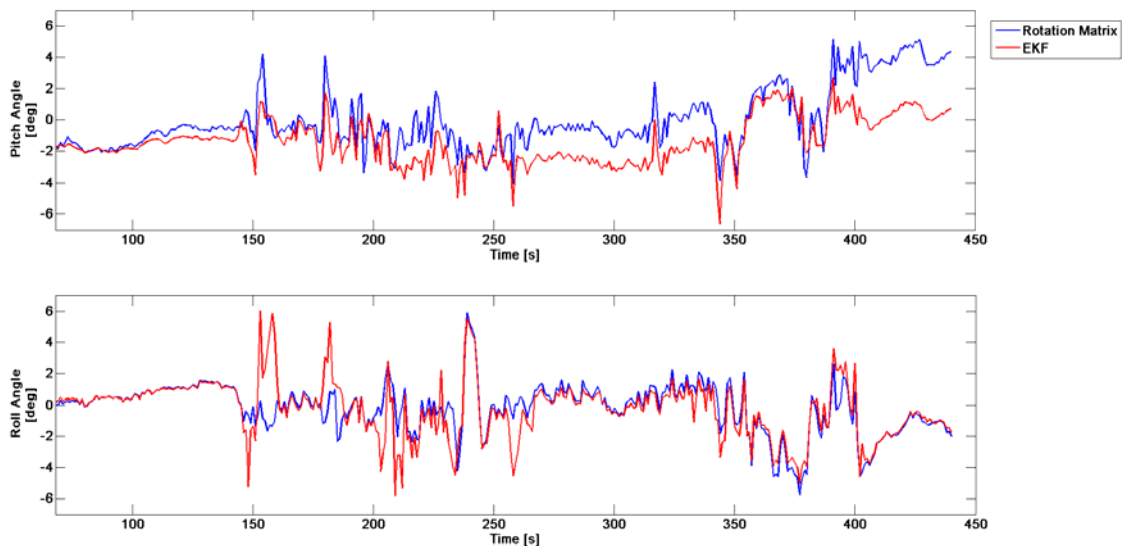


Figure 6.27 – Zoom of pitch and roll angles obtained with the rotation matrix technique and with the quaternion based EKF, for the dynamic trial

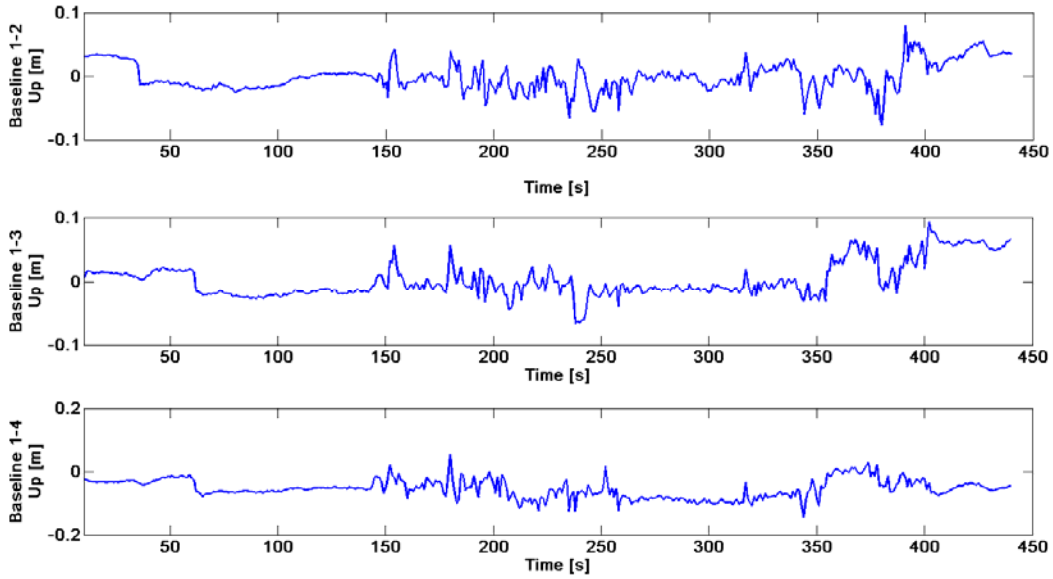


Figure 6.28 – Up coordinate evolution of the three baselines after stabilization

During this trial a positive roll angle was imposed to the car used as platform by climbing the side walk only with the left side wheels, between epochs $t \in [235; 245] s$ and when the vehicle's heading was $\approx -30^\circ$. This test's result is depicted in Figure 6.29, where it is possible to see that the roll angle evolution is approximately 5° for both techniques at epoch $t = 240 s$, which corresponds to the positive rotation about the x -axis applied to the vehicle.

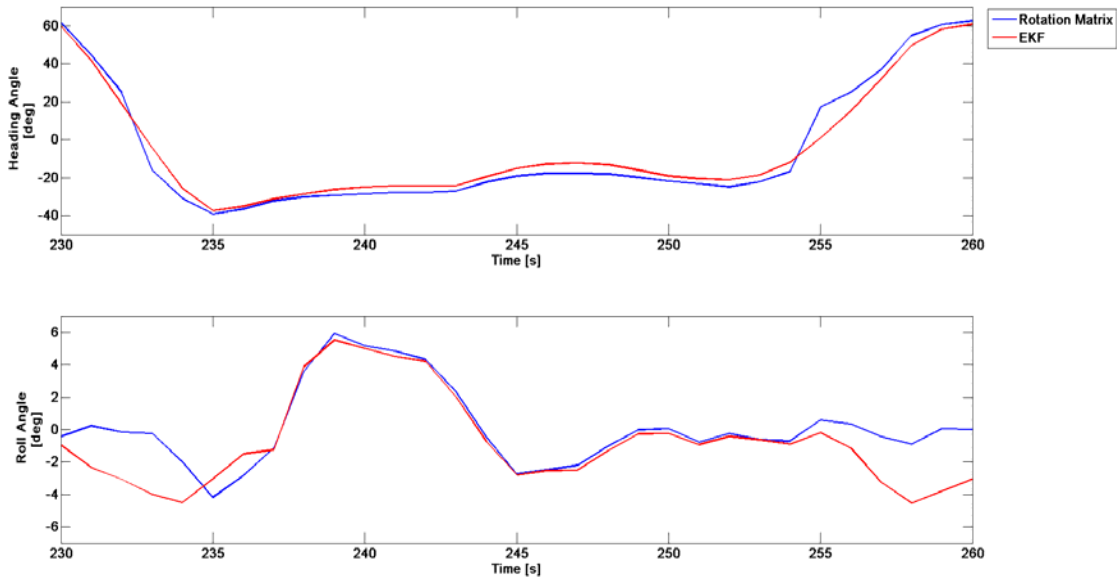


Figure 6.29 – Zoom of heading and roll angles, during a positive rotation about the x axis (positive roll angle), obtained with the rotation matrix technique and with the quaternion based EKF, for the dynamic trial

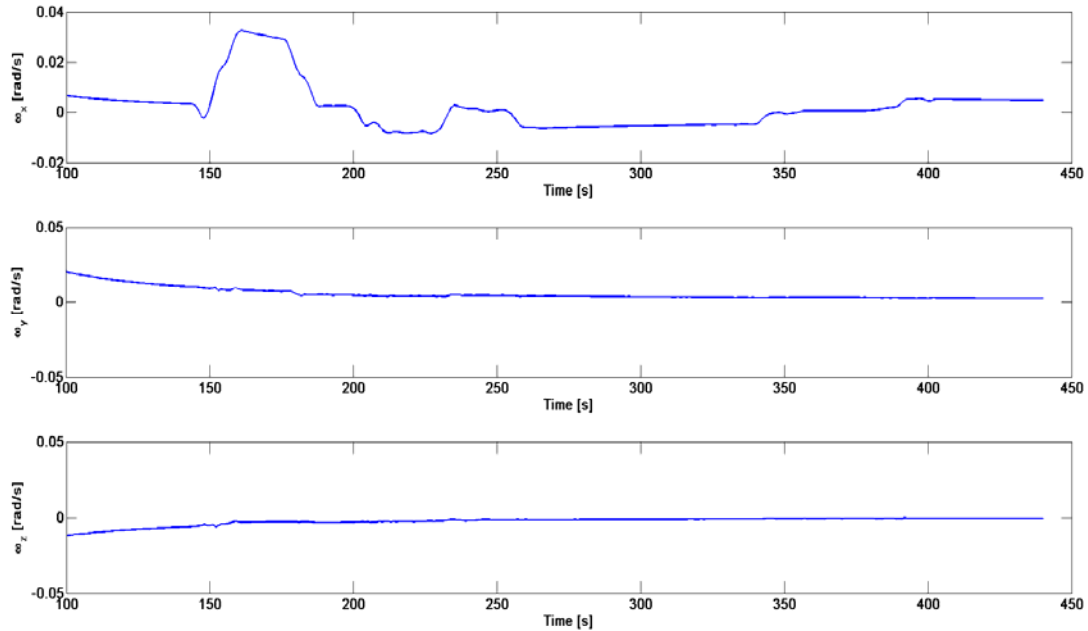


Figure 6.30 – Evolution of the angular velocities estimated by the EKF during the dynamic trial

As for the static case, the innovation process is used to evaluate the performance of the EKF. But in the dynamic trial case, the movement increased the disturbances present in the measurements as already illustrated in Figure 6.28 for the baselines' Up coordinates. This fact is illustrated too in the evolution of the innovation process, where the initial instant $t = 1 s$ corresponds to the epoch when the Ambiguity Filter achieved the optimal solution, that is $t = 57 s$. So the vehicle starts moving when the innovation process is close to $t = 100 s$ in Figures 6.31, 6.32 and 6.33, for the respective baselines. As expected the innovation of each baseline coordinate is zero mean but in contrast with the static case higher residual levels are identified, which are recursively compensated by the Kalman gain. Despite the good results presented by the EKF in this dynamic trial, this solution could not be applicable with highly disturbed measurements that lead to residual levels outside the boundaries of the stability region. The performance of the EKF is resumed in Table 6.7, where it is possible to confirm that the average innovation for each baseline is around zero and that the standard deviation varies from several millimeters to several centimeters, representing a slight degradation as expected when comparing with the results for the static trial in Table 6.6.

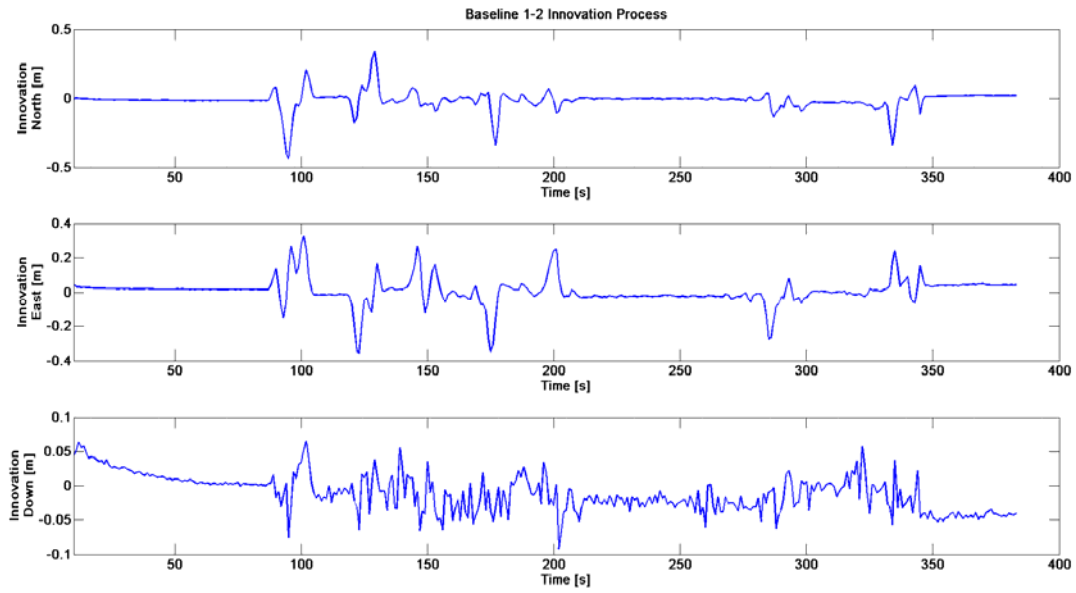


Figure 6.31 – Evolution of the innovation process between the measured baseline1-2 and the one obtained by the estimated quaternion, during the dynamic trial

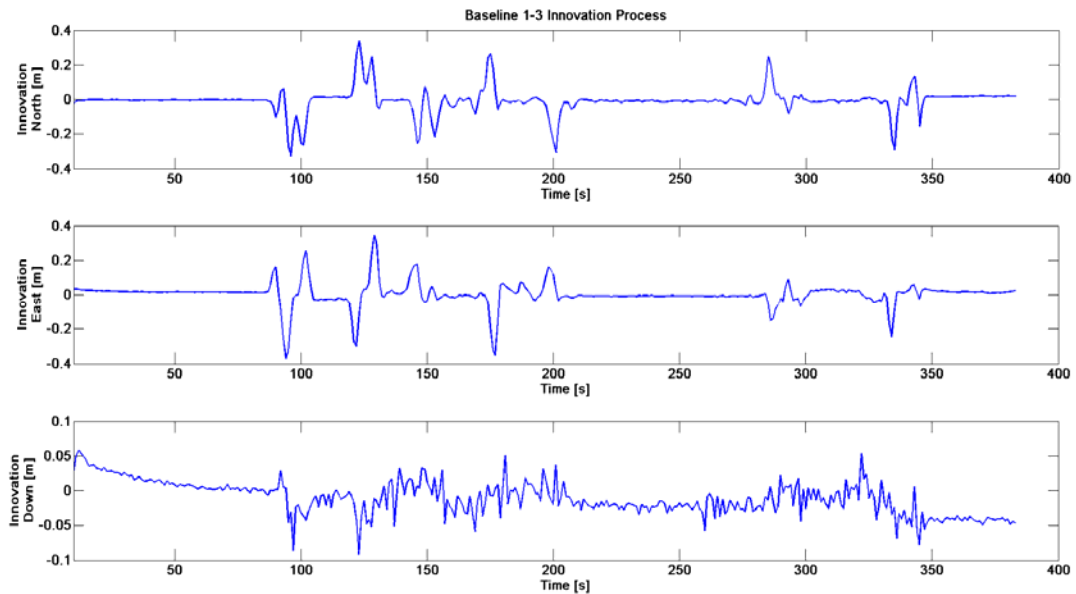


Figure 6.32 – Evolution of the innovation process between the measured baseline1-3 and the one obtained by the estimated quaternion, during the dynamic trial

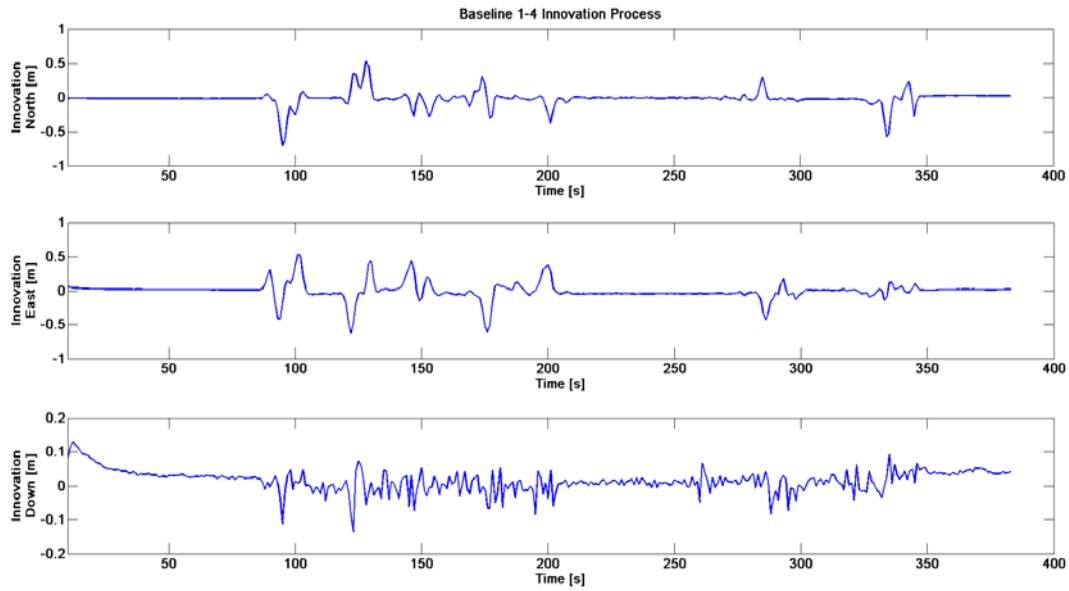


Figure 6.33 – Evolution of the innovation process between the measured baseline1-4 and the one obtained by the estimated quaternion, during the dynamic trial

Table 6.7 – Performance of the innovation process for each baseline, during the dynamic trial

	Baseline 1-2	Baseline 1-3	Baseline 1-4
$\mu_{Innov. North} (m)$	-0.015	-0.007	-0.021
$\sigma_{Innov. North} (m)$	0.066	0.070	0.107
$\mu_{Innov. East} (m)$	0.007	0.002	-0.006
$\sigma_{Innov. East} (m)$	0.076	0.069	0.125
$\mu_{Innov. Down} (m)$	-0.011	-0.011	0.015
$\sigma_{Innov. Down} (m)$	0.027	0.024	0.033

Despite the degradation of the disturbances in a dynamic trial, the EKF performance is good and the results validate this technique. The direct use of the rotation matrix allow similar results, however lacks in the stability that is allowed by a recursive algorithm (i.e. inside the stability region of the EKF) and in the presence of singularities. Better results could be achieved by GNSS/INS coupling techniques.

7 CONCLUSIONS

The implementation of an attitude determination algorithm, using multiple L1 GPS receivers and RTK techniques, was the main objective of this thesis. Based on the results presented in the previous chapter, it is possible to conclude that this objective was successfully achieved.

The static trial results showed that resorting to both the algorithm using the rotation matrix and the quaternion based EKF, it was possible to estimate the Euler angles with precisions smaller than 1° (1σ). However, the quaternion based EKF showed slight improvements regarding the estimation of both pitch and heading angles with an increased precision in the order of approximated 0.3° and 0.05° , respectively, which is understandable since it is a recursive estimation algorithm. The good performance of the EKF is visible in the innovation results, which have millimeter level errors (1σ).

Despite the disturbances augmentation, the dynamic results are representative of the successfully implementation of the attitude determination algorithms, capable of detecting attitude variations along the path made by the test platform. This fact was visible in the detection of a positive roll angle (of approximately 6°), imposed by climbing a sidewalk with the test vehicle. The increase in the level of disturbances is visible in the attitude angles that are function of the Up coordinate (which is more sensible to noise), that is, pitch and roll angles. For the EKF the roll angle is more affected by this phenomenon, since the highly disturbed Up coordinate led to a highly disturbed angular velocity about the x axis. However these disturbances do not affect the correct determination of the Euler angles, which is proved by the performance of the EKF innovation. Despite the disturbances' augmentation, the innovation has errors in the order of the centimeter (1σ).

The static trials showed that the use of the LAMBDA method along with the Ambiguity Filter allows higher confidence in the determination of the correct integer ambiguity, and hence a millimeter level precision in the determination of the baseline vector. In contrast, the baseline solution of the remaining methods (stand alone LAMBDA method, Float Solution and Smoothed Float Solution) was obtained with a meter level precision.

The static results, for single and multiple baselines showed that the proposed improvements within the Ambiguity Filter offer an increase of this algorithm's accuracy. The metric 2, using the baseline length and the Up coordinate in an initial state, offered more confidence in determining the correct integer ambiguity than the metric 1, using the baseline length along with the carrier phase residuals. The introduction of a technique able to keep the correct integer ambiguity solution despite the variation in the satellites' constellation is another improvement within the Ambiguity Filter. This technique avoids resetting the algorithm and hence the restart of the search process for the integer ambiguity determination, which permits the loss of precision in the baseline solution. The results showed that, despite some oscillations due to variations in the satellites' constellation, it is possible to obtain a

millimeter level precision, and hence a precision smaller than 1° (1σ) in the determination of the Euler angles. In the low multipath scenario of the single baseline static trial, the precision of both heading and pitch angles was approximately 0.01° and 0.03° , respectively.

Despite the good results, there are topics that could be improved. Thus some topics regarding future work are presented:

- The research for better metrics and stabilization procedures for the Ambiguity Filter. Despite of the great precision, the technique responsible for avoiding the loss of solution could be improved and tested for longer periods for a more robust validation;
- The research and test of different estimation techniques and different dynamic systems for comparison with the ones implemented in this thesis, in order to improve the presented results;
- The use of techniques like the Constrained Kalman Filter, that allow a coupled estimation of all baselines, making use of the dynamic information given by the GPS receivers' Doppler effect and the satellites' velocity;
- In order to avoid the verified disturbances in the Up coordinate, that were translated in a precision degradation on the estimated angular velocity about the x axis, and consequently in roll angle, the integration of the developed technique with INS sensors (accelerometers in order to improve the estimation of the angular velocities) could lead to great improvements;
- Real time implementation and test in more aggressive environments of the proposed algorithms;
- Even though is not present in this thesis, research regarding the development of an attitude test platform has already been started. A test platform that allows the imposition of different attitude angles could be a great advantage in algorithms validation.

REFERENCES

- [1] E. D. Kaplan and C. J. Hegarty, *Understanding GPS: principles and applications*, 2nd ed. Artech House Publishers, 2006.
- [2] ESA “*Galileo fact sheet*,” 2011.
- [3] P. Misra and P. Enge, *Global Positioning System : Signals , Measurements , and Performance*, 2nd ed. Ganga-Jamuna Press, 2006.
- [4] D. Kim and R. B. Langley, “GPS Ambiguity Resolution and Validation : Methodologies , Trends and Issues,” *International Symposium on GPS/GNSS, Seoul, Korea*, 2000.
- [5] P. Teunissen, “Least-Squares Estimation of the Integer GPS Ambiguities,” *Delft Geodetic Computing Centre LGR series*, no 6., 1993.
- [6] G. Strang and K. Borre, *Linear algebra, geodesy, and GPS*. Wellesley Cambridge Pr, 1997.
- [7] G. Giorgi, P. J. G. Teunissen, and P. J. Buist, “A Search and Shrink Approach for the Baseline Constrained LAMBDA Method : Experimental Results,” *International Symposium GPS/GNSS*, pp. 797-806, Tokyo, 2008.
- [8] J. Reis, “Real-time GPS Heading Determination,” MSc Thesis, Instituto Superior Técnico, Technical University of Lisbon, November 2009.
- [9] J. Reis, J. Sanguino, and A. Rodrigues, “Impact of Satellite Coverage in Single-Frequency Precise Heading Determination,” in *Position Location and Navigation Symposium (PLANS), 2010 IEEE/ION*, Indian Wells, USA, 3-6 May 2010, pp. 592-597.
- [10] J. Reis, J. Sanguino, and A. Rodrigues, “Baseline Influence on Single-Frequency GPS Precise Heading Estimation,” in *Wireless Personal Communications Journal*, Springer, Netherlands, 2012.
- [11] J. Reis, J. Sanguino, A. Rodrigues, “Influence of Baseline Length in Single-Frequency Real-Time Vehicle Heading Estimation,” in *The 13th International Symposium on Wireless Personal Multimedia Communications (WPMC)*, Recife, Brazil, 11-14 October 2010.
- [12] P. Batista, C. Silvestre, and P. Oliveira, “Partial Attitude and Rate Gyro Bias Estimation: Observability Analysis, Filter Design, and Performance Evaluation,” *International Journal of Control*, vol. 84, no. 5, pp. 895-903, May 2011.
- [13] S. Brás, R. Cunha, J. F. Vasconcelos, C. Silvestre, and P. Oliveira, “A Nonlinear Attitude Observer Based on Active Vision and Inertial Measurements,” *IEEE Transactions on Robotics*, vol. 27, no. 4, pp. 664-677, 2011.
- [14] S. Brás, C. Silvestre, P. Oliveira, J. F. Vasconcelos, and R. Cunha, “An Experimentally Validated Attitude Observer Based on Range and Inertial,” *IFAC World Congress*, Italy, September 2011.
- [15] E. Edwan, S. Knedlik, J. Zhou, and O. Loffeld, “A Constrained GPS / INS Integration Based on Rotation Angle for Attitude Update and Dynamic Models for Position Update,” *International Technical Meeting of The Institute of Navigation* pp. 736-743, Anaheim, CA, 2009.

- [16] J. F. M. Lorga , P. F. Silva, J. S. Silva, and A. Fernández, "Attitude Determination Using a Multi-antenna GNSS Receiver Tightly Integrated with a MEMS IMU," *20th International Technical Meeting of the Satellite Division of the Institute of Navigation*, September 2007. September, pp. 25-28, 2007.
- [17] G. Giorgi, P. J. Buist, S. Verhagen, P.J.G. Teunissen, "GNSS-Based Attitude Determination," *InsideGNSS*, July/August 2011.
- [18] J. Tsui, "Fundamentals of Global Positioning System Receivers, A Software Approach. 2nd edition," *John Wiley & Sons, New York*, vol. 2, no. 4, 2005.
- [19] Colonel B. Gruber "Status and Modernization of the US Global Global Positioning System," *Satellite Navigation Summit*, Munich, Germany, March 2012.
- [20] GPS official website, www.gps.gov, visited on April 2012.
- [21] Global Positioning System Wing Systems Engineering & Integration, "Interface Specification IS-GPS-200 (Revision E)," El Segundo, CA, June, 2010.
- [22] R. A. Serway and J. W. Jewett, *Physics for scientists and engineers*, vol. 1. Brooks/Cole Pub Co, 2009.
- [23] B. Hoffmann-Wellenhof, H. Lichtenegger, and J. Collins, "GPS: Theory and practice," *Springer-Verlag, New York*, pp. 2-5, 1994.
- [24] J. Sanguino, Lecture Notes on: "Navigation System," 2010.
- [25] R. E. Kalman, "A New Approach to Linear Filtering and Prediction Problems," *Transactions of the ASME - Journal of Basic Engineering*, vol. 82, no. Series D, pp. 35-45, 1960.
- [26] G. Welch and G. Bishop, "An Introduction to the Kalman Filter," 2006.
- [27] D. Simon, *Optimal state estimation: Kalman, H [infinity] and nonlinear approaches*. John Wiley and Sons, 2006.
- [28] F. V. Graas and M. Braasch, "GPS Interferometric Attitude and Heading Determination: Initial Flight Test Results," *The Institute of Navigation*, vol. IV, pp. 359-378, 1991.
- [29] P. J. D. Jonge, C. C. J. M. Tiberius, P. J. G. Teunissen, and G. C. Centre, "Computational Aspects of the LAMBDA Method for GPS Ambiguity Resolution," *Proceedings of ION GPS-96, 9th International Technical Meeting of the Satellite Division of the Institute of Navigation*, Kansas City, Missouri, Sept.17-20, pp 935-944.
- [30] J. B. Kuipers, *Quaternions and rotation sequences*, vol. 1. Princeton university press Princeton, NJ, 1999.
- [31] J. B. Schleppe, "Development of a Real-Time Attitude System Using a Quaternion Parameterization and Non-Dedicated GPS Receivers," Master Thesis, Department of Geomatics Engineering, University of Calgary, 1996.
- [32] Y. T. Chiang, L. S. Wang, F. R. Chang, and H. M. Peng, "Constrained Filtering Method for Attitude Determination using GPS and Gyro," *IEE Proceedings - Radar, Sonar and Navigation*, vol. 149, no. 5, p. 258, 2002.
- [33] Y. Bar-Shalom, X. Li, and T. Kirubarajan, *Estimation with applications to tracking and navigation*, vol. 9. 2001.

- [34] F. Nunes, Lecture Notes on: "Sistemas de Control de Tráfego," 2010.
- [35] Wilson J. Rugh, *Linear system theory*, Second. 1996.
- [36] Magellan, "A12, B12 & AC12 Reference Manual," 2005.
- [37] U-Blox, "u-blox 6 Receiver Description," 2010.
- [38] Novatel, "531 Rev. 2 and A032 Data Sheets", 1999.
- [39] U-Blox, "ANN Active GPS Antenna," 2003.
- [40] KML Documentation, <https://developers.google.com/kml/documentation/>, visited on April 2012.